UNDRAINED SEISMIC BEARING CAPACITY OF SURFACE STRIP FOUNDATIONS ON COHESIVE SLOPES

by

Mert Öztürk

B.S., Civil Engineering, İstanbul University, 2010

Submitted to the Institute for Graduate Studies in
Science and Engineering in partial fulfillment of
the requirements for the degree of
Master of Science

Graduate Program in Civil Engineering

Boğaziçi University

2015

To my grandmother,

Mediha Cihangiroğlu

ACKNOWLEDGEMENTS

I would like to express my gratitude to my thesis advisor Assoc. Prof. Özer Çinicioğlu who lent his invaluable support me throughout the preparation of my thesis for his guidance, scientific knowledge and encouragement to me a lot for the development of this thesis. I would like to thank the members of my Master's thesis committee, Prof. Gökhan Baykal and Assoc. Prof. Aykut Şenol for their efficient comments and advice.

Moreover, I would like to thank my friends, especially Ahmet Talha Gezgin, for their good wishes. Special thanks to Emel Kahveci for her valuable support and her friendly attitude.

I would like to thank especially to my family for their unconditional support thorough my life.

ABSTRACT

UNDRAINED SEISMIC BEARING CAPACITY OF SURFACE STRIP FOUNDATIONS ON COHESIVE SLOPES

In recent years, some comprehensive research studies have focused on the issue of the undrained seismic bearing capacity in the field of the foundation engineering. However, there is no complete and sufficient solution for calculating the magnitude of the undrained seismic bearing capacity. In this study, a practical and effective method was presented for the calculation of undrained seismic bearing capacity factor for surficial strip foundations on cohesive slopes. Using Finite Element Method, numerous analyses were performed in PLAXIS to investigate the influence of different soil and geometrical parameters on undrained seismic bearing capacity factor. In the analyses, the model was solved as a pseudo-static problem. The considered model has several variables which are possible to influence the numerical results. These variables are the distance between the footing and the slope edge, slope angle, crest height, soil properties and horizontal seismic acceleration coefficient. Using undrained Mohr-Coulomb type of constitutive model in PLAXIS, four different undrained material sets which have different consistency values were defined. Utilizing PLAXIS numerical results obtained; design charts and necessary equations were developed. In addition, charts were developed for identifying the limits of permissible states for the seismic bearing capacity problem of surficial strip foundations.

ÖZET

KOHEZYONLU ŞEVLERİN ÜZERİNDEKİ YÜZEYSEL ŞERİT TEMELLERİN DRENAJSIZ SİSMİK TAŞIMA GÜCÜ

Son yıllarda, temel mühendisliği alanı içinde yer alan drenajsız sismik taşıma gücü konusu ile ilgili detaylı çalışmalar yapılmıştır. Her nasılsa, drenajsız sismik taşıma gücü hesabı konusu hakkında kesin ve yeterli bir çözüm sunulmamıştır. Bu çalışmada, kohezif şevler üzerinde bulunan yüzeysel şerit temeller için drenajsız sismik taşıma gücü faktörü hesabında kullanılabilecek bir pratik ve efektif metot sunulmuştur. Sonlu Elemanlar Yöntemi kullanılarak, farklı zemin ve geometrik parametrelerin drenajsız sismik taşıma gücü faktörü üzerindeki etkisini araştırmak için PLAXIS Programında çok sayıda analiz yapılmıştır. Analizlerdeki model yalancı-statik problem olarak çözülmüştür. Tanımlanan model, sonuçları doğrudan ve önemli ölçüde etkileyebilecek farklı değişkenlere sahiptir. Bu değişkenler; yüzeysel temel ile şev köşesi arasındaki uzaklık, şev yüksekliği, şev açısı, zemin özellikleri ve ivme katsayısıdır. Farklı kıvam durumlarına sahip, dört drenajsız zemin malzemesi, drenajsız Mohr- Coulomb modeli kullanılarak tasarlanmıştır. Elde edilen PLAXIS nümerik sonuçları kullanılarak; tasarım grafikleri ve gerekli denklemler geliştirilmiştir. Ayrıca, yüzeysel şerit temellerin sismik taşıma gücü problemi için izin verilebilir sınır durumlarının tanımlanması için grafikler geliştirilmiştir.

TABLE OF CONTENTS

LIST OF FIGURES

LIST OF TABLES

LIST OF SYMBOLS

A	Horizontal seismic acceleration coefficient
b_c	Base inclination factor
b_q	Base inclination factor
b_γ	Base inclination factor
B	Breadth of foundation
C_u	Undrained strength of soil
d	Equivalent depth of strip foundations
d_c	Depth factor
d_q	Depth factor
d_γ	Depth factor
D	Depth factor
D_f	Depth of strip foundations
E_u	Undrained Young's Modulus
EA	Axial stiffness
EI	Bending stiffness
FS	Factor of safety
g_c	Ground inclination factor
g_q	Ground inclination factor
g_γ	Ground inclination factor
H	Height of strip foundations
I_c	Inclination factor
I_q	Inclination factor
I_γ	Inclination factor
k_h	Horizontal seismic acceleration coefficient
k_{hMAX}	Maximum horizontal seismic acceleration coefficient
k_v	Vertical seismic acceleration coefficient
L	Length of strip foundations
$N_{c,se}$	Seismic bearing capacity factor
N_q	Bearing capacity factor

N_s	Stability number
N_{sMAX}	Maximum stability number
N_γ	Bearing capacity factor
q_f	Distributed load on a strip foundation
q_{ult}	Ultimate bearing capacity
$q_{ult,se}$	Seismic ultimate bearing capacity
s_c	Shape factor
s_q	Shape factor
$s\gamma$	Shape factor
S_u	Undrained strength of soil
v	Poisson ratio
v_u	Undrained poisson ratio
w	Unit weight of strip foundation

β	Slope angle
γ	Unit weight of soil
γ_{sat}	Saturated unit weight of soil
λ	Distance between strip footing and slope edge
ϕ	Soil friction angle
ϕ_u	Undrained soil friction angle
ψ	Angle of Dilatancy

LIST OF ACRONYMS/ABBREVIATIONS

FE	Finite element
FEM	Finite element method

1. INTRODUCTION

1.1. Theory Background

Foundations have a significant influence on the existence and health of structures. Geotechnical design of foundations is done considering several criteria, one of which is the bearing capacity of the foundation under earthquake effects.

Bearing capacity is the ultimate bearing pressure that results in the failure of the foundation. If the considered ultimate bearing pressure is defined for seismic conditions, then it is referred to as seismic bearing capacity. However, computation of seismic bearing capacity is cumbersome, that is why pseudo-static can be preferred. In pseudo-static approach, constant horizontal and vertical seismic body forces defined like the driving forces in the limit equilibrium method represent the influence of earthquake on slopes. Consequently, pseudo-static approach is utilized as a practical method for seismic slope stability analyses.

Foundations are classified as shallow and deep foundations depending on the location of the load bearing layer. If the load bearing layer is near to bottom floor level and the loads of the structure are not heavy, shallow foundations are preferred. Footings, strip foundations and mats can be considered as shallow foundations. In contrast, if the load bearing layer locates in deeper point and the loads of the structure are considerably heavy, deep foundations are preferred. Piles, drilled piers or drilled caissons can be considered as deep foundations.

A strip foundation is the long strip of reinforced concrete supporting the walls of buildings. This foundation type has importance in the field of geotechnical engineering for substructures in the geotechnical projects. Strip foundations are generally built on sloping lands in dwellings zones. Hence, engineering design of the strip foundation located on sloping lands involves calculation complexities.

The main objective of this study is to develop design charts and equations for the calculation of undrained seismic bearing capacity factor for surficial strip foundations. Conditions where the surficial foundations are resting on horizontal ground or sloping ground or near sloping ground are considered. However, analyses were limited to undrained soils since undrained conditions correspond to the most critical conditions. Using Finite Element Method, numerous analyses were performed in PLAXIS to investigate the influence of different soil and geometrical parameters on undrained seismic bearing capacity factors. Furthermore, the concept of the stability number was incorporated to identify the stability of the slopes on which the foundation was on. Finally, the last objective is to improve available charts in the literature for identifying the limits of permissible states when seismic bearing capacity problem is considered for surficial strip foundations.

2. LITERATURE REVIEW

2.1. Shallow Foundations

A foundation, located under the structure, is a subsection that carries the total weight of the structure. Foundations are classified as shallow foundations and deep foundations. Sivakugan and Pacheco (2011) defined the shallow foundation as the load-transferring structure at a relatively shallow depth. Pad footings, strip footings and mats are the kinds of shallow foundations. Shallow foundations differ from deep foundations with an important restriction that the breadth of shallow foundations must have equal or higher values than the depth of shallow foundations.

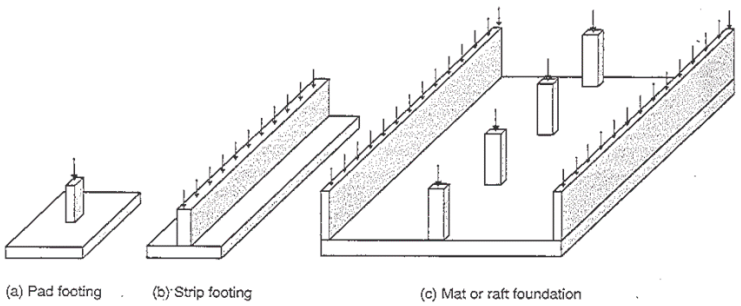

Figure 2.1. Types of Shallow Foundations (Sivakugan and Pacheco, 2011).

Strip foundations are long strip of reinforced concrete substructures which support mainly long structures. Strip foundations, like all other foundations, are designed by considering strength and deformations of the underlying soil. In any case, water is an important factor that can easily influence the strength and naturally deformations values of soil located beneath the foundation. The loads must not be exceeding the capacity of the underlying soils to carry loads and also deformations must be within tolerable limits for a successful foundation design.

2.2. Bearing Capacity of Shallow Foundations

Terzaghi (1943) defined the critical load or the total bearing capacity (Q_u) as the load required causing the failure of the soil support. It depends on the mechanical properties of the soil, the size of the loaded area, foundation shape, and foundation location with reference to the surface of the soil. Provided that the strain which precedes the failure of the soil by plastic flow is very small, the footing does not sink into the ground until a state of plastic equilibrium. This relation between load and settlement is shown by the curve 1 in Figure 2.2. The failure occurs with sliding in the two outward directions, as demonstrated in Figure 2.3. (C_1). This failure type is defined as "the general shear failure". However, if the strain which precedes the failure of the soil by plastic flow increases gradually, the footing sinks into the ground continuously until a state of plastic equilibrium. The corresponding relation between load and settlement is demonstrated with curve 2 in Figure 2.2. The rapid inclination of curve 2 initiates the failure of the soil before the failure reaches to the surface. This failure is named as "the local shear failure".

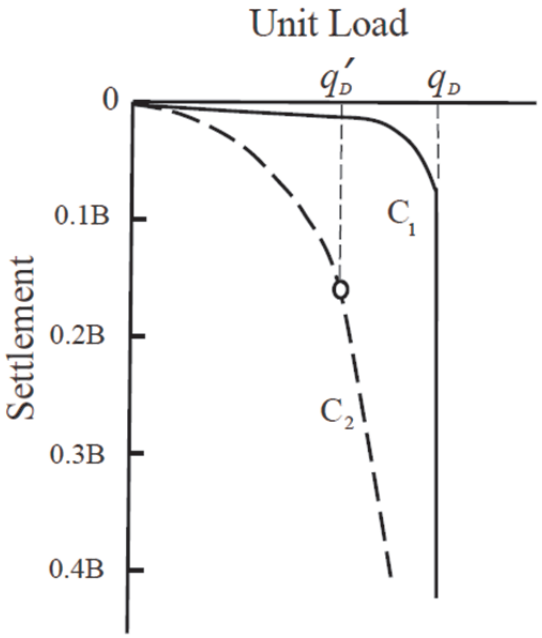

Figure 2.2. Relation Between Load and Settlement on Dense (C_1) and Loose (C_2) Soil (Terzaghi, 1943).

Terzaghi (1943) demonstrated the plastic equilibrium area which is divided into three important zones as shown in Figure 2.3. There are Zone I which is a wedge shaped elastic zone beneath the foundation, Zone II which are the radial shear zones and Zone III which are the passive Rankine zones. (ϕ^o. Top corners of the Rankine passive zones have equal value to (45-ϕ/2). Upper corners of Zone I internal angles' (α) is assumed to equal to soil friction angle.

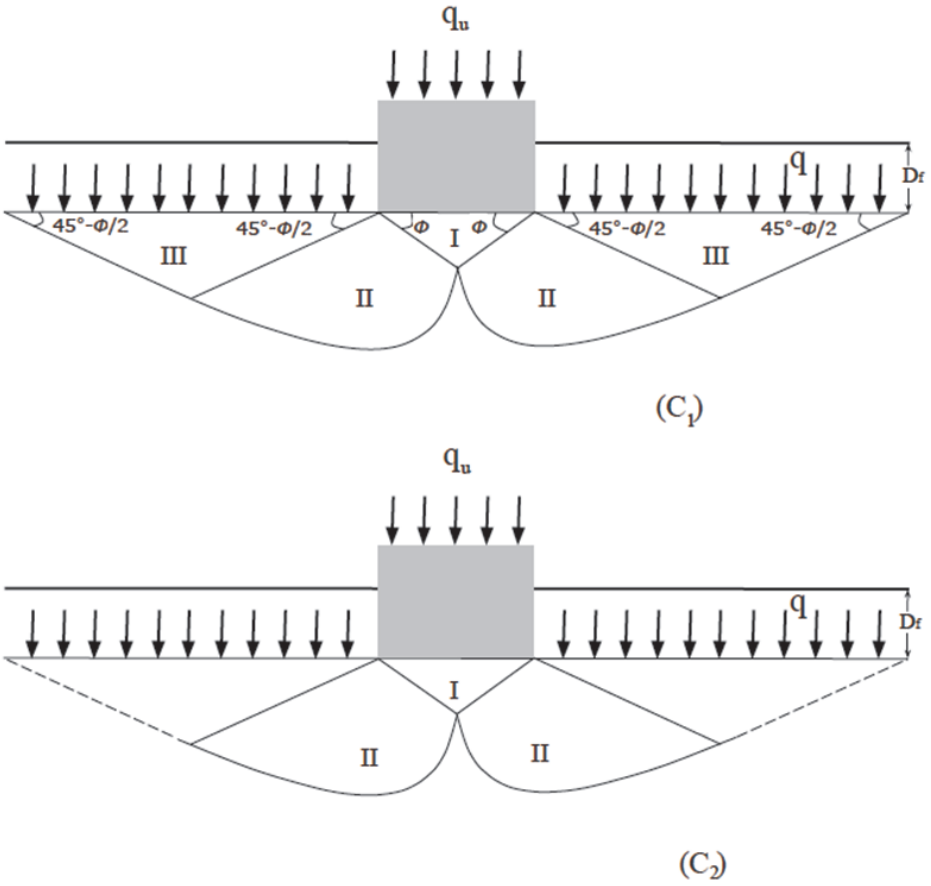

Figure 2.3. Failure Mechanisms of Dense (C_1) and Loose (C_2) Soil (Terzaghi, 1943).

According to Terzaghi's Bearing Capacity Theory (1943), the ultimate bearing capacity of the shallow foundation with the influences of cohesion, friction and weight is calculated using the formula shown below. The coefficients N_c, N_q and N_γ are called the bearing capacity factors. The changes in coefficients occur only if the angle of shearing resistance (ϕ) alters. Bearing capacity factors are indicated below. In N_q formula, $K_{p\gamma}$ signifies that the passive earth pressure coefficient. These formulas shown below are

used in case of general shear failure.

$$q_u = q_c + q_q + q_\gamma \tag{2.1}$$

$$q_u = cN_c + qN_q + \frac{1}{2}\gamma B N_\gamma \tag{2.2}$$

$$N_c = \cot \emptyset \, (N_q - 1) \tag{2.3}$$

$$N_q = \frac{e^{2\left(\frac{3\pi}{4} - \frac{\emptyset}{2}\right)\tan \emptyset}}{2\cos^2\left(45 + \frac{\pi}{2}\right)} \tag{2.4}$$

$$N_q = \frac{1}{2} K_{P\gamma} \tan^2 \emptyset - \frac{\tan \emptyset}{2} \tag{2.5}$$

Skempton (1951) investigated that the bearing capacity of saturated clays (ϕ= 0^o)Skempton presented the simple rules to estimate the bearing capacity factor, N_c:

Table 2.1. Estimation of Bearing Capacity Factor, N_c (Skempton, 1951).

At the surface, where D = 0	
N_{c0} =	5 for strip footings
N_{c0} =	6 for square or circular footings
At depths where D/B < 2 $\frac{1}{2}$	
N_{cD} =	(1 + 0.2D/B) N_{c0}
At depths where D/B > 2$\frac{1}{2}$	
N_{cD} =	1.5 N_{c0}
At any depth the bearing capacity of a rectangular footing	
Nc (rectangle) =	(1 + 0.2 B/L) Nc (strip)

where is the D depth of foundation, is the B breadth of foundation, is the L length of foundation.

Skempton (1951) revised Terzaghi's formula of the allowable foundation pressure:

$$q_{allowable} = \frac{1}{F}\left[cN_c + p_o\left(N_q - 1\right) + \frac{\gamma B}{2}N_\gamma\right] + p \tag{2.6}$$

where is the F the desired factor of safety, is the c cohesion of the soil, is the p_o effective overburden pressure at foundation level, is the p total overburden pressure at foundation level, is the γ density of soil beneath the foundation, is the B breadth of foundation, is the N_c, N_q, N_γ bearing capacity factors, q_{nt} net ultimate bearing capacity.

N_q and N_γ are equal to zero for $\phi = 0^o$. Thus Equation 2.6 becomes the simpler form:

$$q_{allowable} = \frac{c}{F}N_c + p \tag{2.7}$$

The ultimate bearing capacity equation is then shown below:

$$q_t = c_u N_c + p \tag{2.8}$$

The ultimate bearing capacity of clays is calculated with Equation 2.8, if the cohesion of the clay has been determined and the factor Nc has been evaluated for the dimensions of the foundation.

Hansen (1961) emphasized the importance of the dimensions, shape and depth of the foundation area for the bearing capacity. Also, he developed formulas for the inclination of the foundation load. Hansen generalized Terzaghi's formula by multiplying each of terms with a shape, a depth and an inclination factor. The most convenient formula developed by Hansen for the special case of $\phi = 0^o$ (clay), as demonstrated

below.

$$\frac{Q}{BL} = \frac{1}{2}\gamma B N_\gamma s_\gamma d_\gamma i_\gamma + (c + q\tan\emptyset)\, N_c s_c d_c i_c + q \tag{2.9}$$

where is the c cohesion of the soil, is the γ effective unit weight of soil, is the q effective unit load on the surface outside the foundation, is the B breadth of foundation, is the L length of foundation, is the N_c, N_q, N_γ bearing capacity factors, is the s_γ, s_c shape factors, is the d_γ, d_c depth factors, i_γ, i_c inclination factors.

Hansen (1968) revised and extended the bearing capacity formula adding two new factors which were base inclination and a ground inclination factors. In addition, these formulas were for the use of central loading with the symbols B, L and A referred to the effective rectangle. Likewise, Hansen presented a new formula in which the c term was dominant the special case of $\phi = 0^o$ (clay), as shown in Equation 2.11. For inclination factors, H referred to the horizontal component of the applied load and V referred to the vertical component of the applied load, as shown in Figure 2.4.

$$\frac{Q}{A} = \frac{1}{2}\gamma B N_\gamma s_\gamma d_\gamma i_\gamma b_\gamma g_\gamma + q N_q s_q d_q i_q b_q g_q + c N_c s_c d_c i_c d_c i_c b_c g_c \tag{2.10}$$

where is the c cohesion of the soil, is the γ effective unit weight of soil, is the q effective unit load on the surface outside the foundation, is the B breadth of foundation, is the A area of foundation, is the N_c, N_q, N_γ bearing capacity factors, is the s_γ, s_q, s_c shape factors, is the d_γ, d_q, d_c depth factors, is the i_γ, i_q, i_c inclination factors, is the b_γ, b_q, b_c base inclination factors, is the g_γ, g_q, g_c ground inclination factors, is the H horizontal component of the applied load, is the V vertical component of the applied load, is the c_u undrained cohesion of the soil.

$$\frac{Q}{A} = (\pi + 2)\, c_u\, (1 + s_c^a + d_c^a - i_c^a - b_c^a - g_c^a) \tag{2.11}$$

where is the $s_c^a, d_c^a, i_c^a, b_c^a, g_c^a$ additive constants for the case of $\phi = 0^o$.

For $\phi = 0^o$

$$i_c = 0.5 - 0.5\sqrt{1 - {}^{H}/_{Ac_u}} \tag{2.12}$$

For $\phi = 30^o$ and 45^o

$$i_q = [1 - 0.5H : (V + Ac\cot\emptyset]^5 \tag{2.13}$$

For $\phi = 30^o$ and 45^o

$$i_\gamma = [1 - 0.7H : (V + Ac\cot\emptyset]^5 \tag{2.14}$$

For $\phi = 30^o$, ν^o is the angle between base and horizontal.

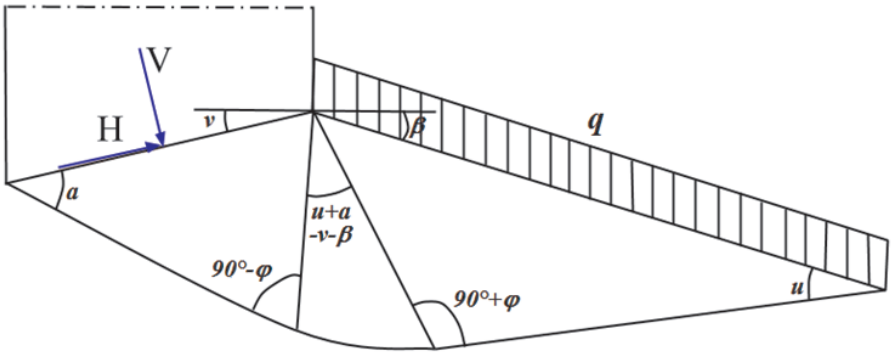

Figure 2.4. Rupture Figure for Calculation of B_c, B_q, G_c and G_q. Frictionless Earth or Weightless Earth With Vertical Surface Load (Hansen, 1968).

For $\phi = 0^o$

$$b_c = \frac{2v}{\pi + 2} = \frac{v^\circ}{147^\circ} \tag{2.15}$$

$$g_c = \frac{2\beta}{\pi + 2} = \frac{\beta^\circ}{147^\circ} \tag{2.16}$$

For $\phi > 0^o$

$$b_q = e^{-2v \tan \emptyset} \tag{2.17}$$

$$b_\gamma = e^{-2.7v \tan \emptyset} \tag{2.18}$$

$$g_q = [1 - 0.5 \tan \beta]^5 = g_\gamma \tag{2.19}$$

For $\phi = 0^o$

$$s_c = 0.2{}^{B}/_{L} \tag{2.20}$$

De Beer proposed these formulas.

$$s_\gamma = 1 - 0.4{}^{B}/_{L} \tag{2.21}$$

$$s_q = 1 + \sin \emptyset {}^{B}/_{L} \tag{2.22}$$

$$d_\gamma = 1 \tag{2.23}$$

These formulas are for the use of D≤B.

$$d_c = 0.4 \tan^{-1} {}^{D}/_{B} \tag{2.24}$$

$$d_q = 1 + 2 \tan \emptyset \, (1 - \sin \emptyset)^{\,2} \tan^{-1} {}^{D}/_{B} \tag{2.25}$$

where is the s_γ, s_q, s_c shape factors, is the d_γ, d_q, d_c depth factors, is the i_γ, i_q, i_c inclination factors, is the b_γ, b_q, b_c base inclination factors, is the g_γ, g_q, g_c ground inclination factors.

Vesic (1975) proposed three distinct modes of failure; general shear failure, local shear failure and punching shear failure; as demonstrated in Figure 2.5. General shear failure is determined by the existence of a well-defined failure pattern comprising of a continuous slip surface from one edge of the footing to the ground surface in Figure 2.5 a, Punching shear failure is characterized by a failure pattern which is not easy to recognize in Figure 2.5 c As the load rises, the vertical movement of the footing exists with the compression of the soil immediately underneath. There is no movement of the soil on the sides of the footing. Local shear failure consists of a wedge and slip surfaces, which start at the edges of the footing and end somewhere in the soil mass. Additionally, soil bulging on the sides of the footing can be visible. Therefore, local shear failure represents a transitional mode between modes of general shear failure and punching shear failure.

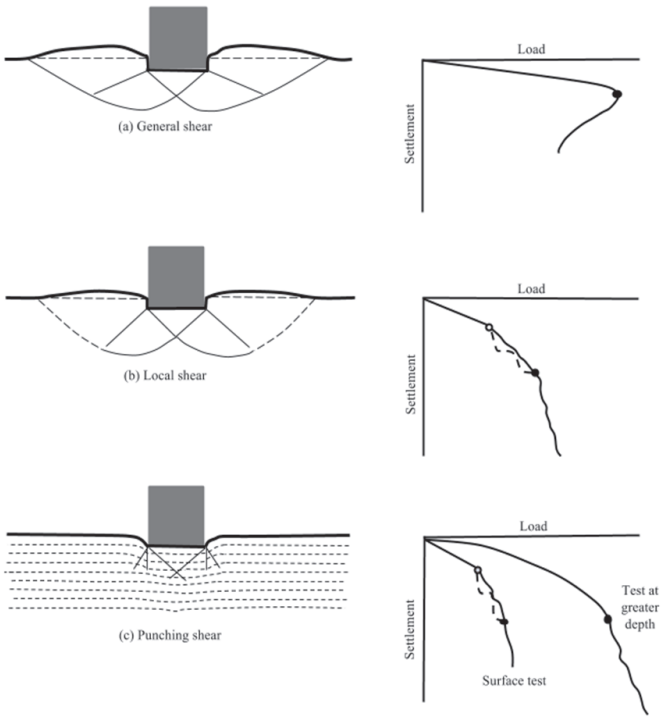

Figure 2.5. Modes of Bearing Capacity Failure (After Vesic, 1963a).

Vesic (1975) emphasized the dependence of the failure mode on the relative compressibility of the soil for particular geometrical and loading conditions. If the soil has incompressible characteristic and low shear strength, it fails in general shear mechanism. However, if the soil has very compressible characteristic, it fails in punching shear mechanism. Furthermore; for a footing on saturated and normally consolidated clay, provided that the loading is slow enough, the soil may fail in punching shear mechanism due to volume change under the action of the load.

Houlsby and Puzrin (1999) conducted the study regarding the problem of failure of a strip foundation on undrained clay subjected to combined moment and horizontal loadings. The researchers obtained apparent upper bound and lower bound solutions (that satisfies equilibrium and nowhere violate the yield criterion). They determined the shape of the failure surface in (V, M, H) space, where principle was written as a function f (V, M, H) = 0. In this study, the contacting area between the strip footing and the clay space was defined by utilizing the effective area concept which is commonly used in the analysis of foundations subjected to moment loading, for lower-bound solution. The effective-width method is equivalent to the assumption that a solution for loads on a footing of width B_0 was also feasible to a footing of larger width B, as shown in Figure 2.6, in which the loads on the two footings were equivalent in static case. Provided that $x = B_0 \ / \ B$, where $0 < x \leq 1$, and the original solution is (v_0, m_0, h_0), then the derived solution was (v, m, h) = (xv_0, $x^2 m_0 \pm 1/2x(1-x)v_0$, xh_0), where the upper sign was used for extension of the footing to the right and the lower sign was used for extension to the left, as shown in Figure 2.6.

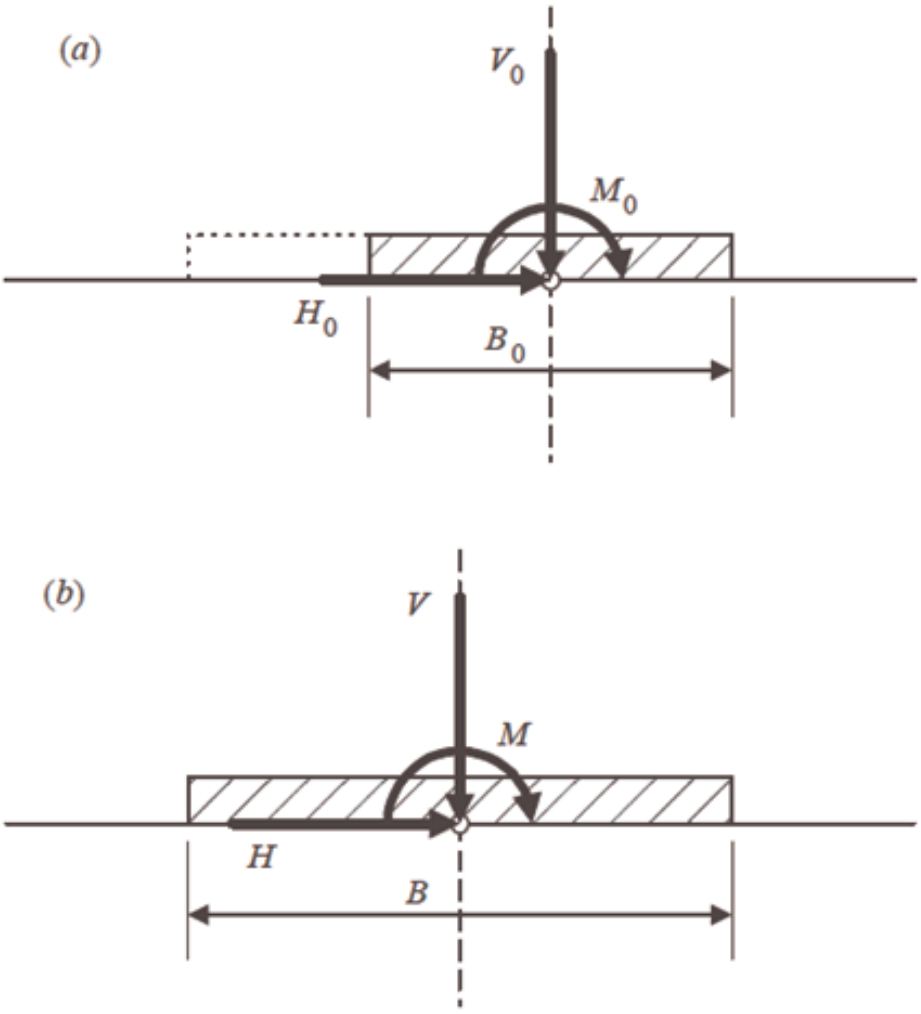

Figure 2.6. The Effective-Width Concept: (a) Original Solution; (b) Derived Solution (Houlsby and Puzrin, 1999).

Taiebat and Carter (2002) determined the shape of the failure locus in (V, M) space using the finite element method. The strip foundation was modeled utilizing isoparametric quadrilateral plane strain elements in load-controlled and also displacement-controlled analyses. In this study, the equivalence between the eccentric bearing capacity of a strip foundation and the vertical bearing capacity of another foundation with a fictitious effective area on which the load is centrally applied were assumed. The failure locus was presented by conducting the two-dimensional finite element analyses for a strip footing under both vertical load and moment, as demonstrated in Figure 2.7. Furthermore; the failure envelopes of the apparent lower-bound and upper-bound solutions proposed by Houlsby and Puzrin (1999) were shown

in Figure 2.7. The load-controlled finite element method of analysis was insufficient to provide the failure load for high M/V ratios. On other hand, the displacement-controlled method of analysis was sufficient to provide a failure load for all conditions. The deformed shape of the model under an eccentric load is shown in Figure 2.8.

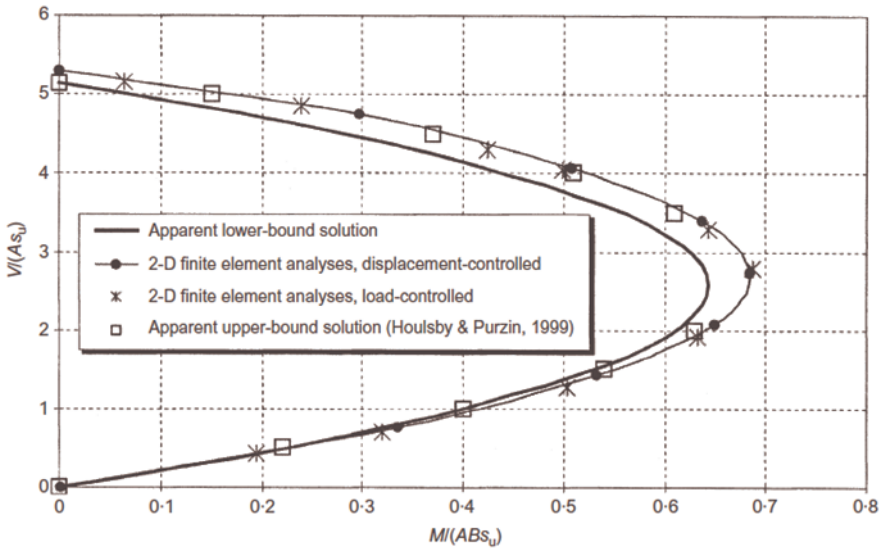

Figure 2.7. Failure Loci for Strip Footing Under Eccentric Loading (Taiebat and Carter, 2002).

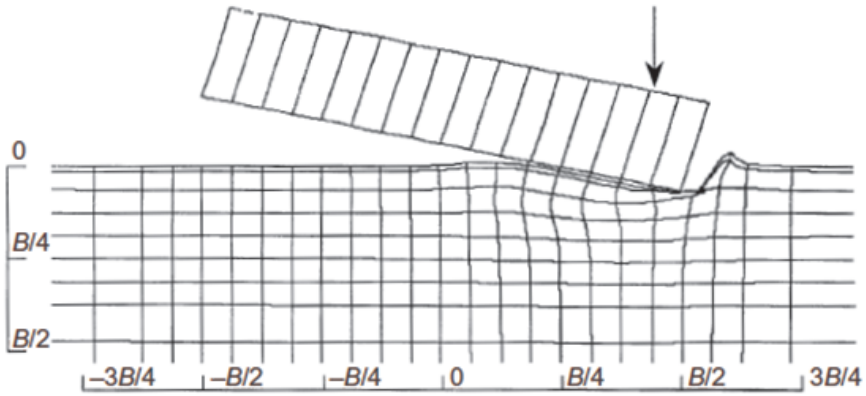

Figure 2.8. Deformed Shape of the Soil and the Strip Footing Under an Eccentric Load (Taiebat and Carter, 2002).

2.2.1. Bearing Capacity of Shallow Foundations on Slopes

Meyerhof (1957) proposed the theory for bearing capacity of a foundation on the top of a slope. When strip foundation is located on the cohesive slope, the bearing capacity of the foundation may be limited due to the probability of the toe or base failure occurrence, as indicated in Figure 2.9. He assumed that N_{cq} in Equation 2.26 as the bearing capacity factor which is utilized for both the influence of the cohesive soil and the overburden pressure. In Figure 2.9, p_0 is the normal stress and s_0 is the shear stress on the surface AE. He emphasized that the bearing capacity factor N_{cq} depends on the distance from the edge of the slope, the slope angle and the stability factor of the slope. N_{cq} diminishes with increasing slope height and slope angle in a smaller extent. The bearing capacity decreases linearly with increasing slope height. When it approaches zero, the height is the critical height of an unloaded slope.

$$q = cN_{cq} + \gamma D \tag{2.26}$$

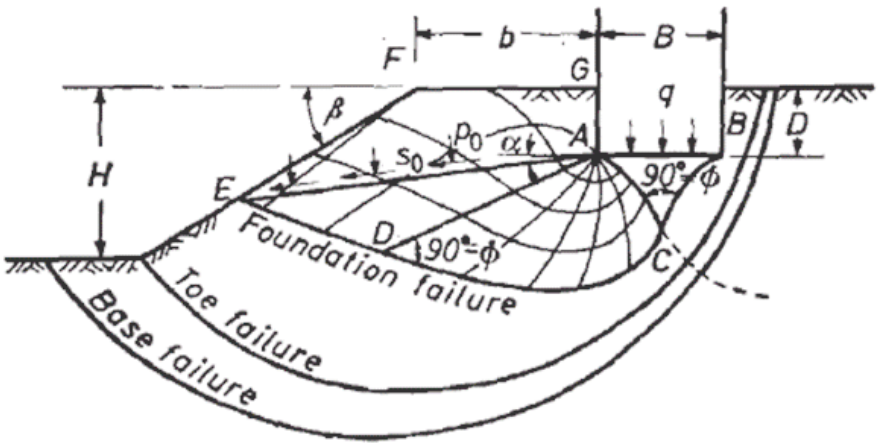

Figure 2.9. Plastic Zones and Slip Surfaces Near Rough Strip Foundation on Top of Slope (Meyerhof, 1957).

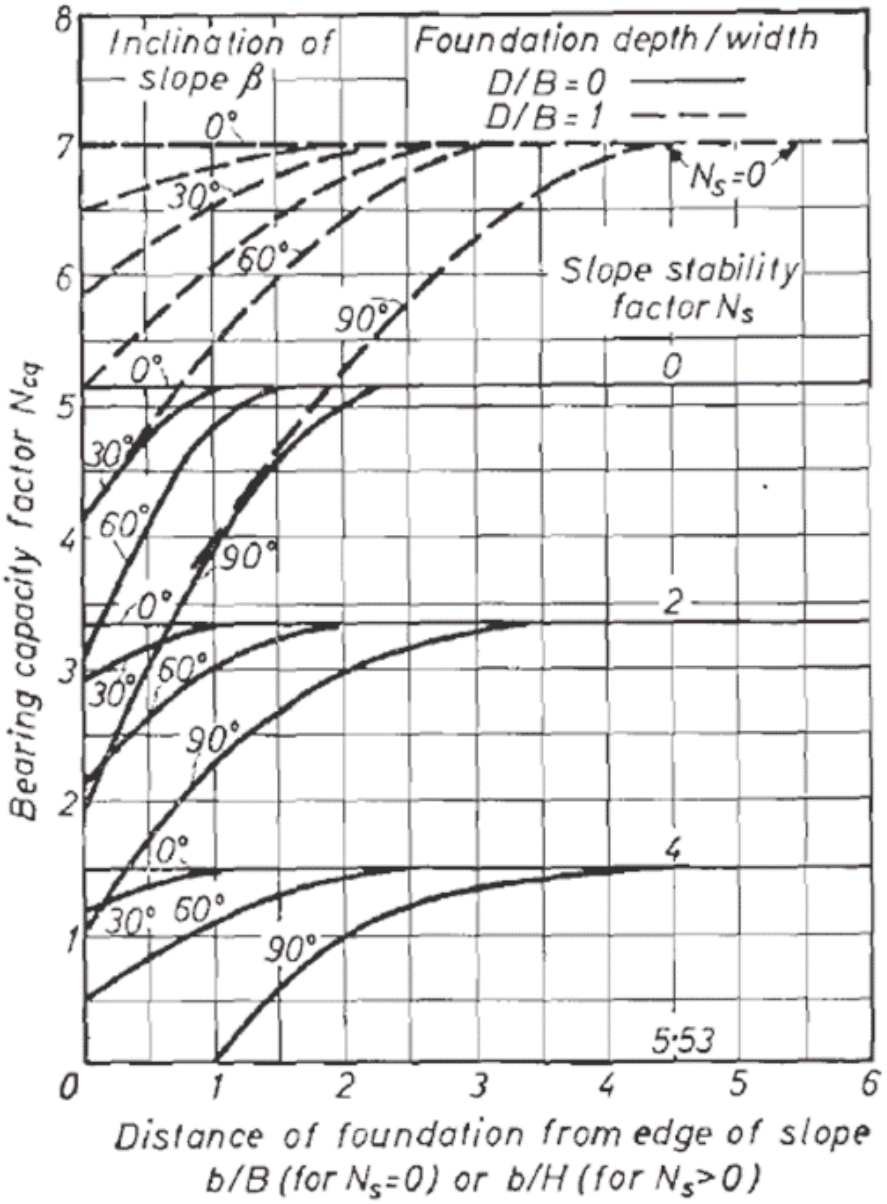

Figure 2.10. Bearing Capacity Factors for Strip Foundation on Top of Slope of Purely Cohesive Material (Meyerhof, 1957).

Kusakabe *et al.*, (1981) investigated that the bearing capacity of slopes on top surfaces using the upper bound theorems. A failure mechanism which was considered as the problem is shown in Figure 2.11. Failure surfaces which emerge below the toe of the slope were not considered in this investigation. As understood, slip line becomes steeper and the area of the radial shear zone becomes smaller while the inclination of the slope increases in Figure 2.12. In addition, the failure surface or slip line and

the bearing capacity factor N_c and N_γ vary with parameter $c/\gamma B$ in Figure 2.13. The relationship in Figure 2.13 is that the slip line becomes incrementally straight and the radial shear zone becomes narrower while $c/\gamma B$ value decreases.

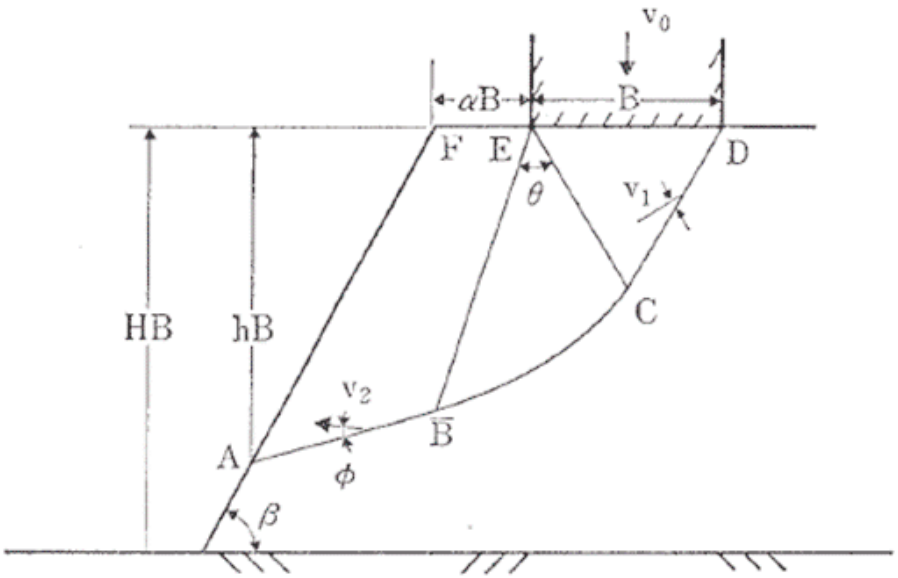

Figure 2.11. Failure Mechanism Adopted of the Present Analysis (Kusakabe *et al.*, 1981).

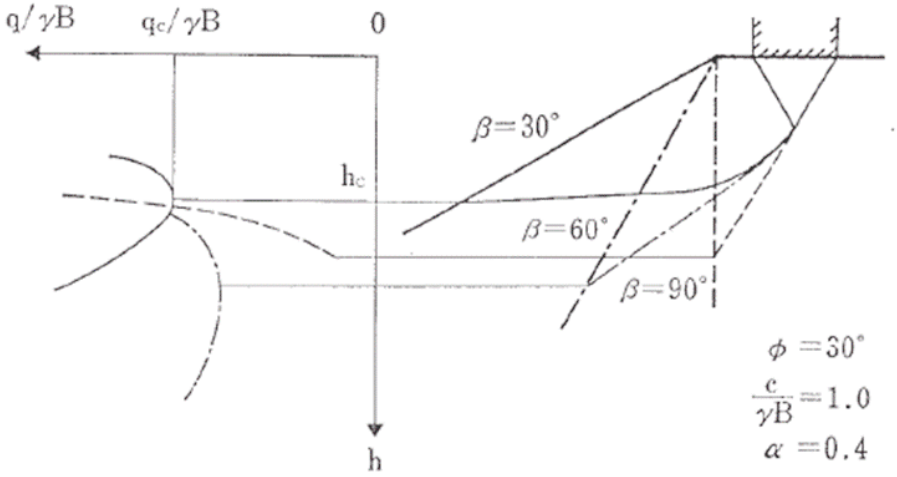

Figure 2.12. Critical Values for $Q/\gamma B$, H and the Failure Surfaces Corresponding to the Critical Slope Height H_c for Various Slope Inclinations (Kusakabe *et al.*, 1981).

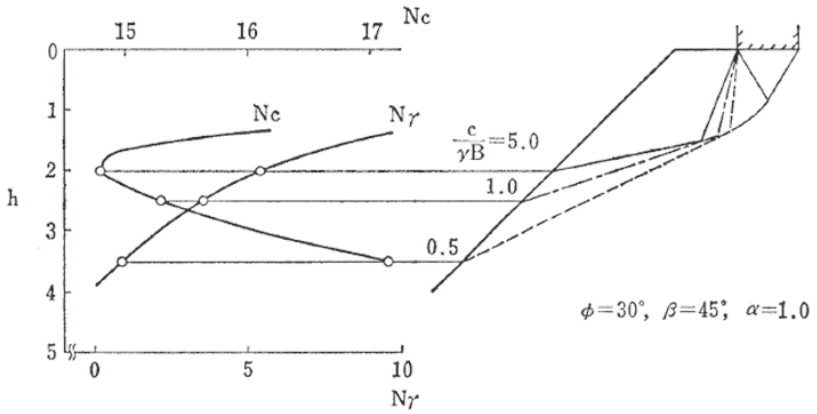

Figure 2.13. Variation of Failure Surfaces and N_c, $N\gamma$ Values With the Value of $C/\gamma B$ (Kusakabe *et al.*, 1981).

Kusakabe *et al.*, (1981) also developed a calculation procedure with diagrams for the bearing capacity of various slopes. One of the diagrams is demonstrated in Figure 2.14. Utilizing these diagrams, the bearing capacity of a footing on slopes (q_s) could be determined by following equation. In Equation 2.27, q_L is the bearing capacity of the footing on a level ground and consists of the bearing capacity factor N_c and N_γ and μ is a dimensionless factor which is plotted versus α and β in the diagrams.

$$q_s = \mu q_L \tag{2.27}$$

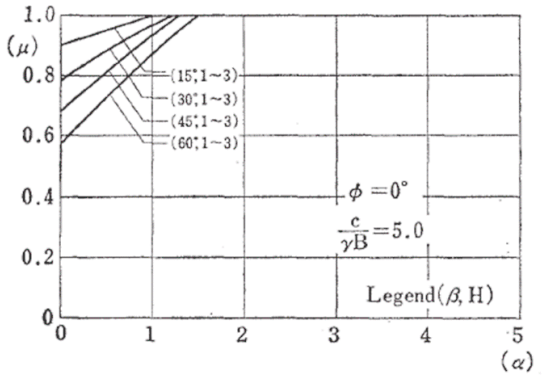

Figure 2.14. The Bearing Capacity Calculation Diagram for Practical Conveniences (Kusakabe *et al.*, 1981).

Azzouz and Baligh (1983) investigated solutions corresponding to a strip load of infinite extent in case of plane strain, as indicated in Figure 2.15. Failure of the model presented takes place as one of two failure modes which are bearing capacity failure and slope failure. Azzouz and Baligh mentioned that if the critical shear surface extends beyond the crest, slope failure occurs; if not, bearing capacity failure is observed. In their study, the effect of strip load on the q^o on the overall slope stability of a slope is assumed by using the circular arc method where the shear surface is regarded as a cylinder of infinite extent. The minimum value of q^o_{cr} is required for the equation of the driving and resisting moments in each unit length of the slope. For this purpose, using Equation 2.28, the minimum value of q^o_{cr} is calculated. $\Delta\gamma H/c$ symbolizes the slope's margin of safety with respect to gravity alone and is defined in Equation 2.28. Smaller values of $\Delta\gamma H/c$ are explained with slopes whose $\Delta\gamma H/c$ are close to $(\Delta\gamma H/c)_{cr}$ for the slope failure due to gravity only.

$$\frac{\Delta\gamma \mathrm{H}}{c} = \left(\frac{\gamma H}{c}\right)_{cr} - \frac{\gamma H}{c} \tag{2.28}$$

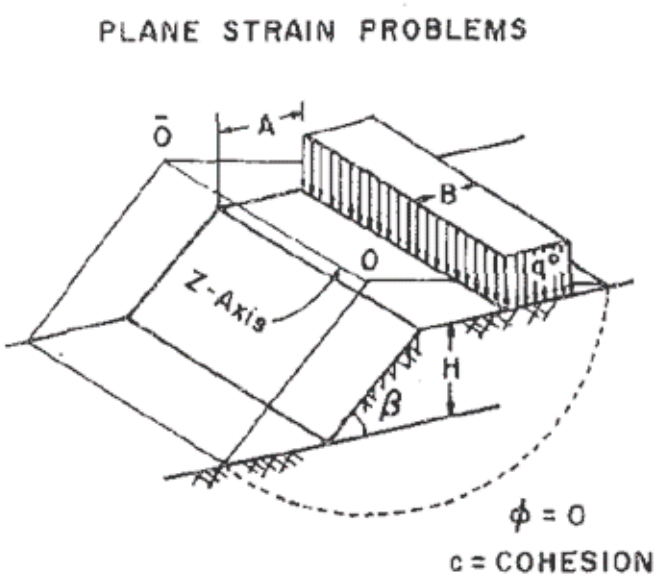

Figure 2.15. Problem Description (Azzouz and Baligh, 1983).

Michalowski (1995) produced a stability chart depending on the kinematic ap-

proach of limit analysis, as shown in Figure 2.16. The failure mechanism with regard to this approach is a log-spiral failure mechanism in Figure 2.17a. According to Figure 2.16, the stability number for $\phi = 0^o$ is not dependent of the slope angle, if the slope angle is less than about 50^o. The failure mechanism for $\phi = 0^o$ is demonstrated in Figure 2.17b. Especially, when the slope angle is less than about 50^o, the failure mechanism extends to infinity. In this case, failure surface radius r has importance rather than the slope height. The rate of work dissipation during collapse with rotational rate ω about point O is formulated by Michalowski in Equation 2.29.

$$D = cr^2\omega\left(\pi - 2\alpha\right) \tag{2.29}$$

The rate of the work of the slope weight for $r >> H$ is indicated below.

$$W_\gamma = \frac{1}{2}\gamma H\omega r^2 \cos^2\alpha \tag{2.30}$$

The dissipation rate and the work rate of the slope weight are equated each other and the maximum stability number in Equation 2.30 is computed (lower bound case) if $\alpha \approx 23.2^o$.

$$\frac{c}{\gamma H} = \frac{\cos^2\alpha}{2\left(\pi - 2\alpha\right)} \tag{2.31}$$

The value in Equation 2.32 is equal to that in Figure 2.16 when $\phi = 0^o$ and the slope angle is less than about 50^o. Michalowski (2002) emphasized this equality is not realistic. Limiting the depth of the failure mechanism to a realist value, he obtained more reasonable stability number. Therefore, two dashed lines in Figure 2.16 express the limitation of the depth of the mechanism in Figure 2.17c (D = 2 and D = 1.25); r_u in Figure 2.16 expresses the distribution of pore water pressure coefficient defined

by Bishop and Morgenstern (1960).

$$\frac{c}{\gamma H} = 0.181 \tag{2.32}$$

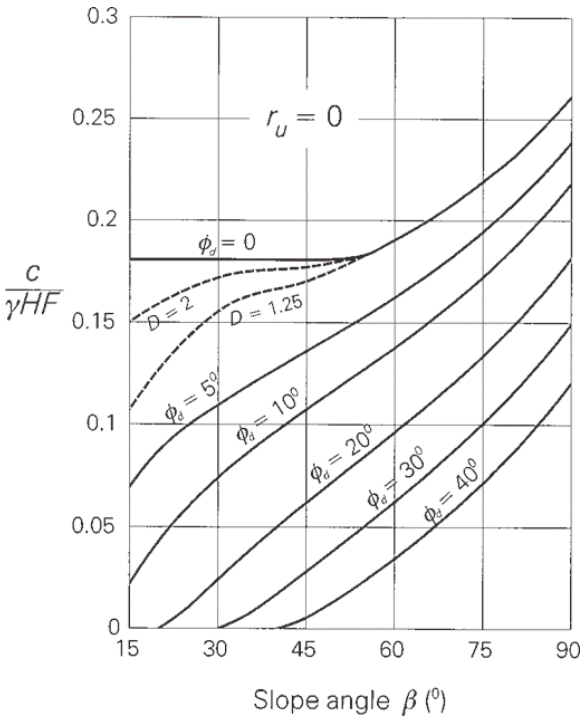

Figure 2.16. Stability Number for Uniform Slopes (Limit Analysis) (Michalowski, 2002).

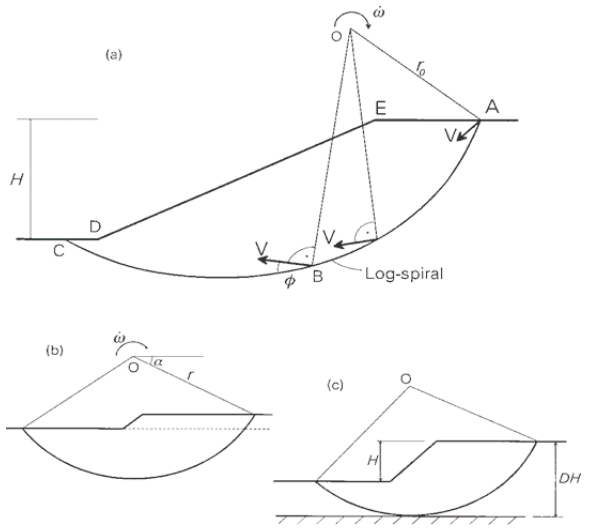

Figure 2.17. Stability Analysis: (a) Rotational Collapse Mechanism; (b)Large-Size Mechanism in Cohesive Soil; and (c) Depth Constraint (Michalowski, 2002).

Georgiadis (2009) conducted finite element analyses of strip footings on or near undrained soil slopes in order to investigate the influence of the various parameters that affect undrained bearing capacity. The influence of slope height, footing distance and soil properties on the undrained bearing capacity was researched by using the program Plaxis. Fifteen-noded triangular elements were utilized to model the soil. Figure 2.18 expresses a typical Finite Element mesh for the case of a 7.5-m-high 45^o soil slope at a distance of 2 m from the footing. Horizontal fixities were defined to the vertical boundaries, both horizontal and vertical fixities to the base of the mesh. The mesh elements were densified beneath the footing for the cases involving bearing capacity failure. The properties of the interface elements have the same properties of the adjacent soil elements. At the end of the analyses, three distinct failure modes were observed, as shown in Figure 2.19. The first two failure modes (bearing capacity failure) occurred in the case of horizontal ground surface, while the other failure mode (overall slope failure) occurred in case of slope stability problem.

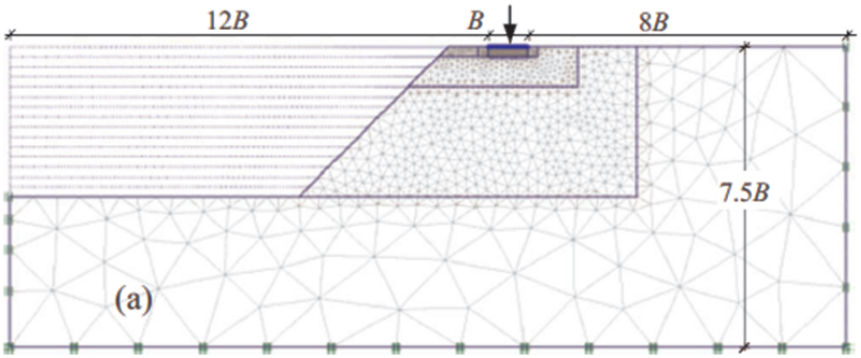

Figure 2.18. FE Mesh with Boundary Conditions (Georgiadis, 2009).

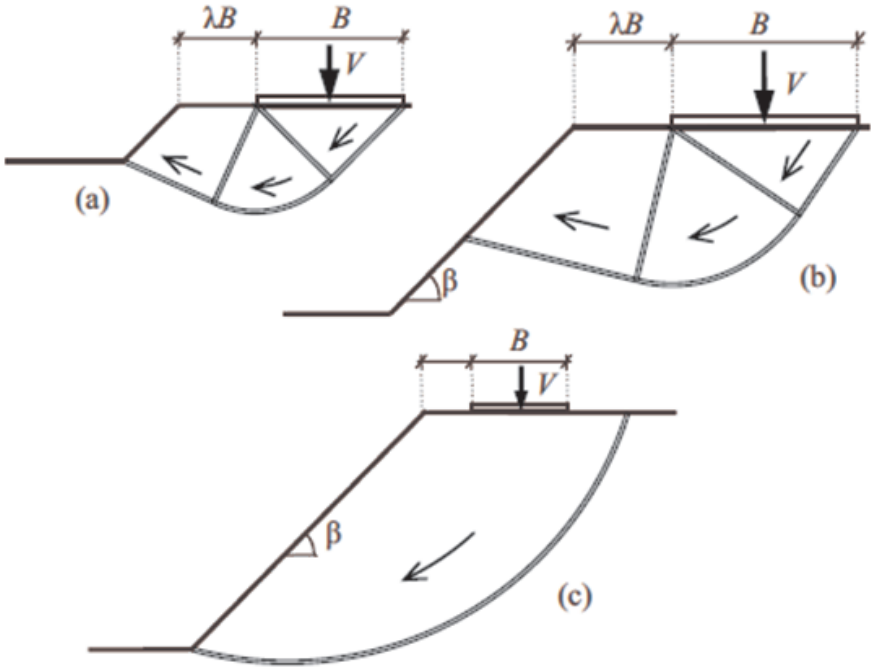

Figure 2.19. Failure Modes [(a) and (b)] Bearing Capacity Failure and (c) Overall Slope Failure (Georgiadis, 2009).

Georgiadis (2009) compared the incremental displacements and principal stress directions at failure obtained from the FE analysis for the case of 0 self weight λ=0 (footing at the crest of the slope) with the optimum upper bound kinematic mechanism for the same case. As seen in Figure 2.20, the FE and upper bound results are in excellent agreement.

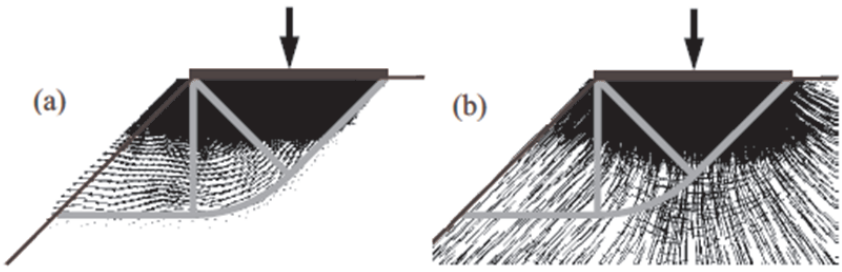

Figure 2.20. Comparison of FE Analysis with Optimum Upper Bound Kinematic Mechanism (Solid Gray Lines) for γ=0: [(a) and (b)] Incremental Displacements and Principal Stress Directions for λ=0 (Georgiadis, 2009).

Georgiadis (2009) demonstrated the variation of the computed values of the undrained bearing capacity factor for a footing at the crest of a slope N_{co} (N_c for λ=0) with the slope angle β for different $cu/\gamma B$ ratios. It can be inferred from Figure 2.21 that N_{co} diminishes linearly with increasing β. It also diminishes slightly with increasing $cu/\gamma B$ ratios. According to these results Equation 2.33 is proposed for the calculation of N_{co}:

$$N_{co} = 5.14 - \frac{2\beta}{1 - \frac{\gamma\beta}{5.14c_u}} \, (where \beta in rads) \tag{2.33}$$

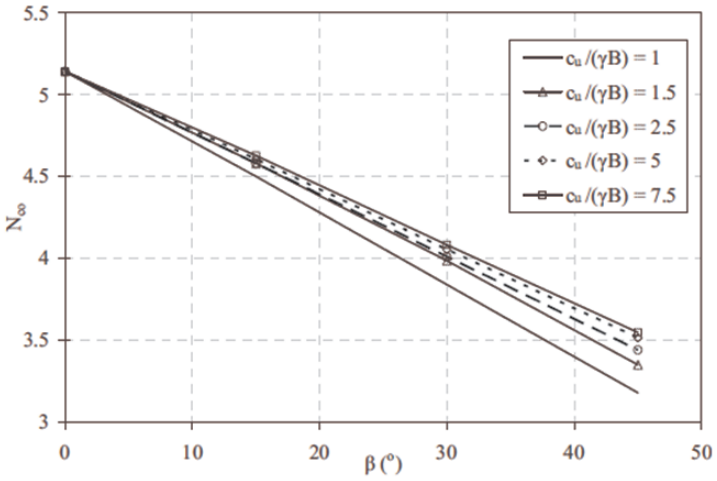

Figure 2.21. Variation of N_{co} with β (Georgiadis, 2009).

Shiau *et al.*, (2011) presented solutions for the ultimate bearing capacity of footings on purely cohesive soils. Applying finite element upper and lower bound methods, design charts were developed for a wide range of parameters, especially a dimensionless strength ratio. The nonlinear curves demonstrated in Figure 2.22b reflect the complex interaction between the footing bearing capacity and the overall slope stability. The transition from bearing capacity failure to overall slope stability failure was marked with three points critical $c_u/\gamma B$ ratios in Figure 2.22b. If $c_u/\gamma B > (c_u/\gamma B)_{crit}$, bearing capacity failure occurred; if $c_u/\gamma B \leq (c_u/\gamma B)_{crit}$, overall slope failure occurred. In other words, after these critical points, the slope is marginally stable and foundation loading triggers an overall slope failure. While $c_u/\gamma B$ diminishes, the failure mecha-

nisms transform from a bearing capacity failure to a base failure at $c_u/\gamma B = 0.556$ in Figure 2.23d. In addition, Shiau *et al.*, (2011) related the stability number to the dimensionless strength parameter $c_u/\gamma B$ in Equation 2.34. In this case, the normalized bearing capacity $p/\gamma B$ will be zero at values of $(c_u/\gamma B)_{crit}$ equal to $N_f H/B$.

$$N_f \frac{H}{B} = \frac{c_u}{\gamma H F_s}\frac{H}{B} = \frac{c_u}{\gamma B} for F_s = 1.0 \tag{2.34}$$

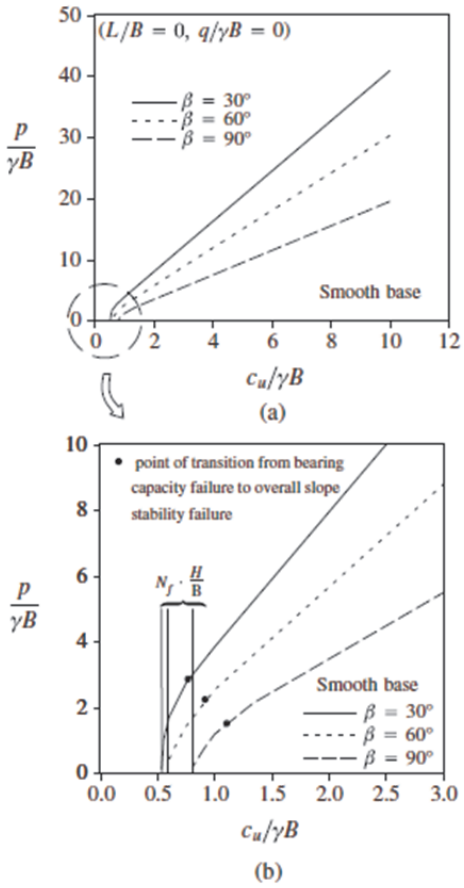

Figure 2.22. Averaged Upper and Lower Bounds for Various Slope Angles (Shiau *et al.*, 2011).

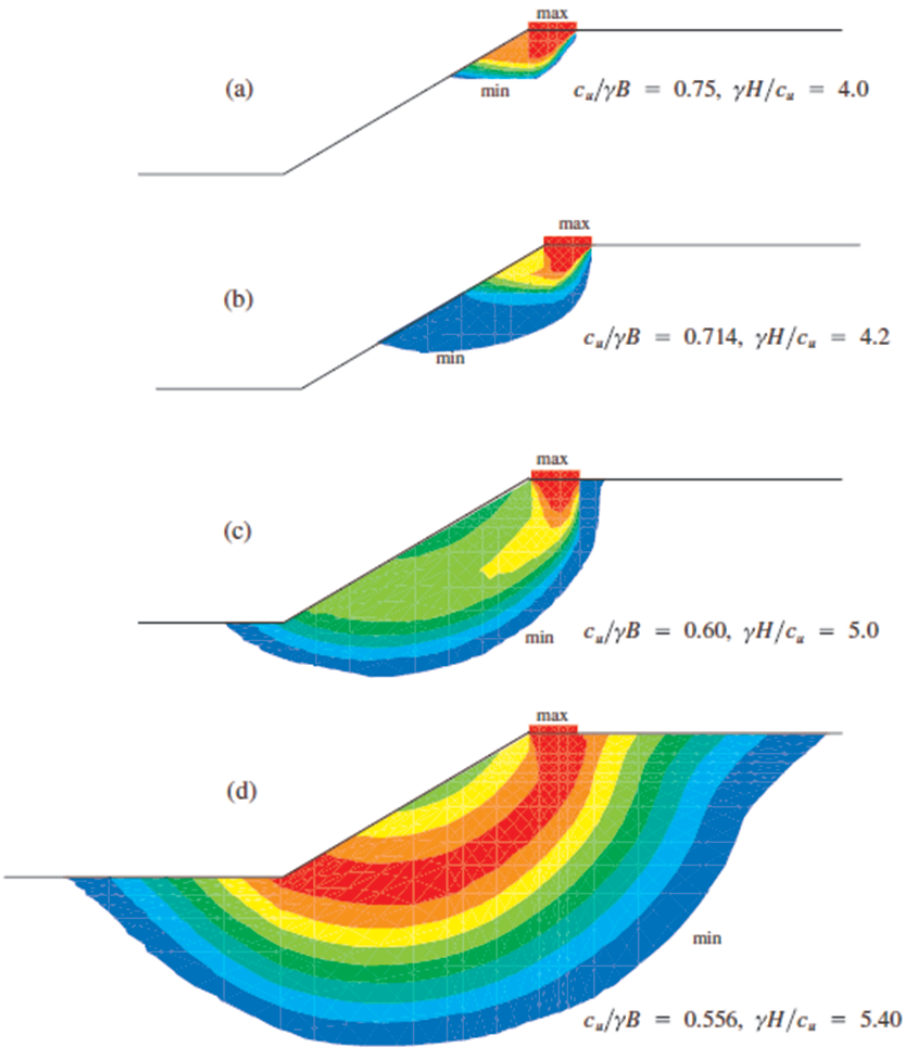

Figure 2.23. Velocity Contours for Decreasing Values of $C_u/\Gamma b$ (Smooth Base, $\beta = 30^o$, L/B = 0, $q/\gamma B$= 0) (Shiau *et al.*, 2011).

2.3. Seismic Bearing Capacity of Shallow Foundations

Sharma (1996) defined Pseudostatic Method as a modified form of the limit equilibrium method with horizontal and vertical static seismic forces that are used to simulate the potential inertial forces owing to ground accelerations in an earthquake.

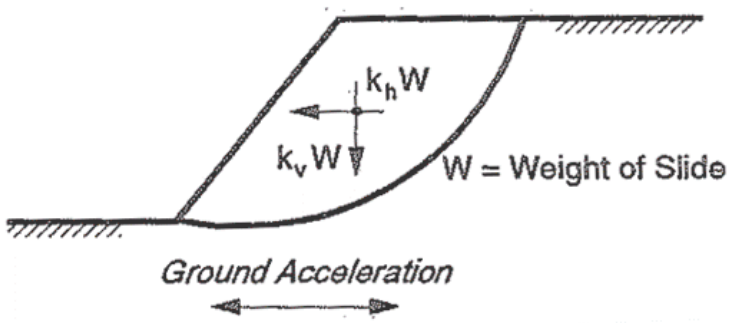

Figure 2.24. Pseudostatic Limiting Equilibrium Analysis for Seismic Loads (Sharma, 1996).

Pecker (1996) reviewed the recent developments regarding seismic bearing capacity of shallow foundations. He summarized the factors affecting the bearing capacity of shallow foundations. These factors are pre-earthquake conditions (the initial static pressure and load eccentricity), soil strength (the rate of loading, degradation under cyclic loading, pore pressure build-up and drainage conditions) and inertia forces in the soil mass. Likewise, he emphasized the most kinematic mechanisms without uplift of the foundation and with uplift obtained by Pecker - Salençon (1991) and Salençon - Pecker (1995 a and b). As seen in Figure 2.25; small load eccentricities or inclinations prevail in the first situation, whereas these parameters become significant in the second situation.

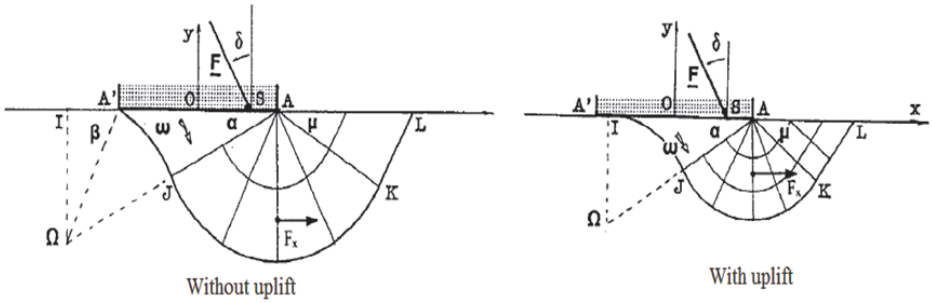

Figure 2.25. Example of Kinematic Mechanisms (Pecker, 1996).

2.3.1. Seismic Bearing Capacity of Shallow Foundations on Slopes

Kumar and Rao (2003) assessed the effect of pseudo-static horizontal earthquake body forces on the bearing capacity of foundations on slopes with the utilization of the method of stress characteristics. They considered two failure mechanisms in carrying out the analysis, as indicated in Figure 2.26. In both-sides failure mechanism, starting from the known boundary stresses on the slope surface, the stress characteristics were expanded from both sides towards the footings base. In single-side failure mechanism, stress characteristics were widened towards the footing base from only one side of the footing. The relationship between N_c and α_h for different values of β and $\phi = 0^o$ is demonstrated in Figure 2.27. According to this relationship, the bearing capacity factor Nc decreases with increase in values of slope angle and α_h.

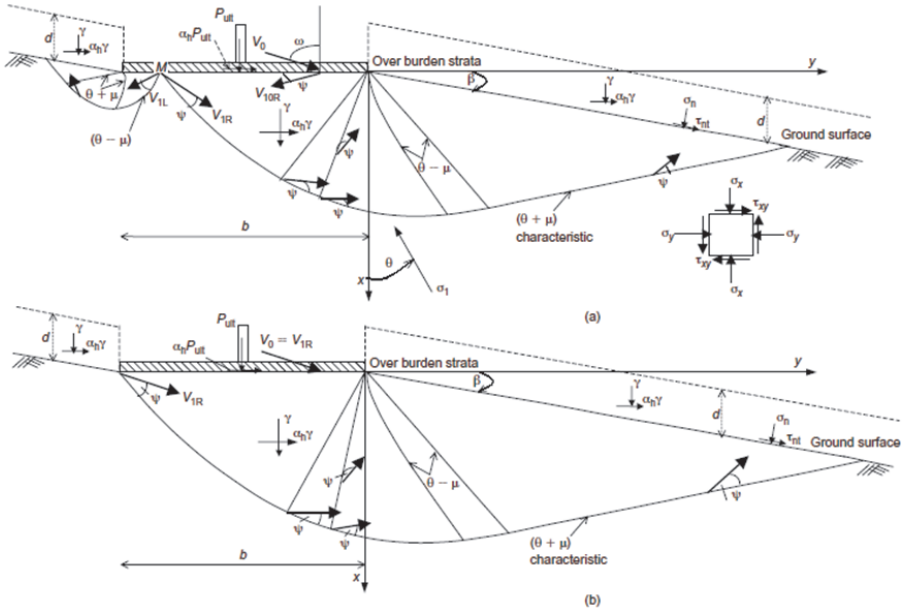

Figure 2.26. Failure Mechanism: (a) Both Sides; (b) Single Side (Kumar and Rao, 2003).

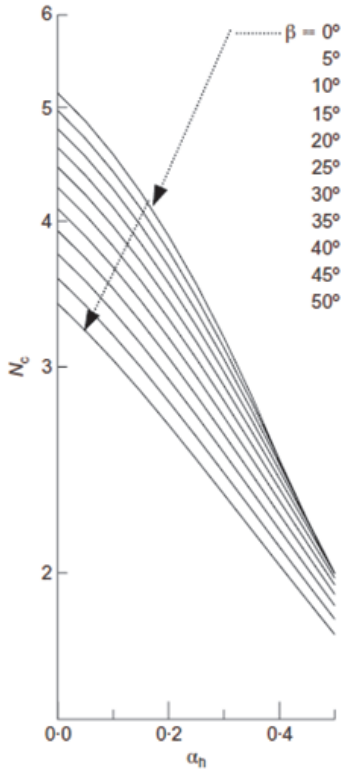

Figure 2.27. Variation of N_c with α_h for Different Values of β and $\phi = 0^{\circ} o$ (Kumar and Rao, 2003).

Shiau *et al.*, (2006) obtained important results regarding yield acceleration of seismic slope stability. They defined yield acceleration as the critical horizontal acceleration at the limit state of the slope stability under pseudo-static earthquake forces in their study. As shown in Figure 2.28, the $(k_h)^{yield}$ value rises depending on the increase in soil friction angle. In addition, while friction angle increases, the failure mechanism becomes narrower due to the gain in soil strength.

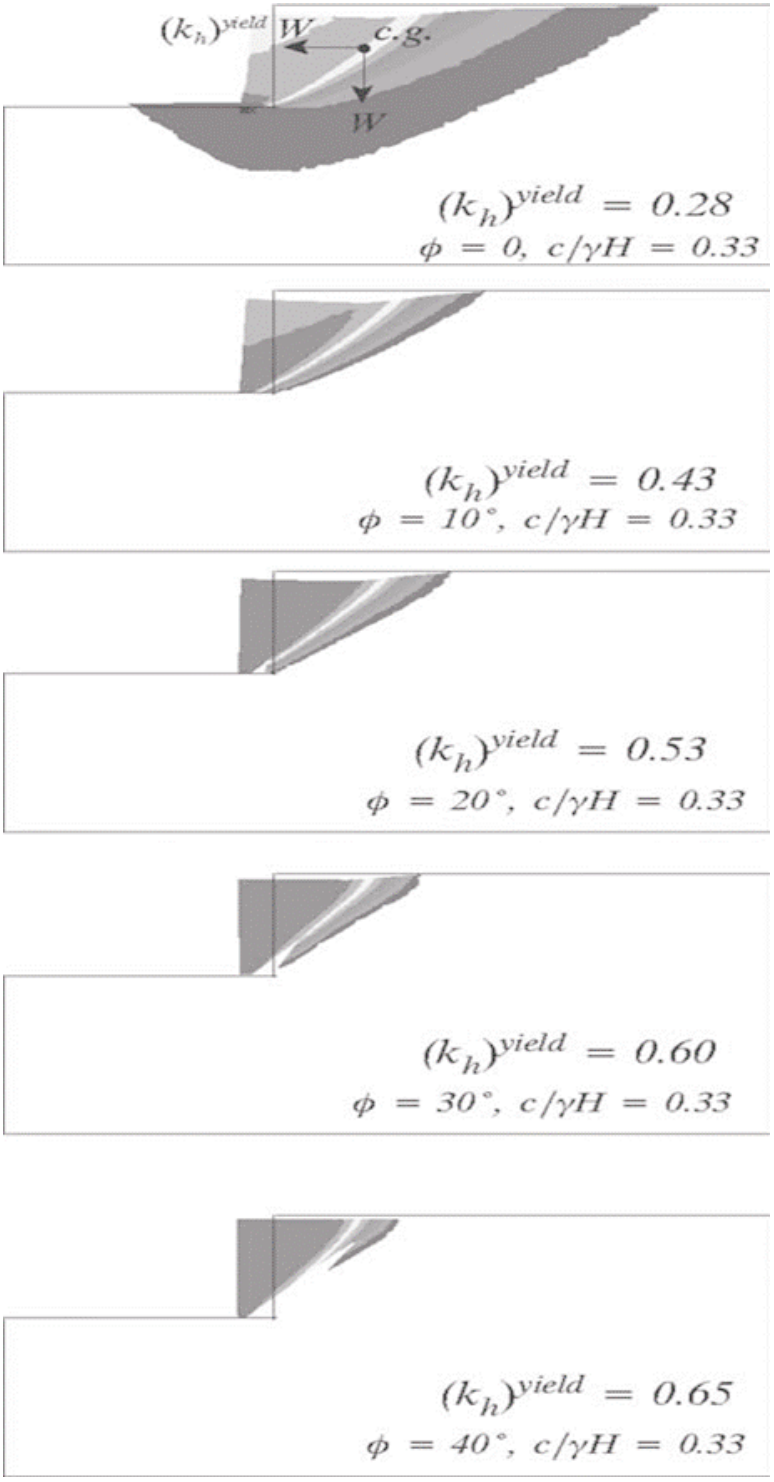

Figure 2.28. Deformed Shapes aAnd Velocity Diagrams Showing Slope Failures Under Critical Yield Accelerations (Shiau *et al.*, 2006).

Castelli and Motta (2009) investigated the bearing capacity of strip footings near slopes depending on the distance of the footing from the edge of the slope. They

conducted the analysis based on the limit equilibrium method, supposing a circular failure mechanism. The results of static case are shown in Figure 2.30 under undrained conditions ($\phi = 0^o$). While the normalized distance of the footing increases, the ground factors, for a not embedded footing, become closer and closer to 1. In Figure 2.31, as in the static case, the bearing capacity has the minimum value when the footing is located at the edge of the slope.

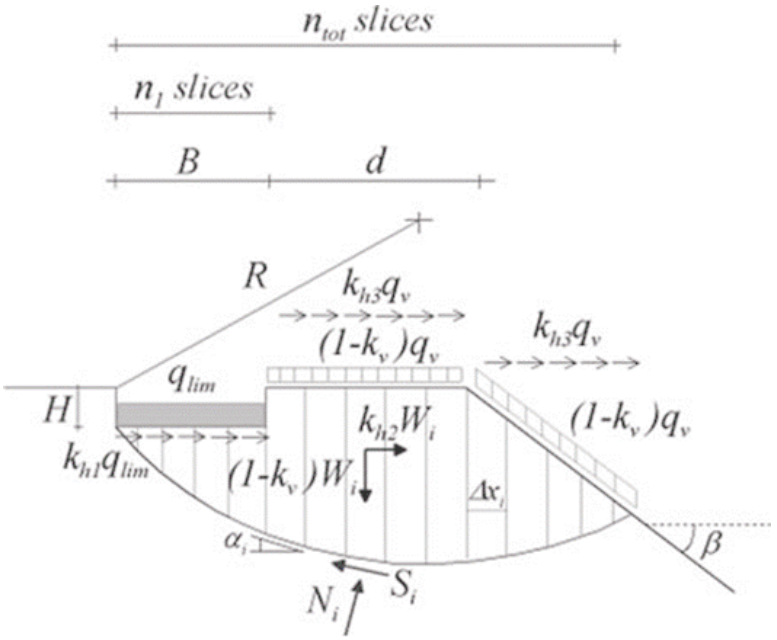

Figure 2.29. Failure Mechanisms and Applied Forces Adopted in the Analysis (Castelli and Motta, 2009).

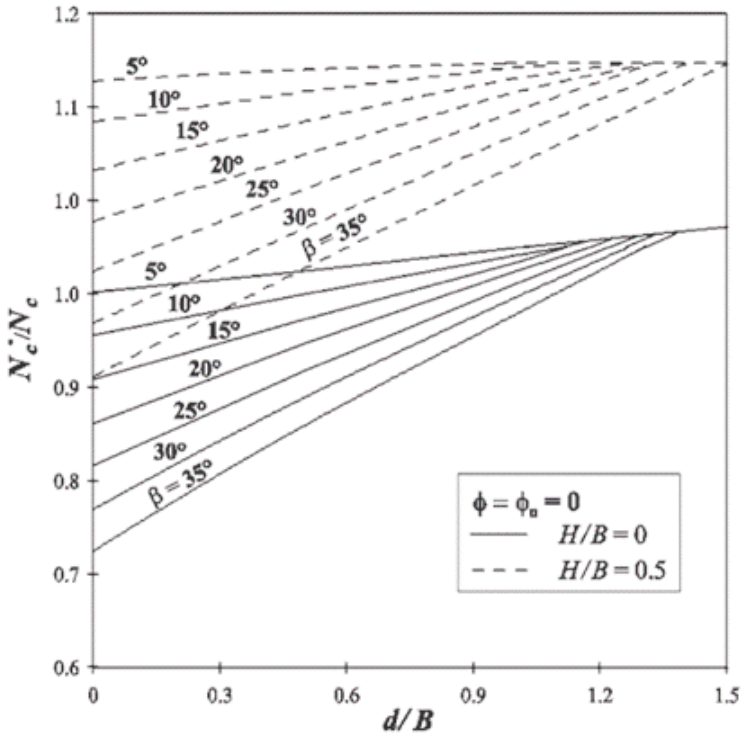

Figure 2.30. Ground Factors G_c as a Function of the Distance From the Edge of the Slope (Castelli and Motta, 2009).

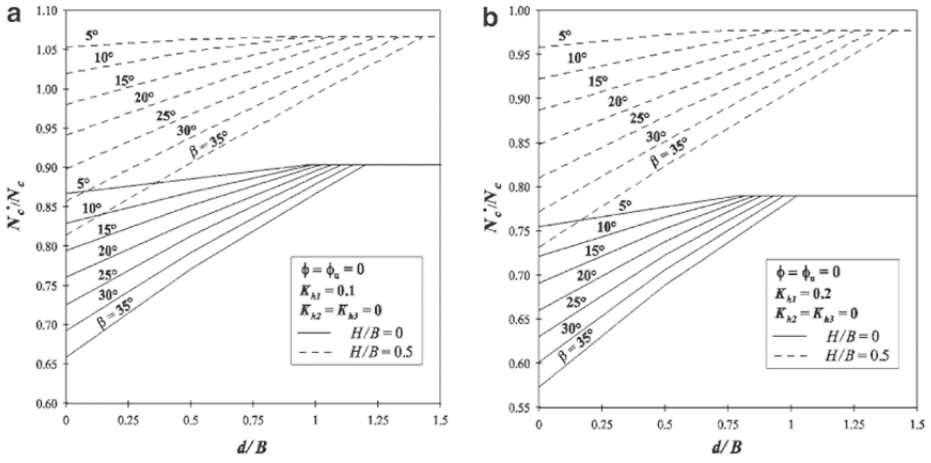

Figure 2.31. N_c^*/N_c Ratios as a Function of the Normalized d/B Slope Distance for $k_{h1} = 0.1$ (a) and $k_{h1} = 0.2$ (b) (Castelli and Motta, 2009).

3. METHODOLOGY

The main objectives of this study are to determine a convenient procedure for the calculation of the seismic bearing capacity of surface strip foundations on slopes and to develop applicable designing charts for the maximum horizontal seismic acceleration which can be tolerated by foundations built on sloping field. For this reason, numerous geotechnical finite element models defined under plane strain conditions were defined and solved using PLAXIS Engineering Software.

Furthermore, Taylor's concept of the stability number (1937) was presented to distinguish the stability of the slopes which the foundation was built on. Moreover, Koppula's concept of the stability number (1984) was presented and utilized for the design examples. By using stability number charts, the stability of one slope which the foundation built on is revealed whether the slope is stable or unstable. Determining the stability of the slope must be confirmed before the design of strip foundations.

Finally, charts indicating allowable values of the horizontal seismic acceleration coefficients were developed for defining the maximum tolerable boundaries of horizontal seismic acceleration for surface strip foundations.

3.1. Overview of PLAXIS Software

PLAXIS Software was utilized for the analysis of this study owing to being a finite element package that has prevalent importance on the geotechnical engineering analyses in geotechnical projects. PLAXIS software consists of the four main sub-programs which are Input program, Calculations program, Output program and Curves program. Each sub-program is used respectively different tasks along Finite Element Modeling.

Input program is utilized mainly to constitute a new model. In this process, initial and constitutional steps follow each other: The geometry of the new model

is drawn precisely. Horizontal and vertical fixities of the model, properties of the foundation material and soil layer material are defined in detail. Interface lines are assigned between foundation and soil. To maximize the ultimate bearable load, the surface load is placed on upper surface of the foundation. After introducing general information regarding the model, the mesh generation is carried out to divide the model cross section into triangular elements. The meshing process can be performed with two kinds of triangular elements: 15-node elements and 6-node elements. 15-node element involves more stress points than 6-node element has. Hence, to conduct more accurate calculation of stresses and ultimate loads, 15-node elements must be opted for mesh generation. After the generation of the model, finite element calculations are conducted.

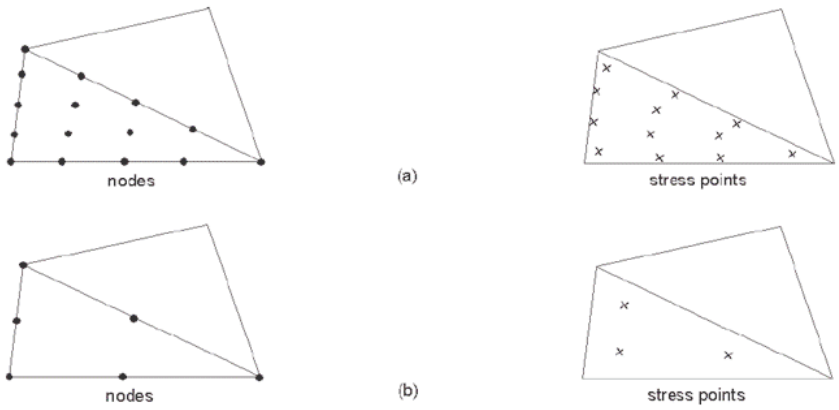

Figure 3.1. (a) 15-Node Triangular Element, (b) 6-Node Triangular Element (PLAXIS TUTORIAL MANUAL).

PLAXIS Calculation program provide four types of calculation which are a plastic calculation, a consolidation calculation, Phi-c reduction analysis and a dynamic calculation. Calculation types are defined as phases for every construction stage, such as the activation of surface loads, the calculation of a safety factor. In addition, each phase of calculations is divided into additional calculation steps due to the non-linear behavior of the soil. The calculation will continue until the number of additional steps has been applied. During calculations, the equilibrium errors are decreased using iterations in each load step (Plaxis Reference Manual).

At calculation process of the models for the study, a plastic calculation type and a safety analysis type were used to perform analyses. The former type enables to carry out an elastic-plastic deformation analyses. Using the undrained option which can be selected in soil material sets, the plastic calculation can be used to set limits for undrained behavior of soil owing to the quick loading of saturated clayey soils (Plaxis Reference Manual). Phi-c reduction (Safety analysis) is executed to calculate a safety factor by reducing strength parameters of soil until a failure occurs. Therefore, this calculation way always ends culminated with the failure.

Output program presents a state of the model in case of visual interpretation for each calculation step. Failure mechanisms occurring are shown visually by using this program. Additionally, Curves program generates the load-displacement curves to indicate the non-linear behavior of the soil.

3.2. Numerical Model

As previously mentioned, the main objective of the thesis is to develop charts for computing undrained seismic bearing capacity factor for strip foundations located on horizontal ground or sloping ground. For this objective, under plain strain conditions, the strip foundation was defined both on the edge of the slope and near the slope in PLAXIS. The foundation had a dimension of 2 m width, B. In order to demonstrate the influence of the slope angle variation, different slope angles were selected; for β, 0^o, 5^o, 15^o, 30^o, 45^o, 60^o and 75^o. Furthermore, different slope heights were also selected; for H, 2 m, 4 m and 8 m. The geometry of the model was generated according to certain geometric dimensions pattern, as shown in Figure 3.2.

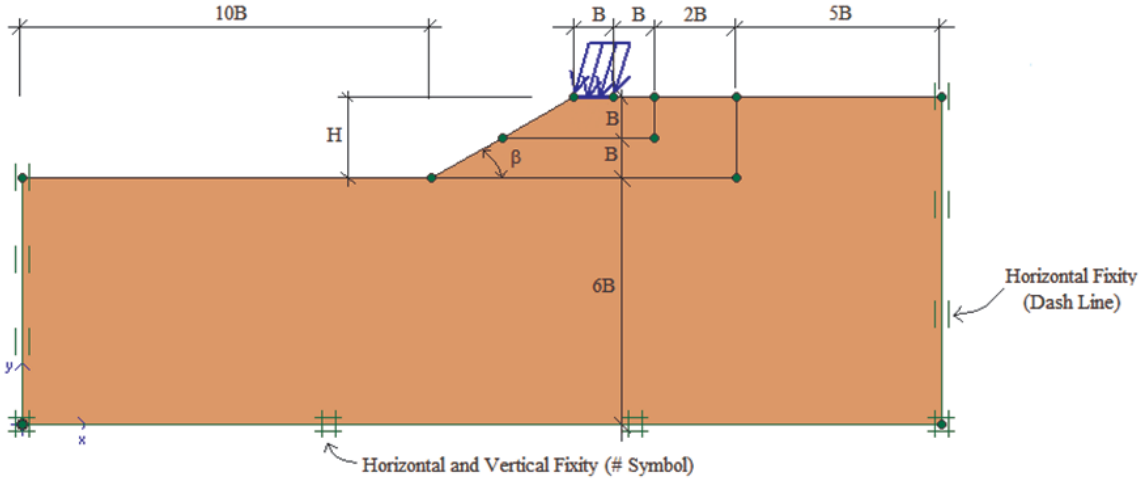

Figure 3.2. Geometry of the Model.

In order to define necessary soil materials; isotropic, homogeneous and purely cohesive soil which has several consistency characteristics was only preferred. Mohr-Coulomb failure criteria defined in terms of cohesion and angle of friction; were opted for the strength characteristic of the soil, because this model is widely utilized for solving foundation problems. Due to the necessity of working in total stress terms for undrained conditions, total stress elastic properties of the soil (E_u and v_u) were used in the analyses. The purpose of defining various material sets was to ascertain the effects of soil having various strength (c_u) and stiffness (E_u) parameters under undrained conditions. Properties of the soil material sets defined in PLAXIS were stated in Table 3.1. The footing is a rigid rough strip footing. The footing was considered weightless with 1m thickness. Flexural rigidity, normal stiffness and thickness of the strip footing were shown in Table 3.1.

Table 3.1. Properties of the Soil Material Sets.

Consistency	Soft	Medium	Stiff	Hard
Undrained Young's Modulus, E_u (Mpa)	5	10	20	40
Undrained Strength, c_u (kPa)	25	50	100	200
Angle of Friction, $\phi(^o)$	0			
Poisson Ratio, ν_u	0.5			
Angle of Dilatancy, $\psi(^o)$	0			
Unit weight of soil, γ_{sat} (kN/m^3)	20			

Table 3.2. Footing Properties.

Axial stiffness, EA	30000000 kN/m
Bending stiffness, EI	2500000 kN.m^2/m
Equivalent depth, d	1m
Unit weight, w	0 kN/m/m
Poisson Ratio, ν	0.2

The horizontal seismic acceleration coefficient was solely defined on the models for seismic conditions. In addition, a distributed load placed on the foundation is implemented with a horizontal component to activate seismic effects. Horizontal seismic acceleration coefficients were presented on Table 3.3.

Table 3.3. Horizontal Seismic Acceleration Coefficients.

k_h
0.1
0.2
0.3
0.4

In order to perform finite element calculations, the model was divided into finite number of elements. To attain more reliable results, 15-node triangular elements were

selected to generate a finite element mesh. The soil layer was separated into three zones according to density of finite elements. The densest mesh zone (very fine mesh zone) was located under the foundation and surrounded along the foundation-soil interfaces and the edge of the slope for more accurate results. The density of meshing decreased with distance from the foundation.

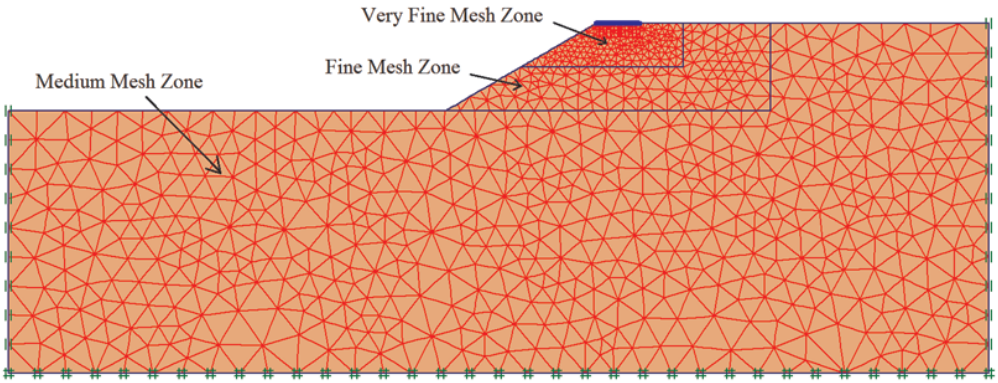

Figure 3.3. Finite Element Mesh.

3.3. Design Procedure

Design Procedure consisted of three stages which were respectively the assessment of a stability number for the slope, the calculation of undrained seismic bearing capacity of the strip foundation, and the determination of the maximum horizontal seismic acceleration endured by the model.

3.3.1. Stability Number (N_s) for Cohesive Slopes

Taylor (1937) developed the stability number as a pure number, depending solely on the slope angle β and friction angle ϕ. Stability number is used to distinguish whether the slope is stable or unstable. For specifying a stability number for the slope, the slope height, the unit weight of soil and the undrained shear strength of soil must

be determined for the stability number formula is given as:

$$N_s = \frac{\gamma H}{c_u} \tag{3.1}$$

Koppula (1984) developed Taylor's stability number concept in Figure 3.4 and Figure 3.5. The stability of the slope as calculated from Equation 3.1 is checked using the N_s graphs given in Figure 3.4 and Figure 3.5. Dept factor is symbolized as D in Figure 3.3. Accordingly, if the value of the calculated stability number is above the corresponding stability number line on the graph, the slope is not stable. If the value of the stability number is below the line, the slope is stable and the calculation of the bearing capacity then can be conducted.

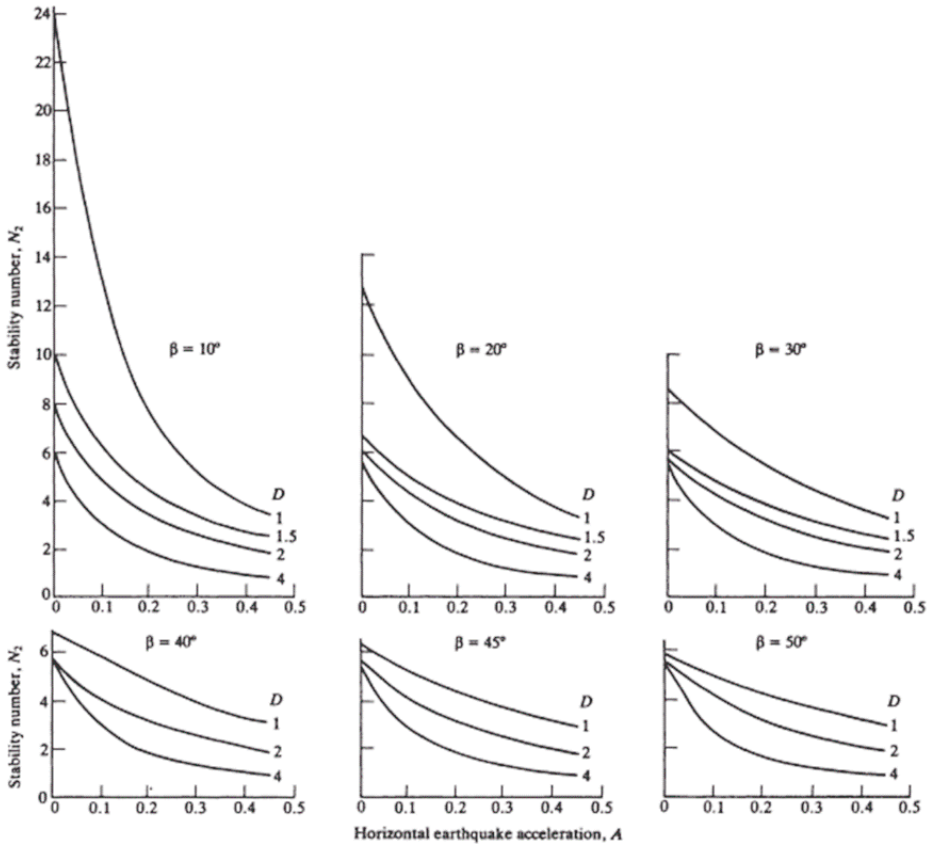

Figure 3.4. Stability Number Versus Horizontal Earthquake Acceleration (Koppula, 1984).

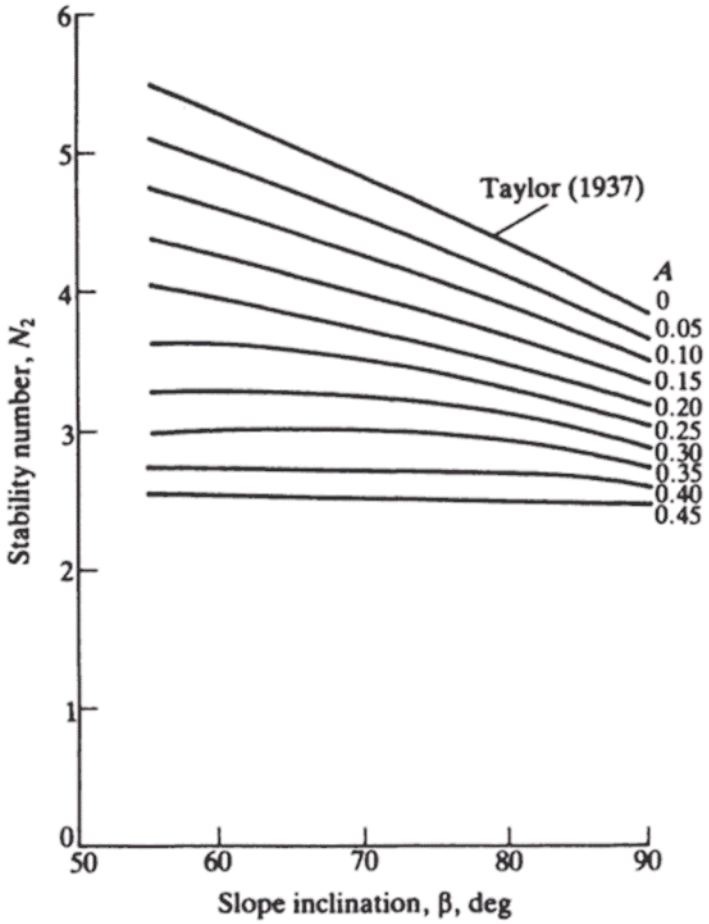

Figure 3.5. Stability Number Versus Slope Inclination (Koppula, 1984).

The horizontal seismic acceleration coefficient has greater impact on the stability number, because stability number lines noticeably fall down under increasing seismic conditions. This inverse relationship derives mainly from that the slope stability is negatively affected under the earthquake impact due to occurring horizontal body forces.

3.3.2. Seismic Bearing Capacity of Strip Foundations

At the calculation stage, according to the four material sets defined and different slope geometries, a great number of models were constituted in PLAXIS. Then, the seismic bearing capacity calculations were conducted for all models. After calculations, seismic bearing capacity values were obtained from PLAXIS calculations. Using bear-

ing capacity values computed, the bearing capacity factors (N_{cse}) were calculated for all models. Depending on N_{cse} values, all horizontal acceleration coefficients and slope angles defined with ratios of H/B, $C_u/\gamma B$ and λ; N_{cse} - β graphs were developed by the values of the parameters plotted. Therefore, the relationships between N_{cse} and all variables could be explained and clarified with these developed graphs.

The seismic bearing capacity of the foundation ($_{qult,se}$) is determined for purely cohesive soils in Equation 3.2. In order to utilize the equation, an appropriate seismic bearing capacity factor (N_{cse}) must be taken from N_{cse} graphs developed.

$$\mathrm{q_{ult,se}} = \mathrm{N_{cse}}.\mathrm{c_u} \tag{3.2}$$

Using N_{cse} - β graphs, N_{cse} value can be determined easily and properly. Then, eventually seismic bearing capacity of the strip foundation (q_{ult}) can be computed.

3.3.3. The Maximum Horizontal Seismic Coefficient ($\mathbf{k}_{hMAX}$)

In case of seismic conditions, the consideration of the bearing capacity of the strip foundation located on the slope was considered as a pseudo-static problem. In the pseudo-static approach, influence of pseudo-static horizontal acceleration on the foundation and soil body should be considered. The goal is to identify the maximum permissible limit of horizontal acceleration that will correspond to the ultimate state of the foundation-soil couple. This is achieved by varying all the variables for different magnitudes of pseudo-static horizontal acceleration values. Magnitudes of bearing capacity have been obtained for many different combinations of k_h, c_u, β, H, and λ. The results were presented in a graphical format.

4. EVALUATION OF PLAXIS ANALYSES RESULTS

In this chapter, the numerical results of the undrained seismic bearing capacity analyses for the strip foundation were presented. Likewise, each relationship between the seismic bearing capacity factor (N_{cse}) and other all variables were plotted on graphs with necessary inferences. In order to illustrate the design procedure, three different design examples were presented and solved in detail. Finally, typical failure mechanism types observed in PLAXIS Output Program were visually indicated and the differences among all failure types were discussed in detail.

All analyses performed in PLAXIS were named systematically: For example "C-30-4-0-25-0,2", the first capital letter means that the soil material type which was the cohesive soil, the second number is the slope angle (β^o), the third number is the slope height (H), the fourth number is the distance between the footing and the slope edge (λ), the fifth number is the undrained strength (c_u), the last number is the horizontal seismic coefficient (k_h).

4.1. Relationship between Ncse and $\beta(^o)$

In order to calculate the seismic bearing capacity of the strip foundation on sloping land, it is necessary to determine an appropriate bearing capacity factor (N_{cse}). According to the numerical results of the seismic bearing capacity for PLAXIS analyses; N_{cse} - β graphs were developed for the ratios of $C_u/\gamma B$, H/B and λ. Then, N_{cse} - β graphs were formulated mathematically. As shown below the each N_{cse} - β graph, every coefficients of each equation are close values. For this reason, all equations of N_{cse} - β graphs were averaged mathematically.

Bearing capacity factor (N_{cse}) versus slope angle (β)relationships are dependent on the value of horizontal seismic coefficient. Figure 4.1, Figure 4.2 and Figure 4.3 show these relationships for the combinations that are stable.

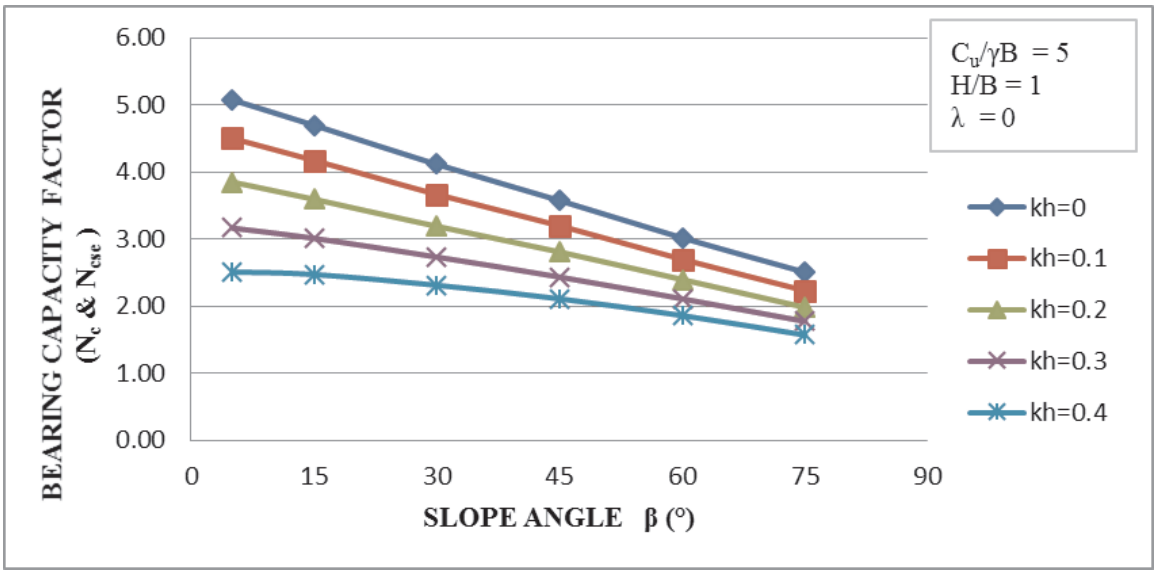

Figure 4.1. Variation of Bearing Capacity Factor with Slope Angle for $C_u/\gamma B = 5$ and H/B=1.

$$N_{c,se} = (0.0612k_h - 0.0377)\,\beta + \left(-6.642k_h + N_{c,se(\beta=0°)}\right) \tag{4.1}$$

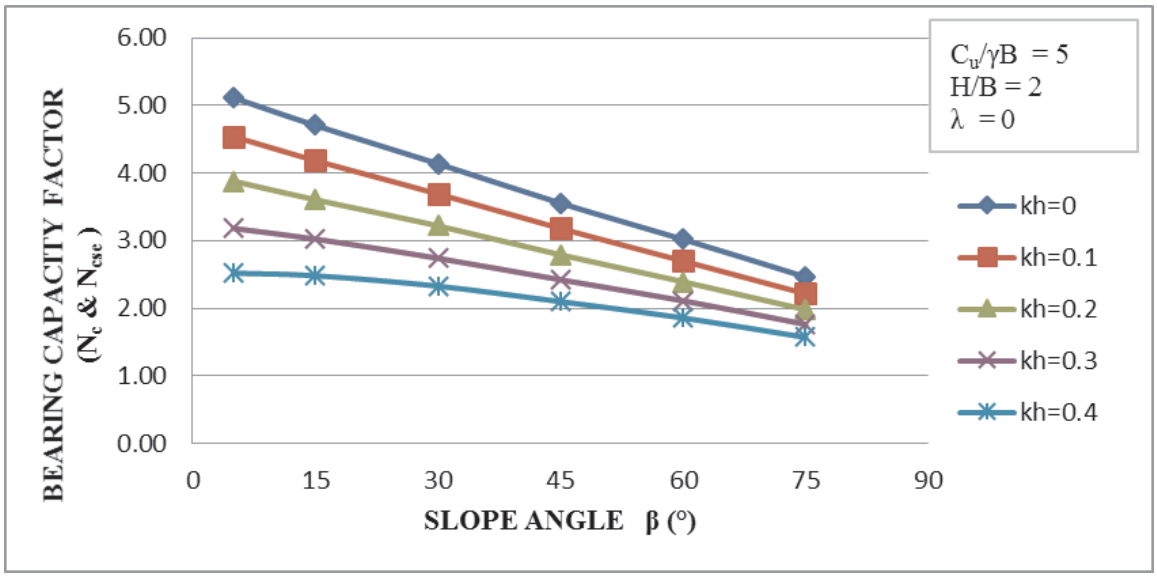

Figure 4.2. Variation of Bearing Capacity Factor With Slope Angle for $C_u/\gamma B = 5$ and H/B=2.

$$N_{c,se} = (0.0626k_h - 0.0384)\,\beta + \left(-6.6844k_h + N_{c,se(\beta=0^\circ)}\right) \tag{4.2}$$

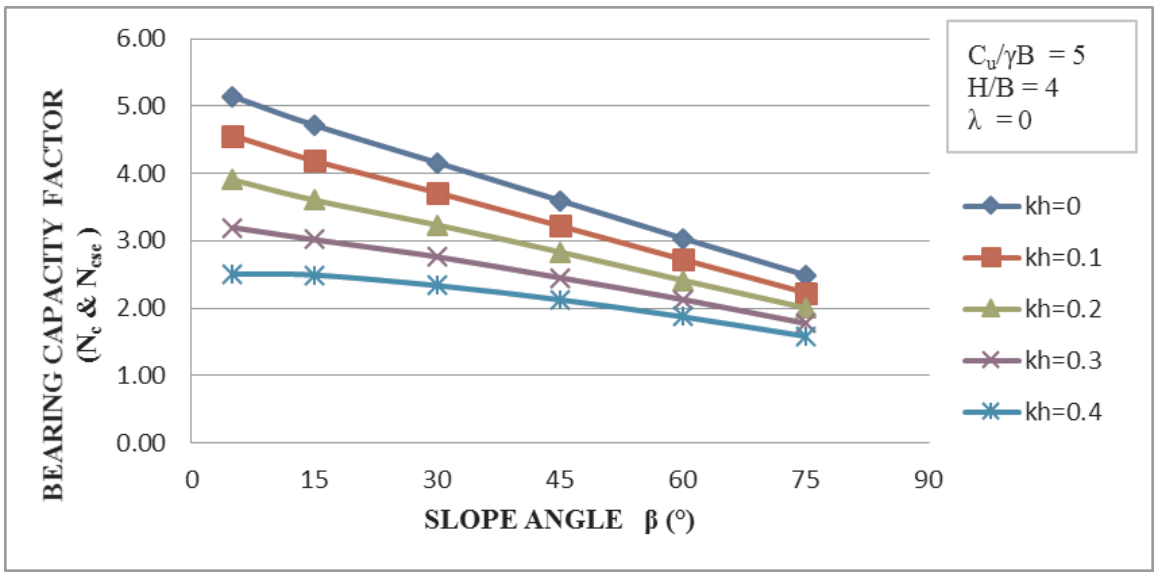

Figure 4.3. Variation of Bearing Capacity Factor With Slope Angle for $C_u/\gamma B = 5$ and H/B=4.

$$N_{c,se} = (0.0626k_h - 0.0381)\,\beta + \left(-6.7172k_h + N_{c,se(\beta=0^\circ)}\right) \tag{4.3}$$

Considering $C_u/\gamma B$= 2.5, bearing capacity factor (N_{cse}) was related to the slope angle (β)for the increase in the horizontal seismic coefficients. Figure 4.4, Figure 4.5 and Figure 4.6 represents an inverse relationship between N_{cse} and β for k_h. While the slope angle increases, bearing capacity factor value falls down. Apart from this relation, the increase in horizontal seismic acceleration causes to the decrease in bearing capacity factor value. The effect of H/B on seismic bearing capacity factor for $c_u/\gamma B$ =2.5 is ignored, due to the sameness of all k_h lines for these figures.

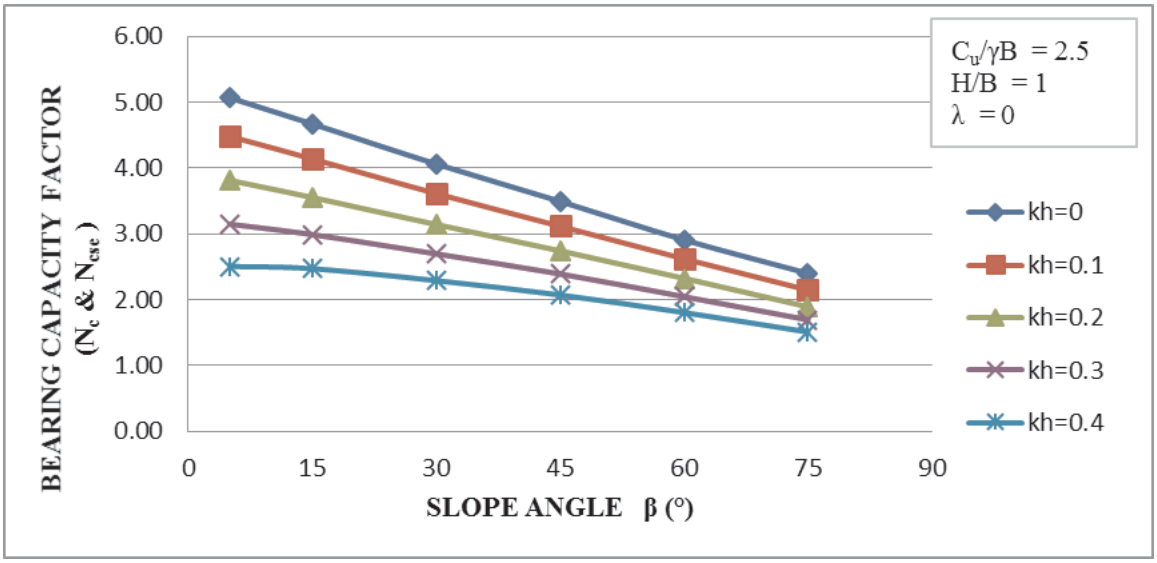

Figure 4.4. Variation of Bearing Capacity Factor With Slope Angle for $C_u/\gamma B$= 2.5 and H/B=1.

$$N_{c,se} = (0.0637k_h - 0.0394)\,\beta + \left(-6.6682k_h + N_{c,se(\beta=0°)}\right) \tag{4.4}$$

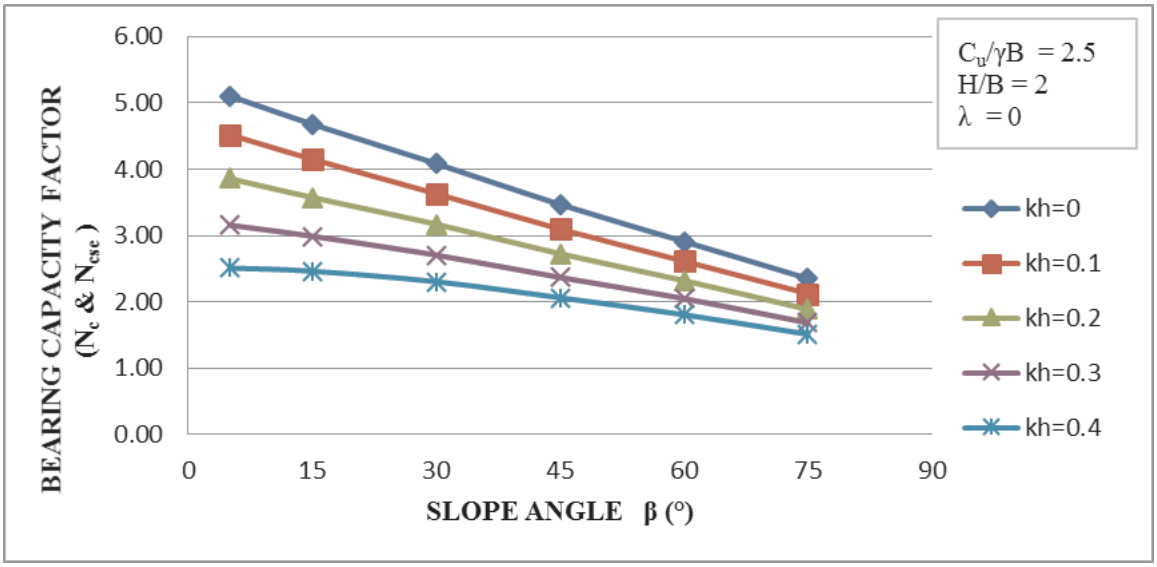

Figure 4.5. Variation of Bearing Capacity Factor With Slope Angle for $C_u/\gamma B$= 2.5 and H/B=2.

$$N_{c,se} = (0.0645k_h - 0.0397)\,\beta + \left(-6.6674k_h + N_{c,se(\beta=0^\circ)}\right) \tag{4.5}$$

In Figure 4.6, the model failed to reach the ultimate seismic bearing capacity value for k_h=0.4 and β= 5^o, because the stability number did not satisfy the stability of the slope. For this reason, there is no point plotted in that case.

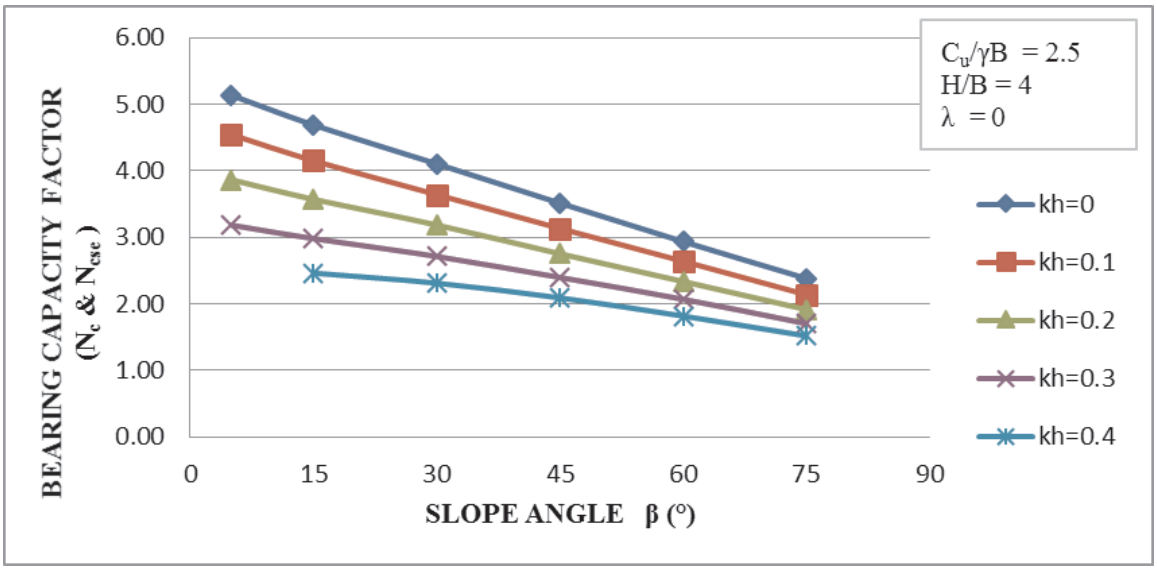

Figure 4.6. Variation of Bearing Capacity Factor With Slope Angle for $C_u/\gamma B$= 2.5 and H/B=4.

$$N_{c,se} = (0.0637k_h - 0.0394)\,\beta + \left(-6.6682k_h + N_{c,se(\beta=0^\circ)}\right) \tag{4.6}$$

For $C_u/\gamma B$= 1.25, the relationship between bearing capacity factor (N_{cse}) and the slope angle (β) for the horizontal seismic coefficient (k_h) was given in Figure 4.7, Figure 4.8 and Figure 4.9. There are no different characteristics of these figures with previous figures for $C_u/\gamma B$= 2.5 and $C_u/\gamma B$= 5. However, in Figure 4.7 the model failed to reach the ultimate seismic bearing capacity value for k_h= 0.4 and for all slope

angles. Therefore, N_{cse} line for k_h= 0.4 couldn't be drawn. Similar failings were found for k_h= 0.3, 0.4 in Figure 4.8 and for k_h= 0.2, 0.3, 0.4 Figure 4.9.

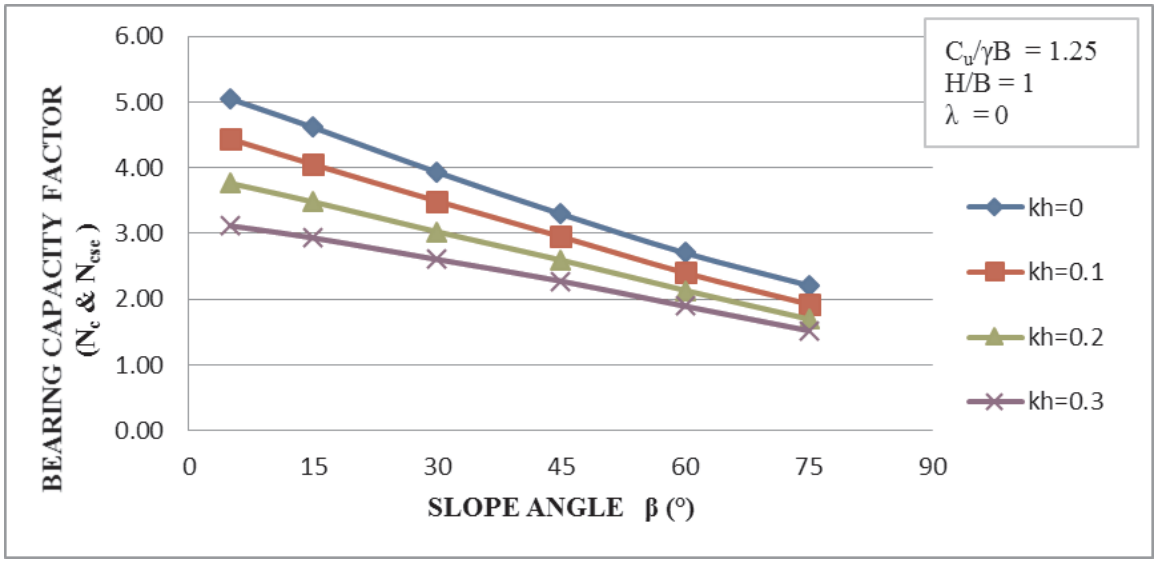

Figure 4.7. Variation of Bearing Capacity Factor With Slope Angle for $C_u/\gamma B$= 1.25 and H/B=1.

$$N_{c,se} = (0.0631k_h - 0.0417)\,\beta + \left(-6.6153k_h + N_{c,se(\beta=0°)}\right) \tag{4.7}$$

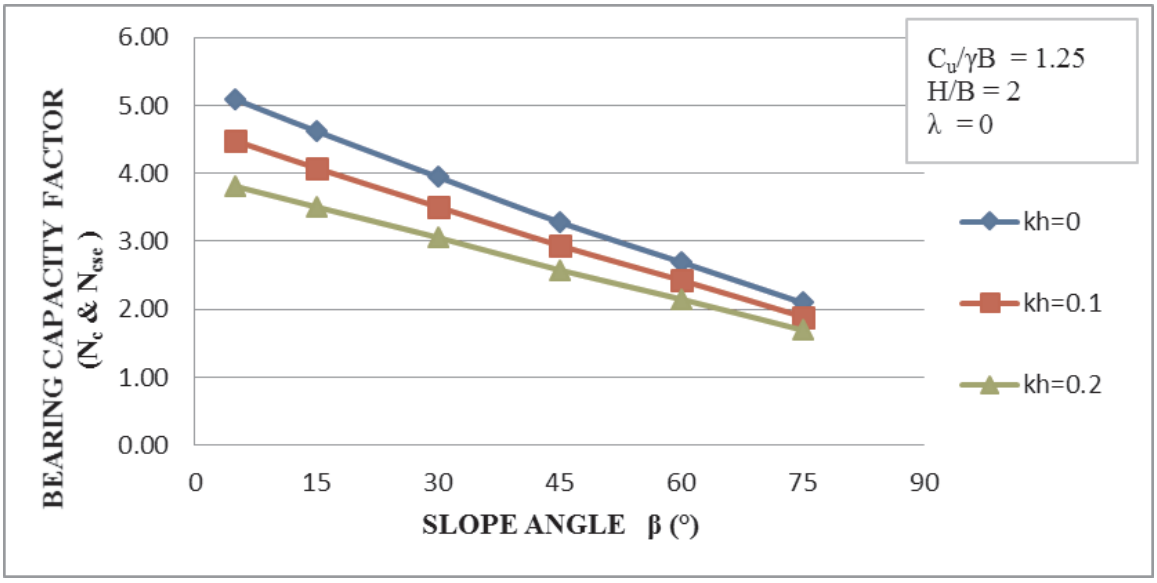

Figure 4.8. Variation of Bearing Capacity Factor With Slope Angle for $C_u/\gamma B$= 1.25 and H/B=2.

$$N_{c,se} = (0.064k_h - 0.0427)\,\beta + \left(-6.573k_h + N_{c,se(\beta=0°)}\right) \tag{4.8}$$

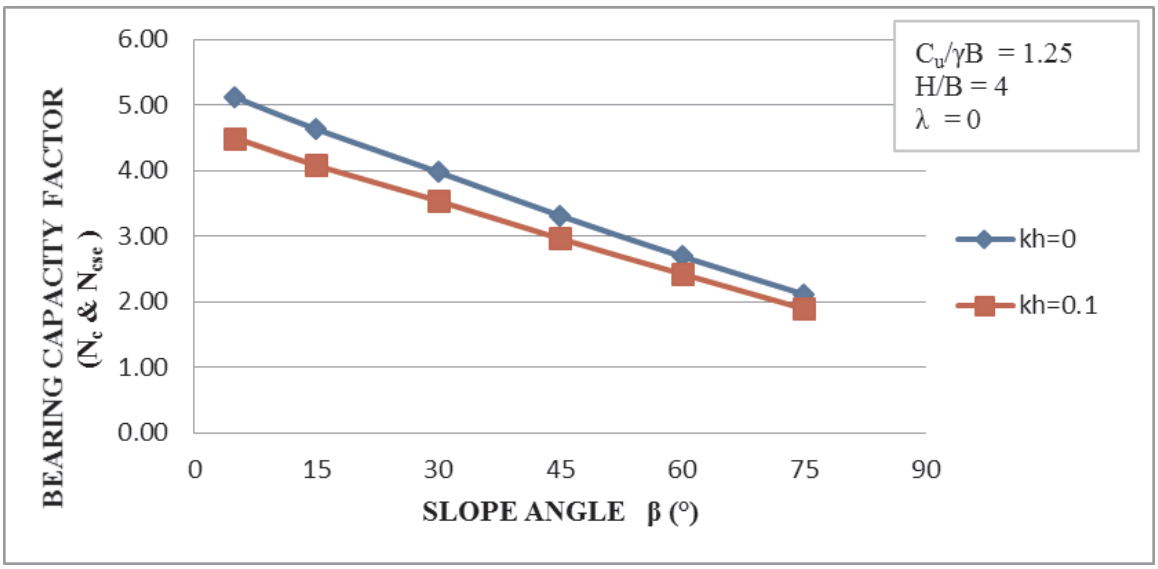

Figure 4.9. Variation of Bearing Capacity Factor With Slope Angle for $C_u/\gamma B$= 1.25 and H/B=4.

$$N_{c,se} = (0.058k_h - 0.0425)\,\beta + \left(-6.307k_h + N_{c,se(\beta=0^\circ)}\right) \tag{4.9}$$

For $C_u/\gamma B$= 0.625, the relationship between bearing capacity factor (N_{cse}) and the slope angle (β)for the horizontal seismic coefficient (k_h) was given in Figure 4.10 and Figure 4.11. There are no different characteristics of these figures with previous figures for $C_u/\gamma B$=1.25, $C_u/\gamma B$= 2.5 and $C_u/\gamma B$= 5. However, the model failed to reach the ultimate seismic bearing capacity value for all models which had H/B=4 ratio. Therefore, N_{cse} - β graph for $C_u/\gamma B$= 0.625 and H/B=4 couldn't be generated.

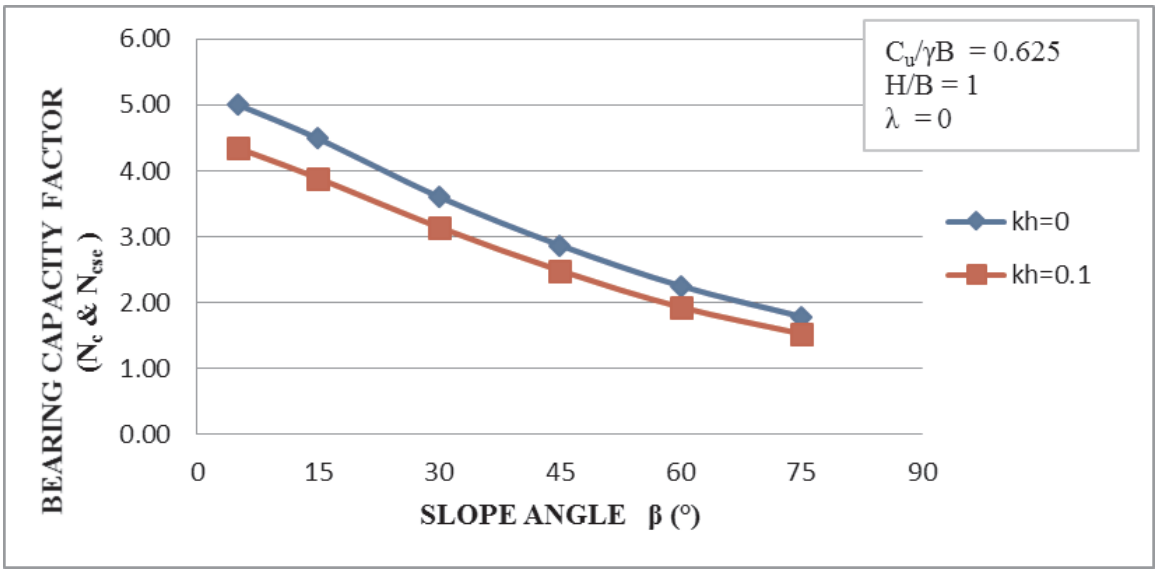

Figure 4.10. Variation of Bearing Capacity Factor With Slope Angle for $C_u/\gamma B$= 0.625 and H/B=1.

$$N_{c,se} = (0.06k_h - 0.0475)\,\beta + \left(-6.8k_h + N_{c,se(\beta=0^\circ)}\right) \tag{4.10}$$

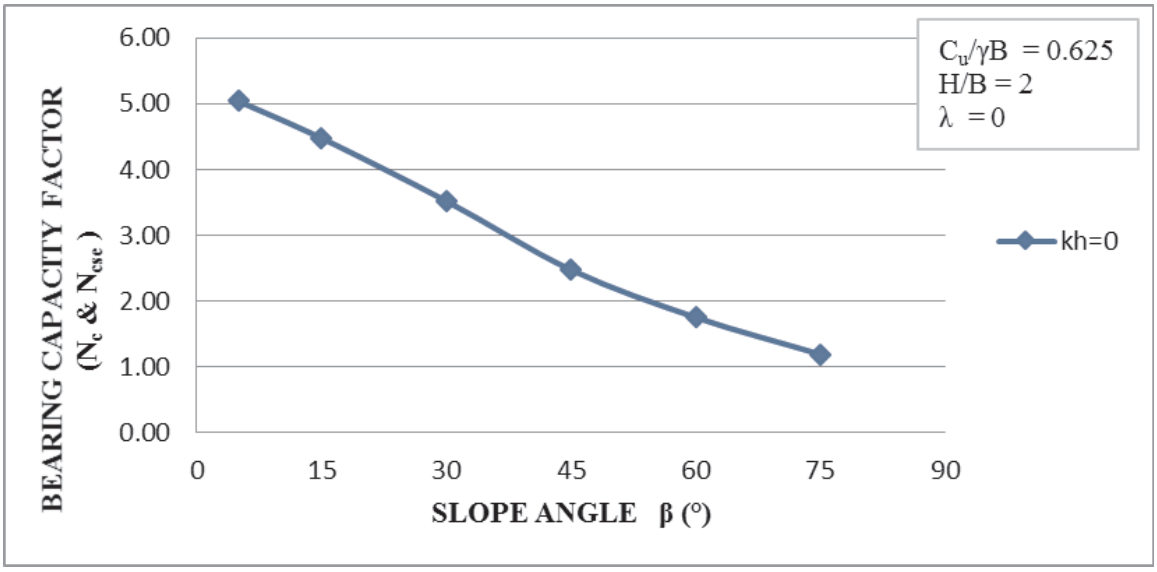

Figure 4.11. Variation of Bearing Capacity Factor With Slope Angle for $C_u/\gamma B$= 0.625 and H/B=2.

$$N_{c,se} = -0.0565\beta + N_{c,se(\beta=0^\circ)} \tag{4.11}$$

In order to calculate the seismic bearing capacity factor, N_{cse} for any situation that can be given; all equations of N_{cse} - β graphs were averaged mathematically and Equation 4.12 was obtained as the ultimate design equation.

$$N_{c,se} = (0.0566k_h - 0.0421)\,\beta + \left(-6.0317k_h + N_{c,se(\beta=0^\circ)}\right) \tag{4.12}$$

4.2. Design Examples

Three different design examples were presented and solved in detail to exemplify the use of the equations developed.

4.2.1. Design Example I

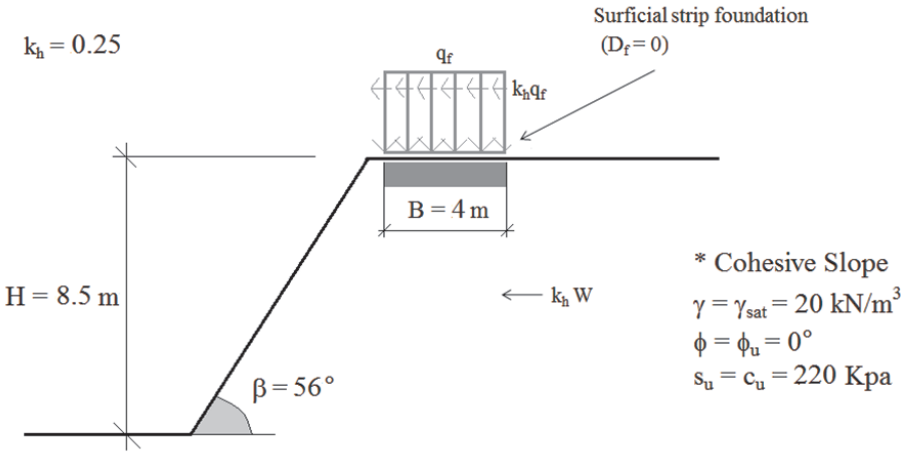

Figure 4.12. Design Example I.

In order to solve the problem given, stability number (N_s) is firstly calculated to check the stability of the slope. For this purpose, Equation 3.1 is utilized for the stability number calculation.

$$N_S = \frac{\gamma H}{c_u} = \frac{20x8.5}{220} = 0.77 \tag{4.13}$$

To determine the necessary stability number line for k_h= 0.25; N_s - β graph based on Taylor's and Koppula's analysis for $\beta \geq 55^o$ is utilized.

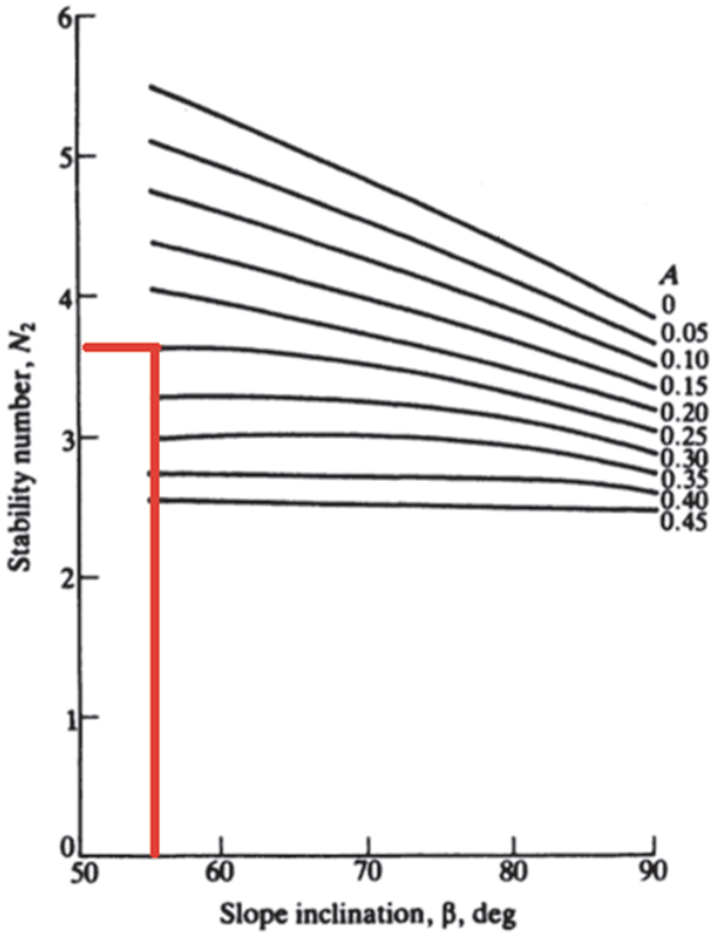

Figure 4.13. Stability Number Versus Slope İnclination (Koppula, 1984).

$$N_{SMAX} = 3.7 \tag{4.14}$$

$$N_S \leq N_{SMAX} \tag{4.15}$$

Therefore, the slope is stable and capable of bearing the ultimate seismic load.

At the second stage, N_{cse} was obtained for β= 56^o and k_h= 0.25 by using Equation

4.12.

$$N_{c,se} = ((0.0566x0.25) - 0.0421)\,x56) + \left((-6.0317x0.25) + N_{c,se(\beta=0°)}\right)$$
$$N_{c,se} = 2.06 \tag{4.16}$$

The undrained seismic bearing capacity of the surficial strip foundation was calculated by using Equation 3.2.

$$q_{ult,se} = 220x2.06 = 453.2kN/m^2 \tag{4.17}$$

4.2.2. Design Example II

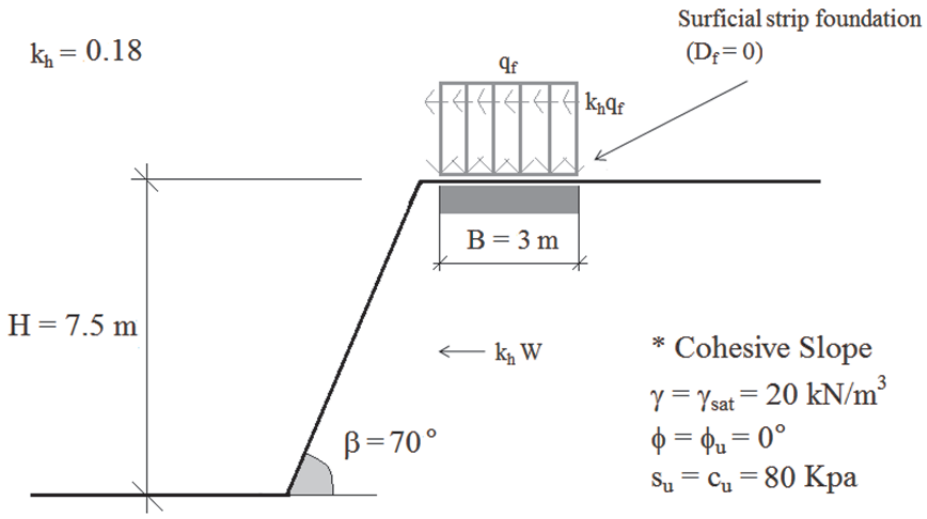

Figure 4.14. Design Example II.

In order to solve the problem given, stability number (N_s) is firstly calculated to check the stability of the slope. For this purpose, Equation 3.1 is utilized for the stability number calculation.

$$N_S = \frac{\gamma H}{c_u} = \frac{20x7.5}{80} = 1.875 \tag{4.18}$$

To determine the necessary stability number line for k_h= 0.18; N_s - β graph based on Taylor's and Koppula's analysis for $\beta \geq 55^o$ is utilized.

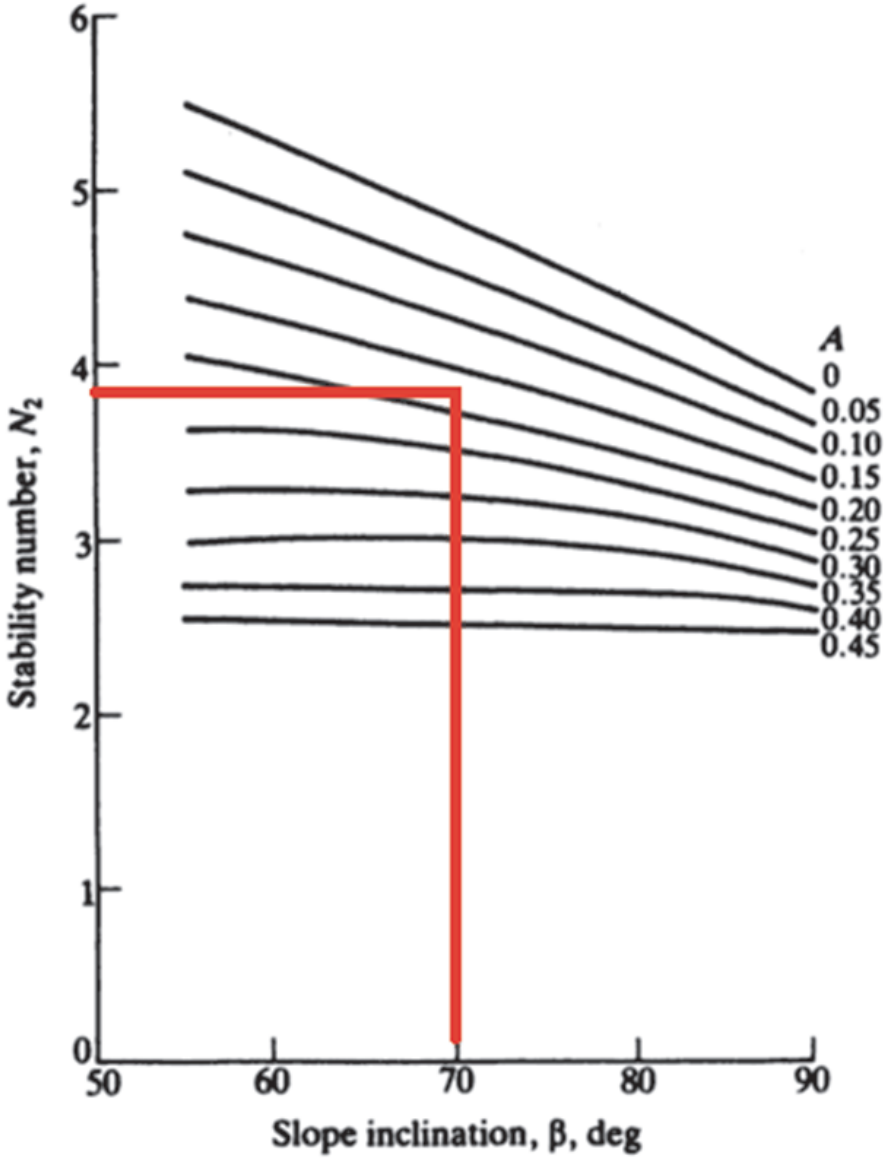

Figure 4.15. Stability Number Versus Slope Inclination (Koppula, 1984).

$$N_{SMAX} = 3.9 \tag{4.19}$$

$$N_S \leq N_{SMAX} \tag{4.20}$$

Therefore, the slope is stable and capable of bearing the ultimate seismic load.
At the second stage, N_{cse} was obtained for β=70^o and k_h= 0.18 by using Equation 4.12.

$$N_{c,se} = ((0.0566x0.18) - 0.0421)\,x70) + \left((-6.0317x0.18) + N_{c,se(\beta=0°)}\right)$$
$$N_{c,se} = 1.82 \tag{4.21}$$

The undrained seismic bearing capacity of the surficial strip foundation was calculated by using Equation 3.2.

$$q_{ult,se} = 80x1.82 = 145.6kN/m^2 \tag{4.22}$$

4.2.3. Design Example III

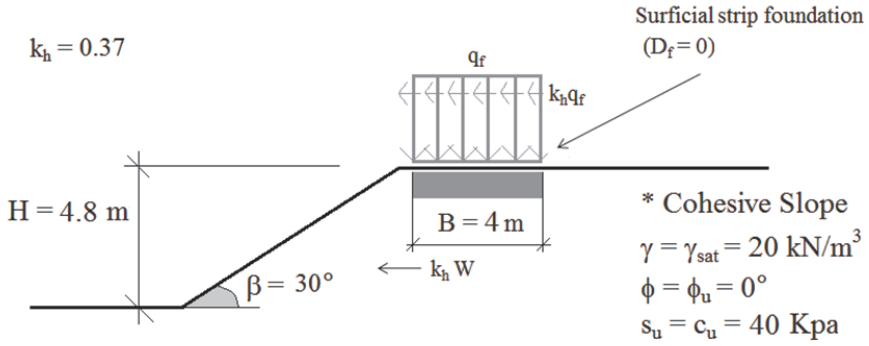

Figure 4.16. Design Example III.

In order to solve the problem given, stability number (N_s) is firstly calculated to check the stability of the slope. For this purpose, Equation 3.1 is utilized for the stability number calculation.

$$N_S = \frac{\gamma H}{c_u} = \frac{20x4.8}{40} = 2.4 \tag{4.23}$$

To determine the necessary stability number line for k_h= 0.37; N_s - k_h graphs based on Koppula's analysis for β= 30^o is utilized. Depth factor is assumed as D = 4.

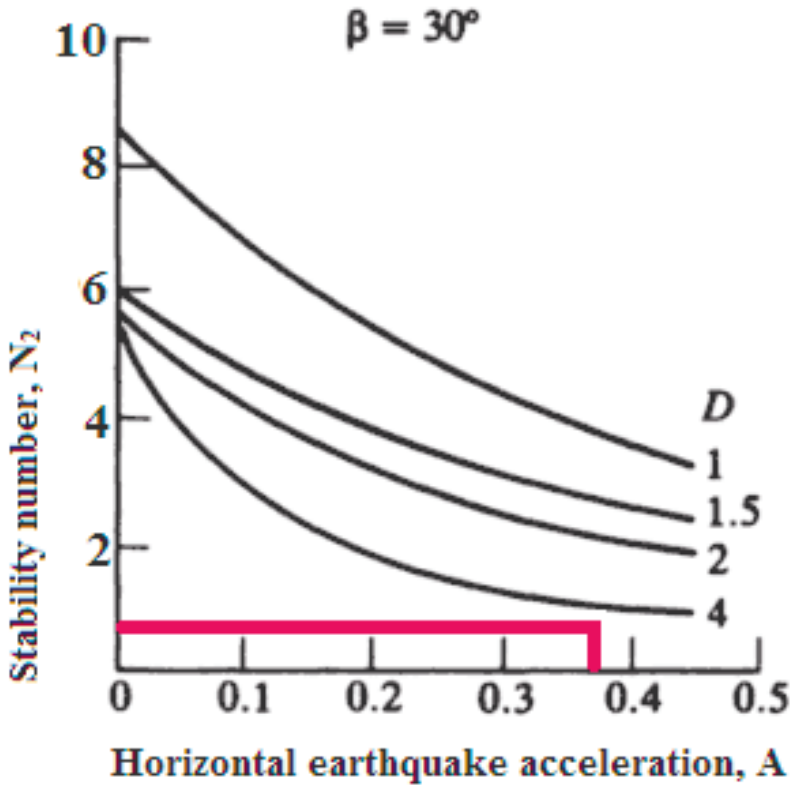

Figure 4.17. Stability Number Versus Horizontal Earthquake Acceleration (Koppula, 1984).

$$N_{SMAX} = 0.9 \tag{4.24}$$

$$N_S > N_{SMAX} \tag{4.25}$$

Therefore, the slope is unstable and not capable of bearing the ultimate seismic load.

4.3. Failure Mechanisms

At the end of analyses, different types of failure mechanisms were observed in PLAXIS Output program. Terzaghi's bearing capacity mechanism was observed in only horizontal ground models, as shown in Figure 4.12. Terzaghi's three zones which are the wedge shaped elastic zone beneath the foundation, the radial shear zones and the passive Rankine zones could be easily recognized. The bearing capacity mechanism without passive zone is generally initial failure type for sloping ground models. When the foundation was located on sloping ground under seismic conditions especially for k_h; 0 and 0.1; Terzaghi's bearing capacity mechanism without the passive Rankine zones occurred, as indicated in Figure 4.13. When this type of mechanism occurs, the slope does not completely fail. In Figure 4.14, Terzaghi's bearing capacity mechanism with the slope failure was observed especially for low slopes. At this type, the foundation failure causes the slope failure from the end of the distributed load to the edge of the slope. In Figure 4.15, overall slope failure occurred when the slope was unstable and not capable of bearing the ultimate seismic load. The fundamental difference between Figure 4.14 and Figure 4.15 is the location of the upper starting point of the failure circle. In Figure 4.15, the slope stars to fail at the far away point from the end of the distributed load. In Figure 4.16, the base failure mechanism was the precursor of deep seated failure mechanism and also an advanced form of Figure 4.14 with the increase in seismic influence. The boundary of the failure mechanism reaches to the firm layer in the deep. Sliding failure mechanism was mainly observed when the horizontal seismic acceleration had seriously higher values than values which could be tolerated by the model. Due to higher horizontal seismic acceleration, the model slides altogether immediately and the failure mechanism zone does not occur clearly, as demonstrated in Figure 4.17. The deep seated was the ultimate failure mechanism occurred for the permissible limit values of horizontal seismic accelerations, in Figure 4.18. In this case; the slope and the foundation seated deeply and also collapsed, because of the profound effect of the earthquake. Likewise, the deep seated mechanism indicates that the load bearing layer is not capable of bearing the ultimate load and also the foundation.

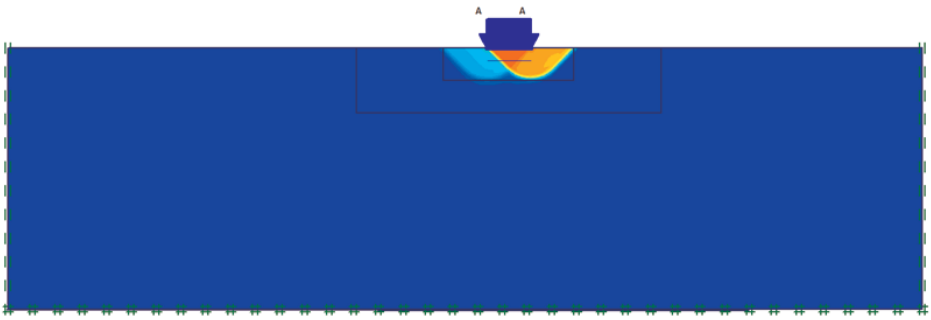

Figure 4.18. Terzaghi's Bearing Capacity Mechanism.

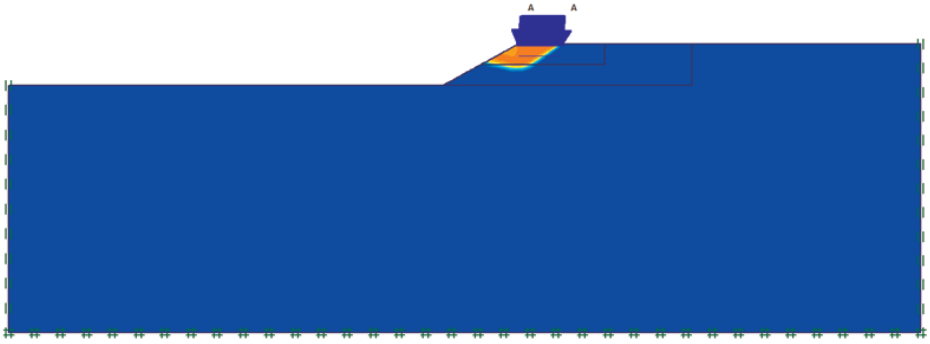

Figure 4.19. Terzaghi's Bearing Capacity Mechanism Without Passive Zone.

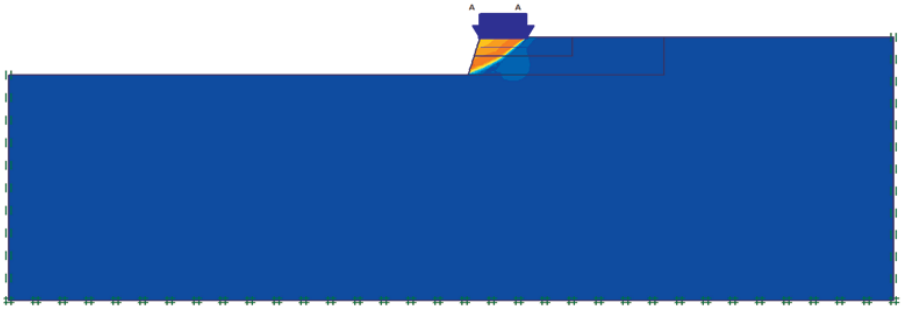

Figure 4.20. Terzaghi's Bearing Capacity Mechanism with Slope Failure.

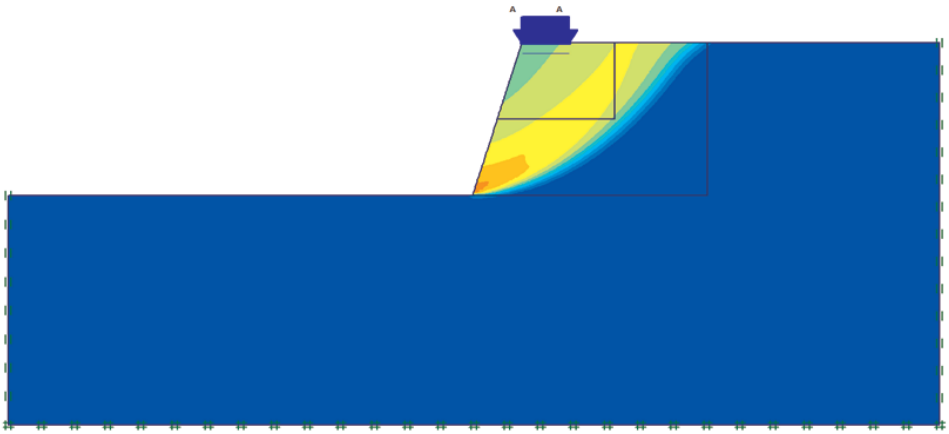

Figure 4.21. Overall Slope Failure.

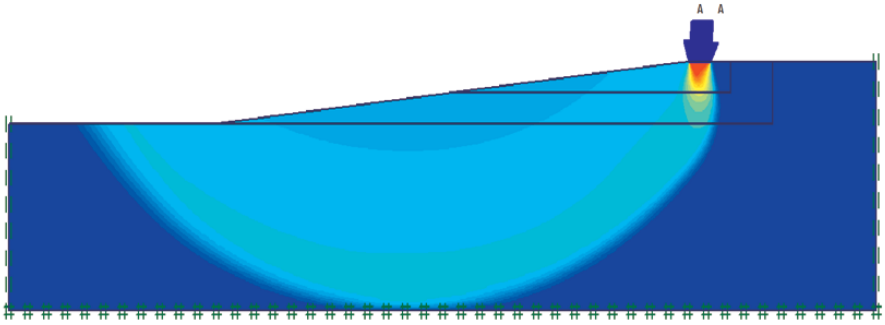

Figure 4.22. Base Failure Mechanism.

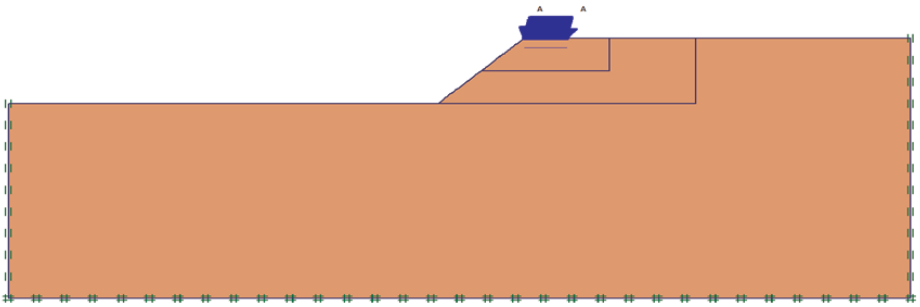

Figure 4.23. Sliding Failure Mechanism.

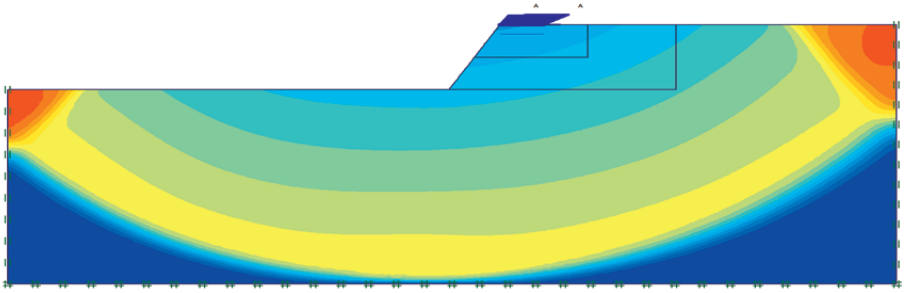

Figure 4.24. Deep Seated Mechanism.

5. DISCUSSION

Hansen (1968) proposed ground inclination factors for the bearing capacity calculation of the shallow foundations on sloping lands. Using Hansen's approach, the bearing capacity factors were determined for the slope angles defined previously, and plotted on the comparison graph. Except for $\beta = 5^o$ points on each line nearly coincided in Figure 5.1.

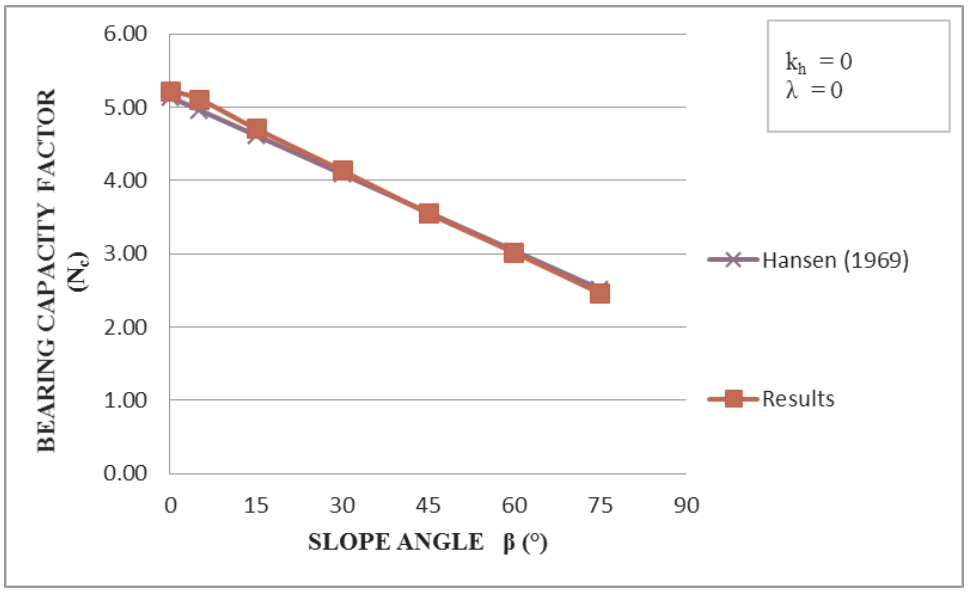

Figure 5.1. Comparison of the Bearing Capacity Factor Values of Hansen's Study and the Analyses Results.

Kusakabe (1981) investigated the bearing capacity of loaded slopes, using the upper bound theorem. Kusakabe's the numerical results of the bearing capacity factor were compared with the numerical results of the bearing capacity factor. As seen in Figure 5.2, the lines are collinear.

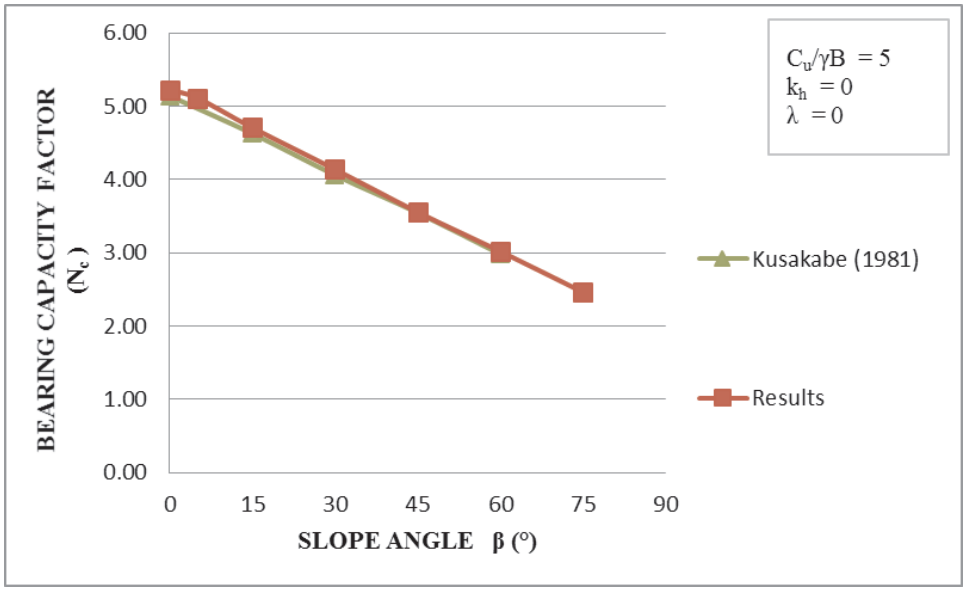

Figure 5.2. Comparison of the Bearing Capacity Factor Values of Kusakabe's Study and the Analyses Results.

Castelli and Motta (2009) developed a model using the limit equilibrium method. They presented convenient design charts as the diagram for ground factors with the distance from the slope edge under undrained conditions. Thus, bearing capacity factors depending on the ground factors for β= 5^o, 15^o, 30^o and D/B=0 were compared with the bearing capacity factors obtained from analyses, as seen in Figure 5.3. The bearing capacity factors for β=15^o were especially coherent each other.

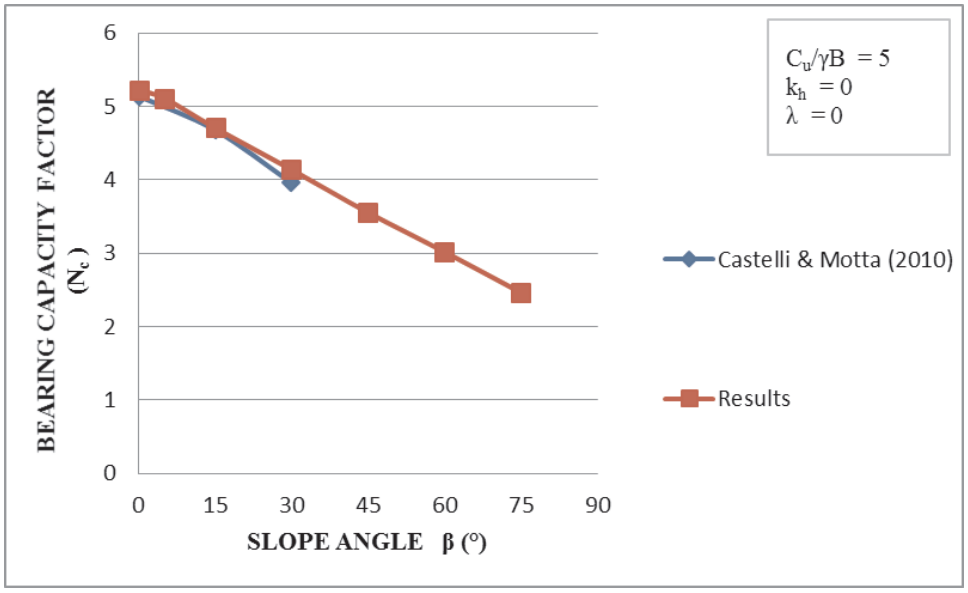

Figure 5.3. Comparison of Bearing Capacity Factor Values Of Castelli's and Motta's Study and the Analyses Results.

Georgiadis (2010) proposed the design charts for the calculation of the undrained static bearing capacity factor by utilizing finite element analyses in Plaxis. Therefore, undrained static bearing capacity factors depending Georgiadis's study were especially opted for the discussion part. According to Figure 5.4, the results of the bearing capacity analyses were consistent with Georgiadis's values.

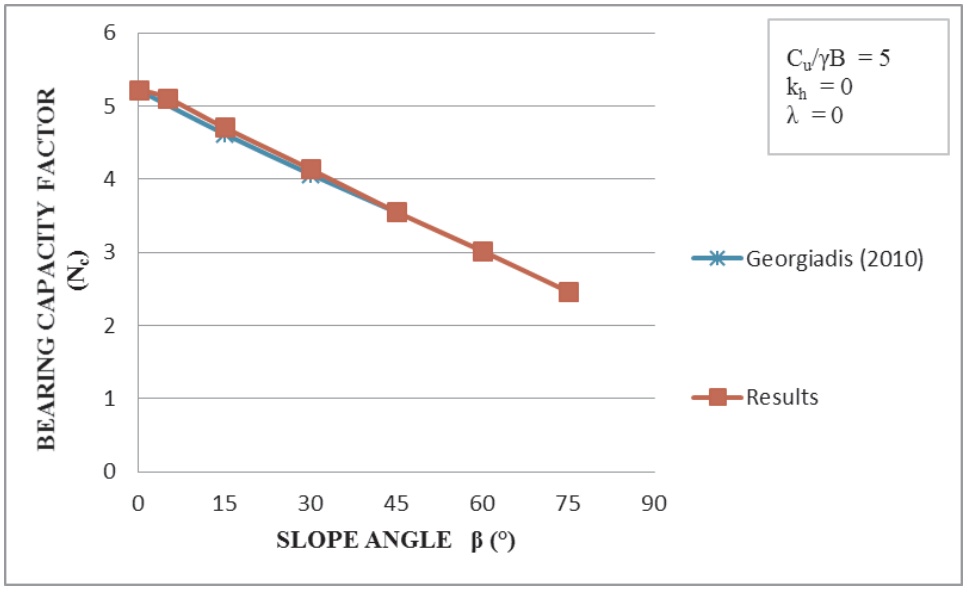

Figure 5.4. Comparison of Bearing Capacity Factor Values of Georgiadis's Study and the Analyses Results.

The analyses were conducted mainly for the calculation of the undrained seismic bearing capacity. For this purpose, results were contrasted with comparable studies in the literature. The results were more coherent Kumar and Ruo (2003) study results than Castelli and Motta (2010) study results. Seismic bearing capacity factor values proposed by Castelli and Motta were slightly small than other studies' values.

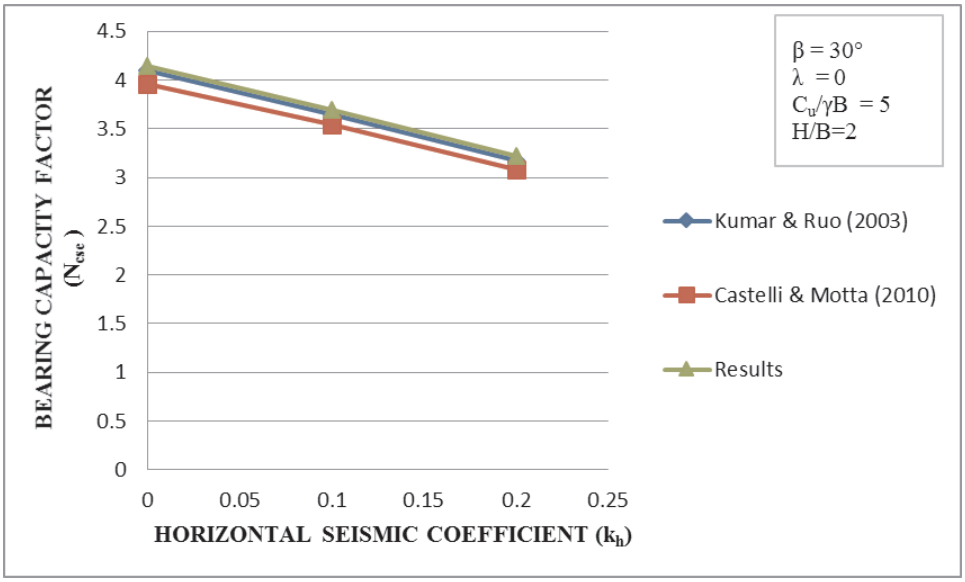

Figure 5.5. Comparison of Seismic Bearing Capacity Factor Values of Studies in the Literature and the Analyses Results.

As seen on the graphs in the previous chapter, while the slope angle is increased, the undrained seismic bearing capacity of the foundation reduces noticeably. Furthermore, the increase in horizontal seismic acceleration coefficient causes the fall in the seismic bearing capacity factor.

In addition, different types of the failure mechanism were observed at end of the analyses. For $C_u/\gamma B$ =0.625 and $\beta \geq = 30^0$, all models especially ended with bearing capacity with slope due to the low cohesion value of the soil. On the other hand, if the higher strength parameters are defined, the observation of sliding failure mechanism was more probable than the other types of mechanisms. Moreover, the deep seated mechanism indicates that the load bearing layer has not capability to bear the ultimate load and the foundation.

According to $k_h MAX$ - β graphs in Appendix A, as the slope angle is increased, the limit horizontal seismic acceleration coefficients increase. For the slopes which consisted of purely cohesive soil, the proneness to collapse decreased and correspondingly an increase in the maximum horizontal seismic acceleration was observed. This is attributed to the decreasing inertial forces at greater slope angles due to the decreases in the mass of the soil body. On the other hand, H/B ratio influences inversely the maximum horizontal seismic acceleration value. In addition, as $C_u/\gamma B$ ratio is increased, maximum horizontal seismic coefficients noticeably increase due to being greater strength characteristic of soil.

6. CONCLUSION

By using Finite Element Method, numerous analyses were performed in PLAXIS to investigate the influence of the various parameters on undrained seismic bearing capacity of surficial strip foundations located on horizontal ground or sloping ground or near sloping ground. Finally, charts indicating the values of maximum horizontal seismic acceleration coefficients for surficial strip foundations were improved to indicate the maximum tolerable boundaries of horizontal seismic acceleration.

(i) In order to calculate the undrained seismic bearing capacity; N_{cse} - β graphs for all horizontal acceleration coefficients and ratios of H/B, $C_u/\gamma B$ were developed.

(ii) The seismic bearing capacity factor, N_{cse} decreases while the slope angle, β increases. Furthermore, the increase in the horizontal seismic acceleration coefficient causes to the fall in the seismic bearing capacity factor, N_{cse}. Likewise, the change in undrained strength, c_u or the slope height, H has no the noticeable influence on the seismic bearing capacity factor.

(iii) It is observed that while the slope angle increases, the maximum horizontal seismic acceleration limit increases. Moreover, the increase in the soil shear strength affects the maximum horizontal seismic acceleration positively. However, the increase in the slope height causes the decrease in the maximum horizontal acceleration limit.

(iv) It is investigated that the relationship among all types of failure mechanisms occurred at end of the analyses. Until the deep seated failure occurred, the horizontal seismic acceleration coefficient reaches to the maximum. The overall slope failure was observed for the slope that was unstable and not capable of bearing the ultimate seismic load. The sliding failure was detected mostly for the analyses with high strength characteristics of soil or under high seismic accelerations. On the other hand, the base failure rarely occurs in the analyses.

APPENDIX A: MAXIMUM HORZONTAL SEISMIC COEFFICIENT (k_{hMAX})

Maximum horizontal seismic acceleration, which the foundation is capable of tolerating, is a significant issue for the seismic bearing capacity notion. For this reason, models previously defined were reanalyzed to determine a limit permissible horizontal seismic acceleration. Thus, the horizontal seismic acceleration coefficient was gradually increased to the maximum value until resulting deep seated failure occurs. In other words, the ultimate analyses were before the seismic horizontal acceleration causing deep seated failure. Consequently, the deep seated failure mechanism is an important indicator to fix the maximum value, because the deep seated failure is the ultimate state. When the deep seated failure mechanism occurs, the slope and the strip foundation seat deeply together and also collapse. However, despite resulting deep seated failure, the values of seismic bearing capacity was obtained for some analyses in Plaxis, but these values obtained were not practically evaluable. The last analysis on each line was marked with its failure mechanism type on Ncse - kh graphs to demonstrate the relationship between the maximum horizontal seismic coefficient and failure mechanism types.

A.1. Relationship between N_{cse} and k_{hMAX} for $C_u/\gamma B$=5

The increase in horizontal seismic acceleration causes obviously the decrease in the seismic bearing capacity. For $C_u/\gamma B$=5, all H/B lines are coincident in Figure A.1, Figure A.2, Figure A.3, Figure A.4, Figure A.5 and Figure A.6. Therefore, the slope height has no influence on the undrained seismic bearing capacity, but affects inversely the maximum horizontal seismic acceleration coefficient.

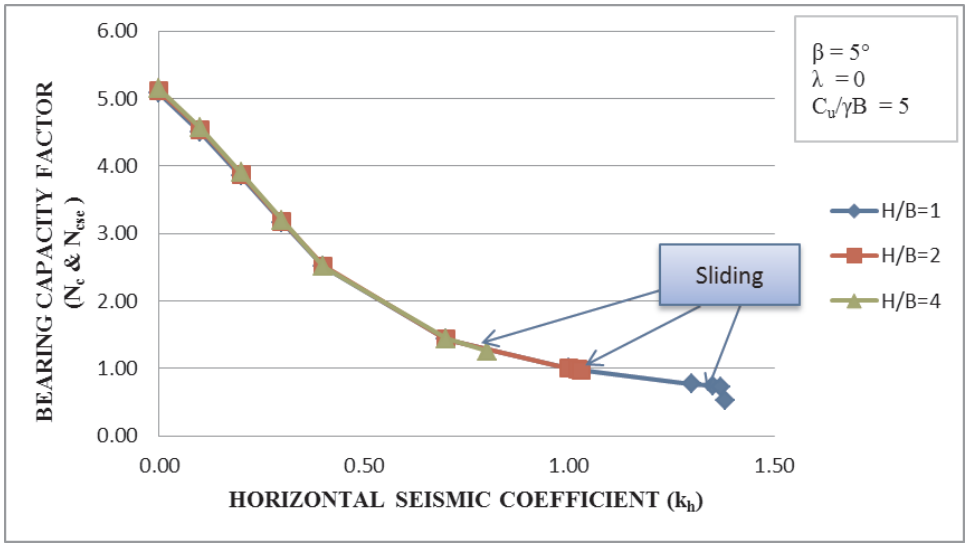

Figure A.1. Variation of Bearing Capacity Factor With Maximum Horizontal Seismic Coefficient for $C_u/\gamma B$=5 and β=5$^{\circ}o$.

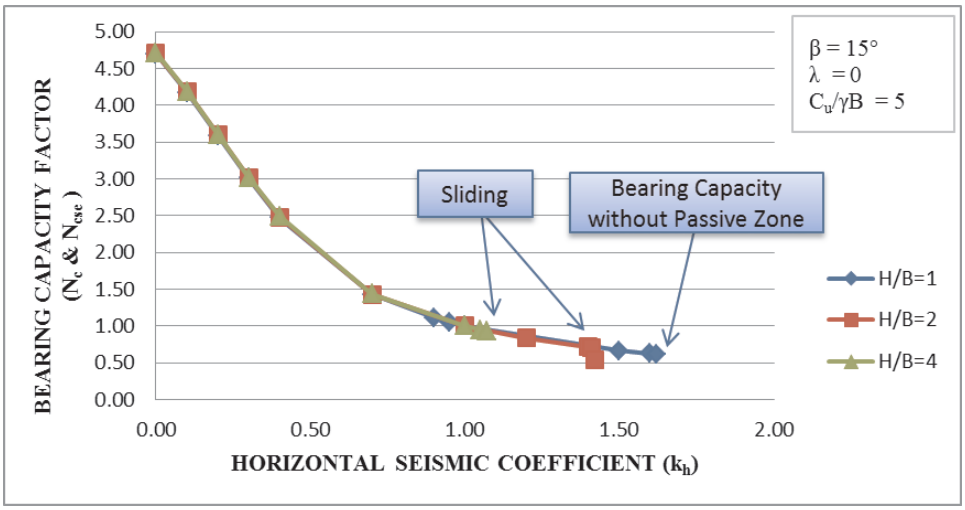

Figure A.2. Variation of Bearing Capacity Factor With Maximum Horizontal Seismic Coefficient for $C_u/\gamma B$=5 and β=15$^{\circ}o$.

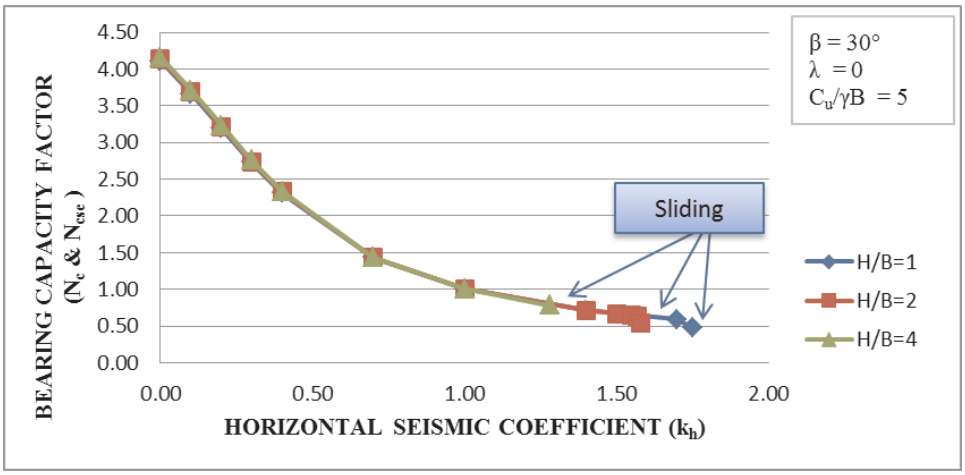

Figure A.3. Variation of Bearing Capacity Factor With Maximum Horizontal Seismic Coefficient for $C_u/\gamma B$=5 and β=30$^{\circ}o$.

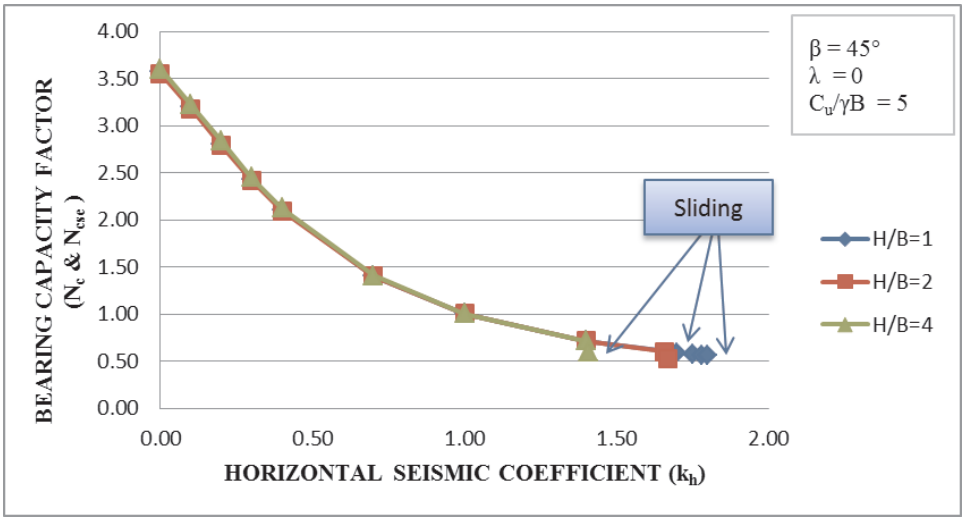

Figure A.4. Variation of Bearing Capacity Factor With Maximum Horizontal Seismic Coefficient for $C_u/\gamma B$=5 and β=45$^{\circ}o$.

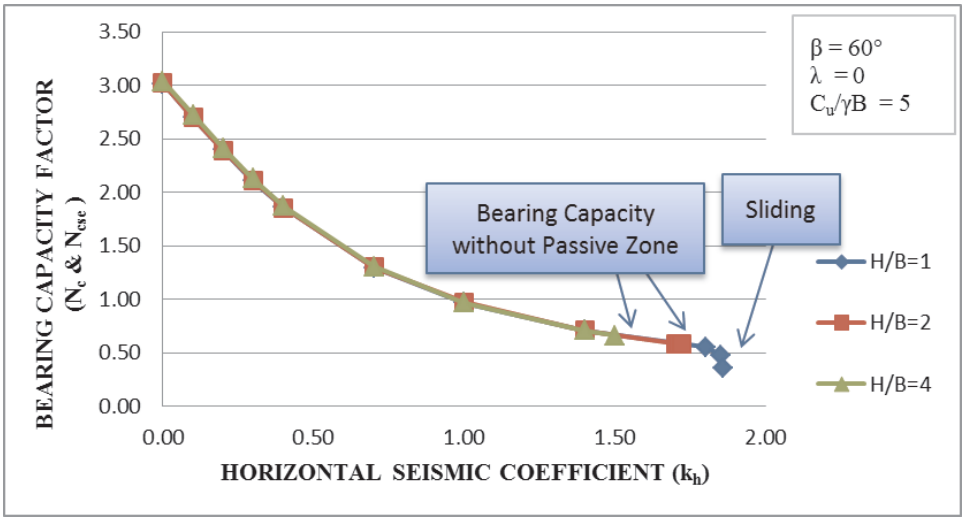

Figure A.5. Variation of Bearing Capacity Factor With Maximum Horizontal Seismic Coefficient for $C_u/\gamma B$=5 and β=60$^{\circ}o$.

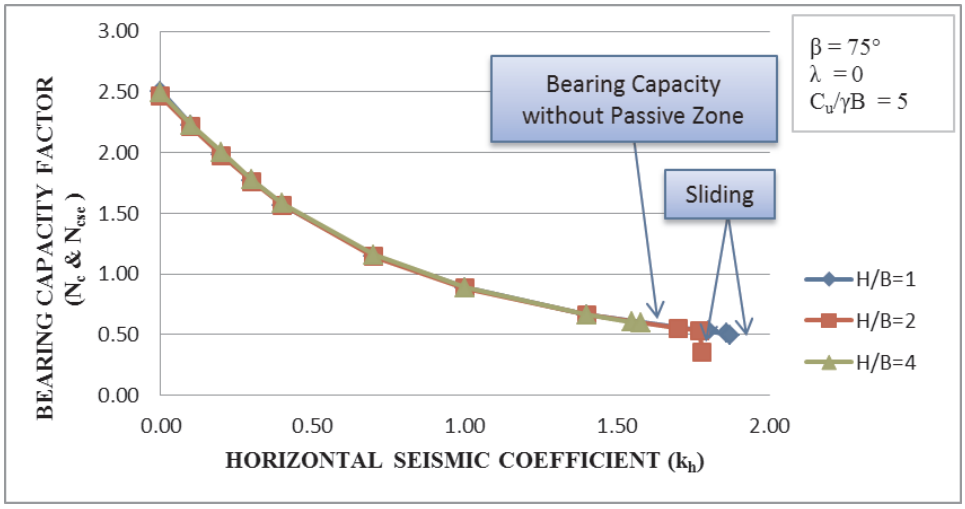

Figure A.6. Variation of Bearing Capacity Factor With Maximum Horizontal Seismic Coefficient for $C_u/\gamma B$=5 and β=75$^{\circ}o$.

A.2. Relationship between k_{hMAX} and $\beta(^o)$ for $C_u/\gamma B$=5

According to Figure A.7, as the slope angle is increased, the limit horizontal seismic acceleration coefficients increase. For the slopes which consisted of purely cohesive soil, the proneness to collapse decreased and correspondingly an increase in the maximum horizontal seismic acceleration was observed. This is attributed to the decreasing inertial forces at greater slope angles due to the decreases in the mass of

the soil body.

In addition, H/B ratio influences inversely the maximum horizontal seismic acceleration value. Furthermore, H/B=1 line and H/B=2 line are closer each other because of the smaller difference of slope height than H/B=4 line.

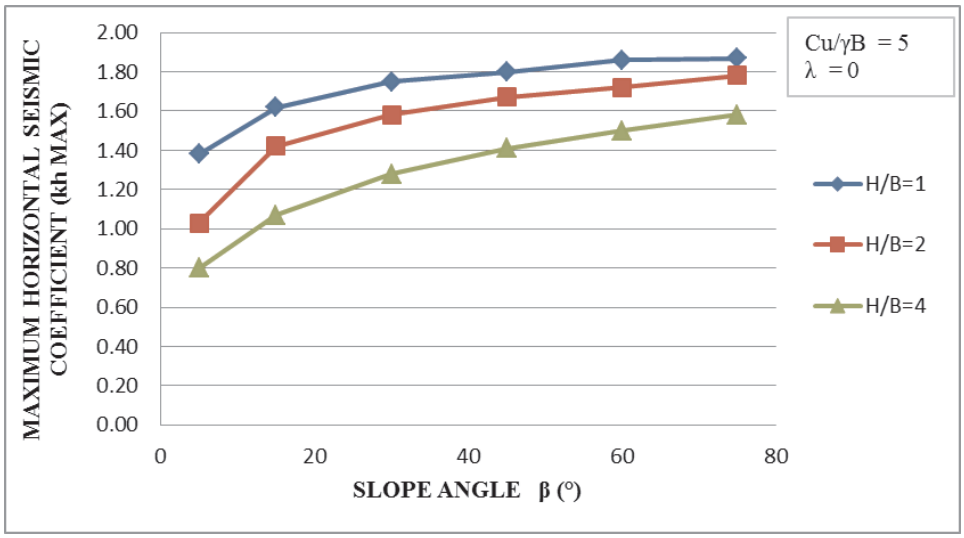

Figure A.7. Variation of Maximum Horizontal Seismic Coefficient With Slope Angle for $C_u/\gamma B$= 5.

A.3. Relationship between N_{cse} and k_{hMAX} for $C_u/\gamma B$=2.5

The increase in horizontal seismic acceleration causes the decrease in the undrained seismic bearing capacity. For $Cu/\gamma B$= 2.5, all H/B lines are coincident in Figure A.8, Figure A.9, Figure A.10, Figure A.11, Figure A.12 and Figure A.13. Therefore, the slope height has no influence the seismic bearing capacity value, but affects inversely the maximum horizontal seismic acceleration coefficient. The maximum horizontal seismic acceleration coefficient for $C_u/\gamma B$=2.5 are smaller than values for $C_u/\gamma B$=5 owing to the decrease in the strength characteristics of soil.

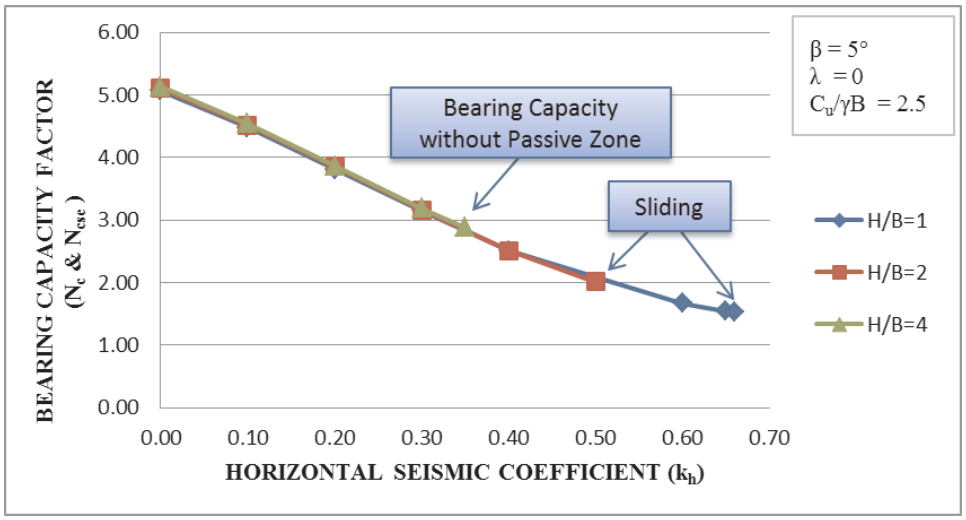

Figure A.8. Variation of Bearing Capacity Factor With Maximum Horizontal Seismic Coefficient for $C_u/\gamma B$=2.5 and β= 5^o.

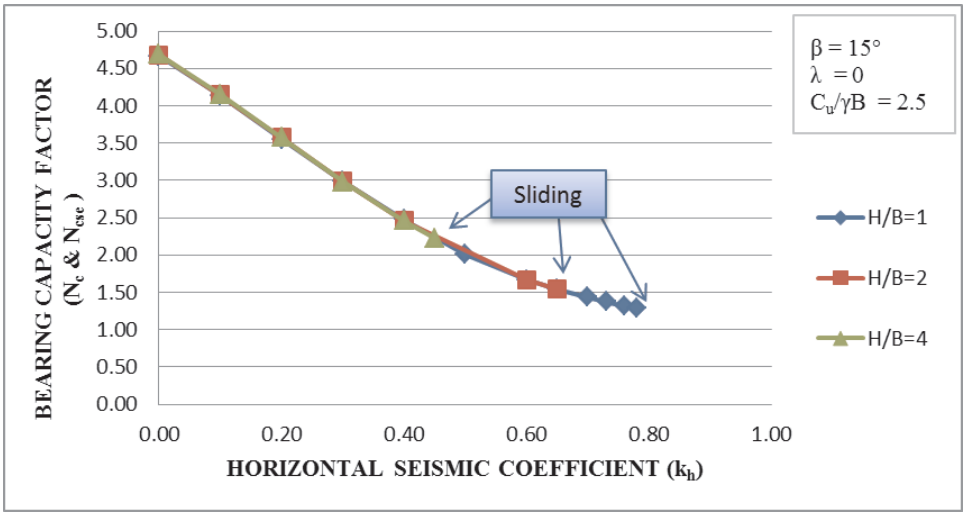

Figure A.9. Variation of Bearing Capacity Factor With Maximum Horizontal Seismic Coefficient for $C_u/\gamma B$= 2.5 and β= 15^o.

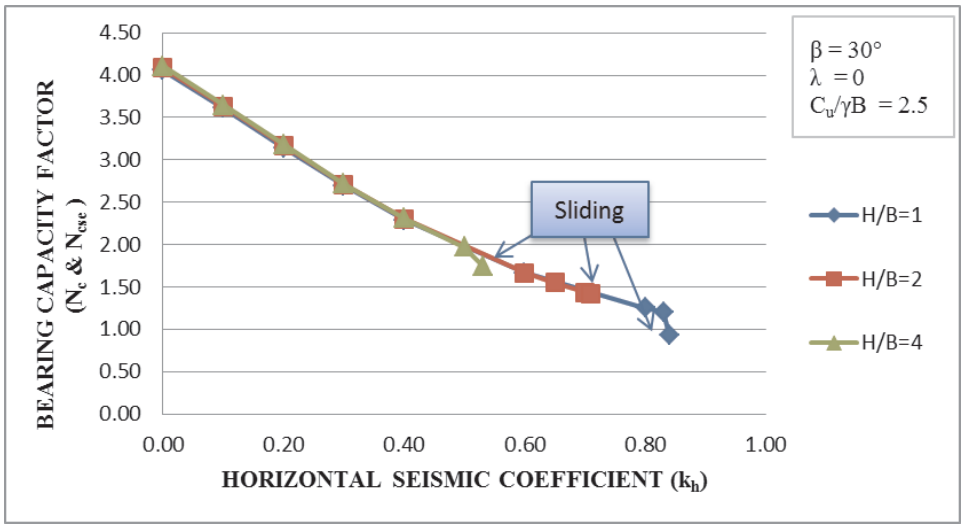

Figure A.10. Variation of Bearing Capacity Factor With Maximum Horizontal Seismic Coefficient for $C_u/\gamma B$= 2.5 and β= 30^o.

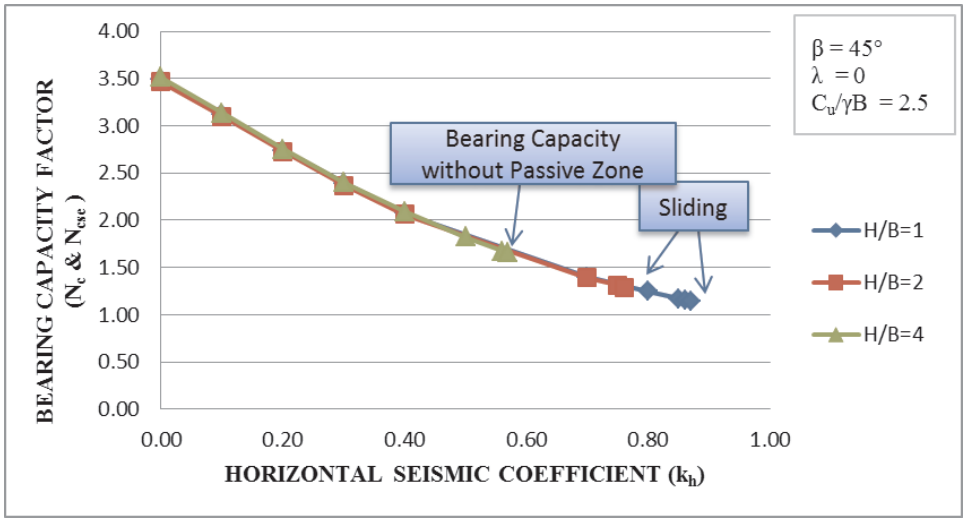

Figure A.11. Variation of Bearing Capacity Factor With Maximum Horizontal Seismic Coefficient for $C_u/\gamma B$= 2.5 and β= 45^o.

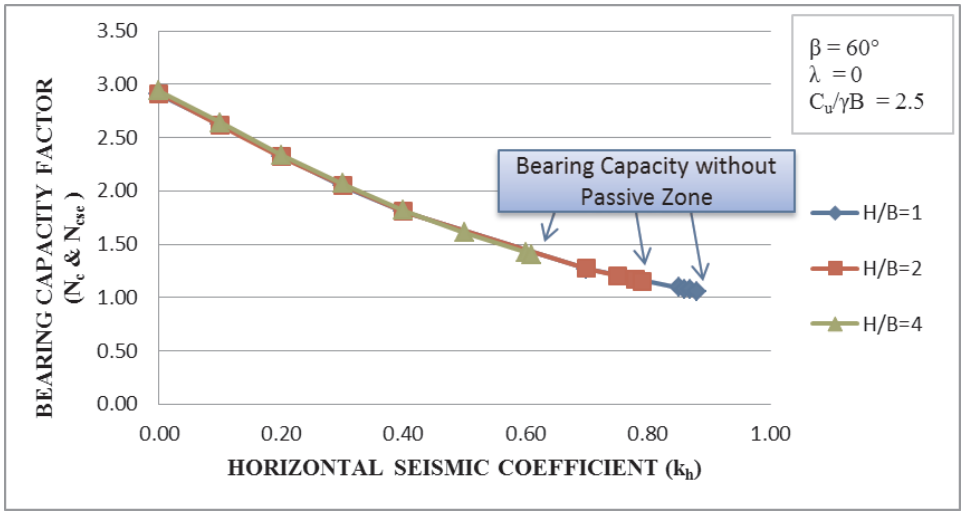

Figure A.12. Variation of Bearing Capacity Factor With Maximum Horizontal Seismic Coefficient for $C_u/\gamma B$= 2.5 and β= 60^o.

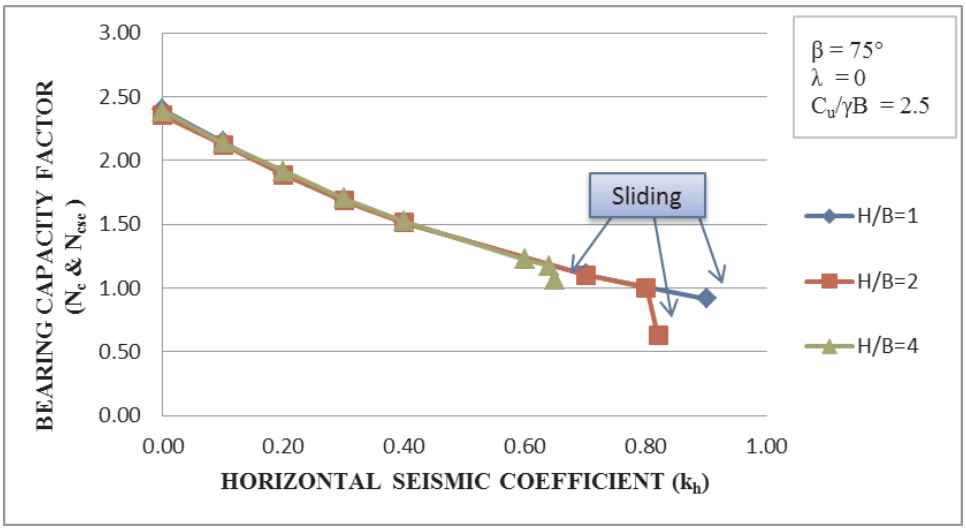

Figure A.13. Variation of Bearing Capacity Factor With Maximum Horizontal Seismic Coefficient for $C_u/\gamma B$= 2.5 and β= 75^o.

A.4. Relationship between k_{hMAX} and $\beta(^o)$ for $C_u/\gamma B$=2.5

The numeric difference among the maximum horizontal seismic coefficients for each line in Figure A.14 is less than the numeric difference for $C_u/\gamma B$= 5 in Figure A.7 owing to decreasing strength characteristics of soil.

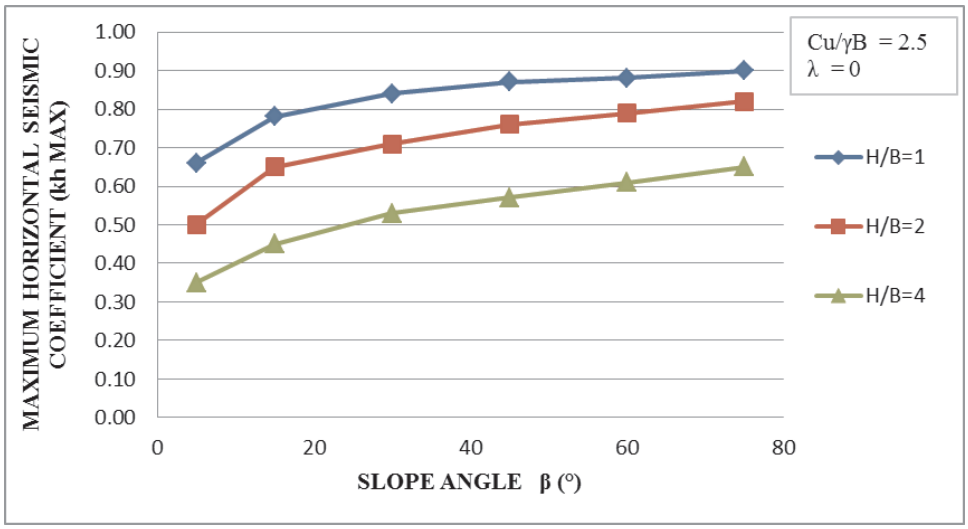

Figure A.14. Variation of Maximum Horizontal Seismic Coefficient With Slope Angle for $C_u/\gamma B$= 2.5.

A.5. Relationship between N_{cse} and k_{hMAX} for $C_u/\gamma B$=1.25

N_{cse} - k_h graphs for $C_u/\gamma B$= 1.25 indicate similar relations to previous graphs for $C_u/\gamma B$= 2.5 and $C_u/\gamma B$= 5. The maximum horizontal seismic acceleration coefficients for $C_u/\gamma B$= 1.25 are smaller than values for $C_u/\gamma B$= 2.5 owing to the decrease in the soil strength.

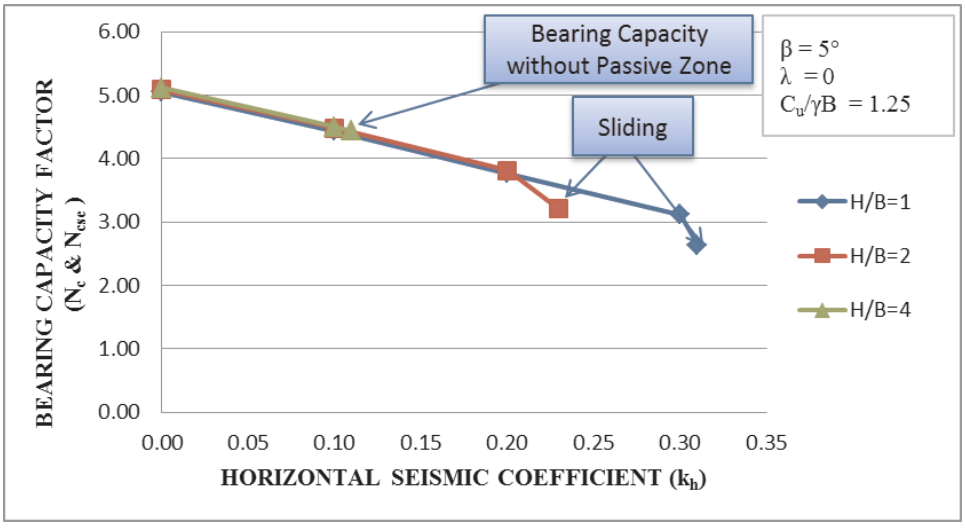

Figure A.15. Variation of Bearing Capacity Factor with Maximum Horizontal Seismic Coefficient for $C_u/\gamma B$= 1.25 and β=5°.

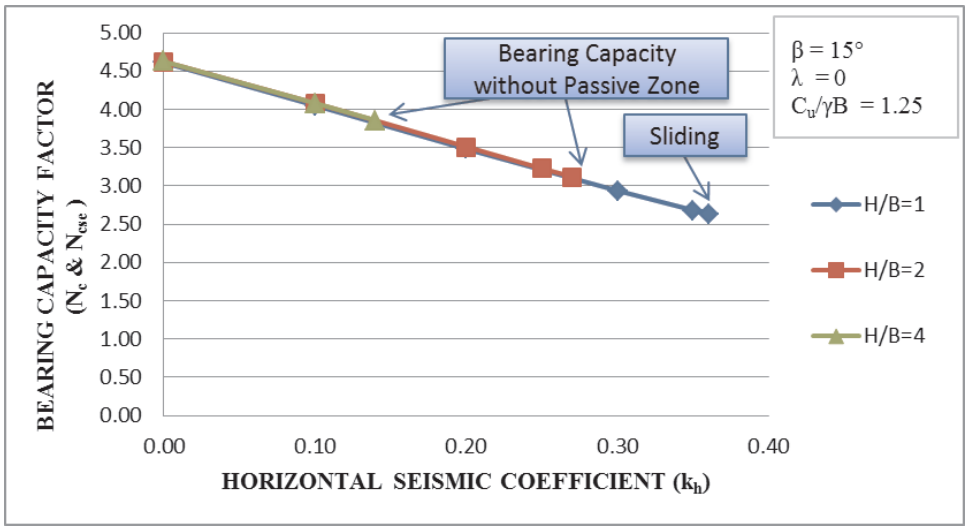

Figure A.16. Variation of Bearing Capacity Factor with Maximum Horizontal Seismic Coefficient for $C_u/\gamma B$= 1.25 and β= 15^o.

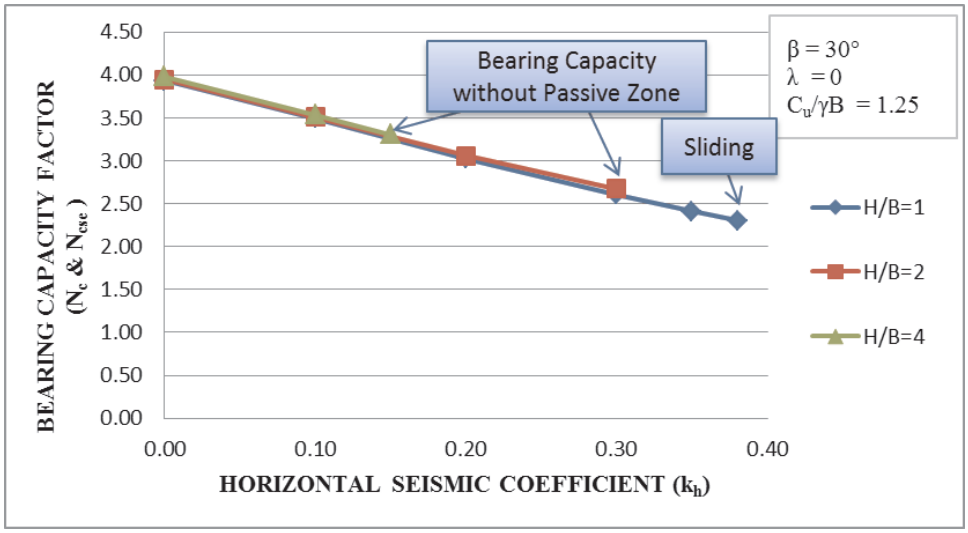

Figure A.17. Variation of Bearing Capacity Factor with Maximum Horizontal Seismic Coefficient for $C_u/\gamma B$= 1.25 and β= 30^o.

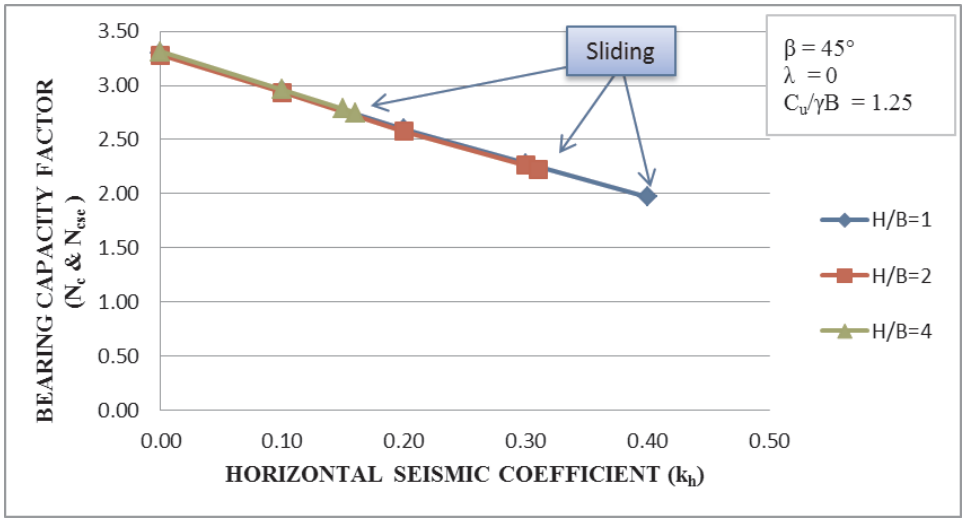

Figure A.18. Variation of Bearing Capacity Factor with Maximum Horizontal Seismic Coefficient for $C_u/\gamma B$= 1.25 and β= 45^o.

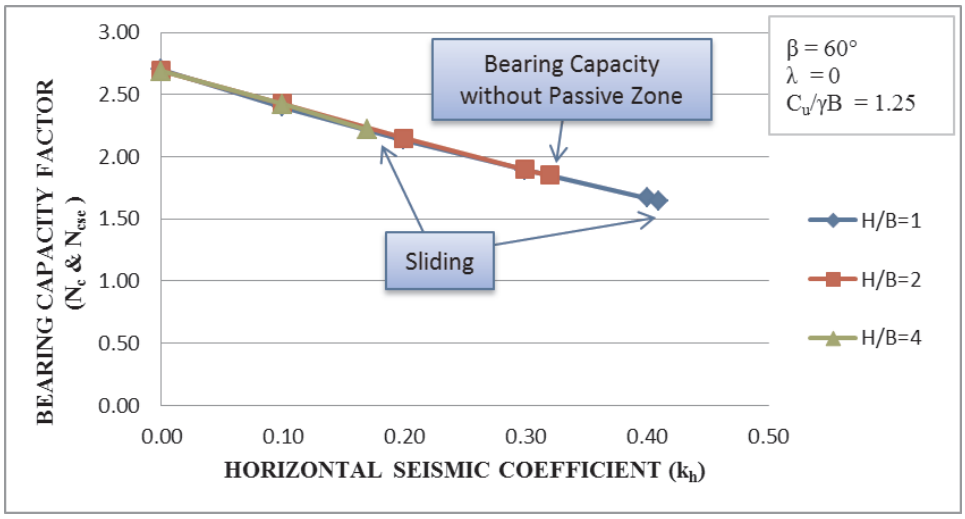

Figure A.19. Variation of Bearing Capacity Factor with Maximum Horizontal Seismic Coefficient for $C_u/\gamma B$= 1.25 and β= 60^o.

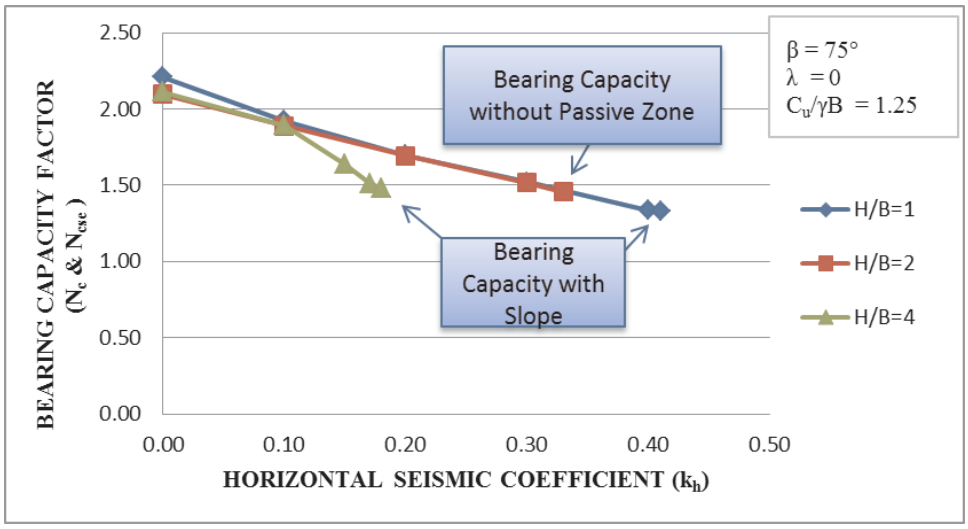

Figure A.20. Variation of Bearing Capacity Factor with Maximum Horizontal Seismic Coefficient for $C_u/\gamma B$= 1.25 and β= 75^o.

A.6. Relationship between k_{hMAX} and $\beta(^o)$ for $C_u/\gamma B$= 1.25

The numeric difference among the maximum horizontal seismic coefficients for each line for $C_u/\gamma B$= 1.25 in Figure A.21 is less than the numeric difference in Figure A.14 for $C_u/\gamma B$= 2.5 owing to decreasing strength characteristics of soil.

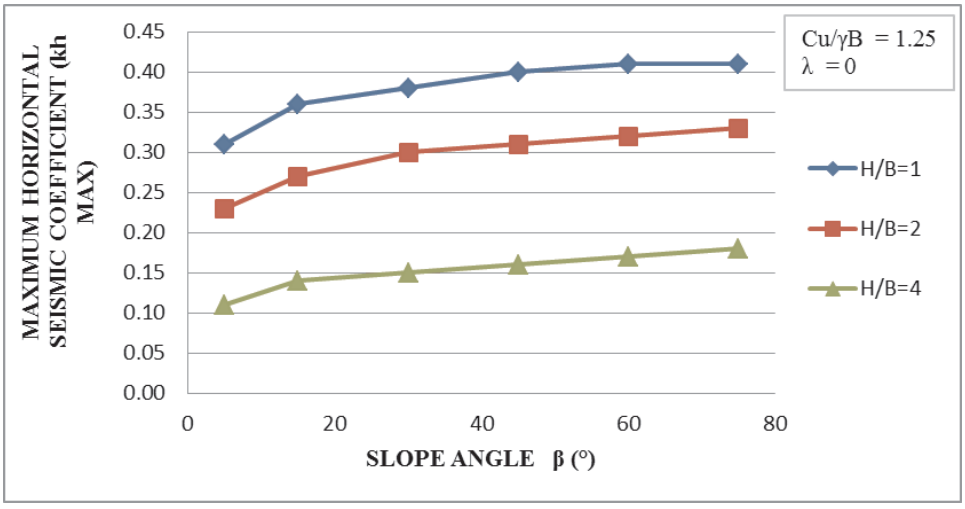

Figure A.21. Variation of Maximum Horizontal Seismic Coefficient With Slope Angle for $C_u/\gamma B$= 1.25.

A.7. Relationship between N_{cse} and k_{hMAX} for $C_u/\gamma B$= 0.625

N_{cse} - k_h graphs for $C_u/\gamma B$= 0.625 indicate similar relationships like previous graphs for $C_u/\gamma B$= 1.25, $C_u/\gamma B$= 2.5 and $C_u/\gamma B$= 5. The maximum horizontal seismic acceleration coefficients for $C_u/\gamma B$= 1.25 are smaller than the results for $C_u/\gamma B$= 2.5 owing to the decrease in the soil strength. In addition, there are no H/B=4 lines obtained in k_{hMAX} graphs of $C_u/\gamma B$= 0.625 except for $\beta = 5^o$, because of the lowest soil strength characteristics defined. Likewise, due to the weakest strength characteristics of soil, H/B lines don't coincide with each other in the graphs, as shown in Figure A.22, Figure A.23, Figure A.24, Figure A.25, Figure A.26 and Figure A.27.

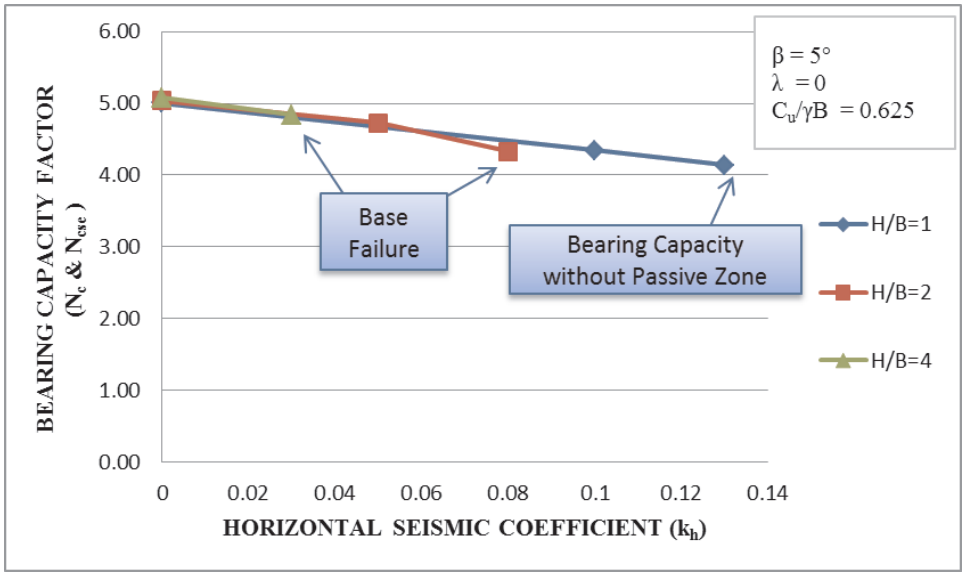

Figure A.22. Variation of Bearing Capacity Factor with Maximum Horizontal Seismic Coefficient for $C_u/\gamma B$= 0.625 and β= 5^o.

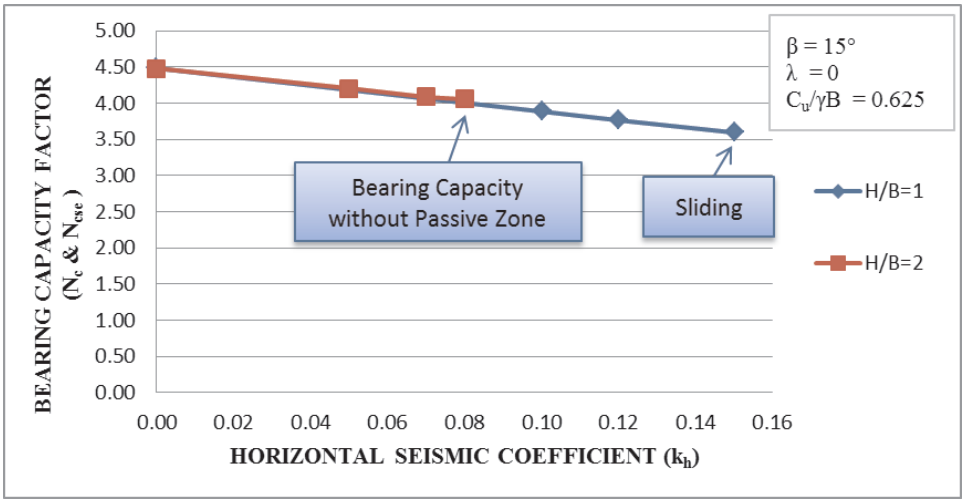

Figure A.23. Variation of Bearing Capacity Factor with Maximum Horizontal Seismic Coefficient for $C_u/\gamma B$= 0.625 and β= 15^o.

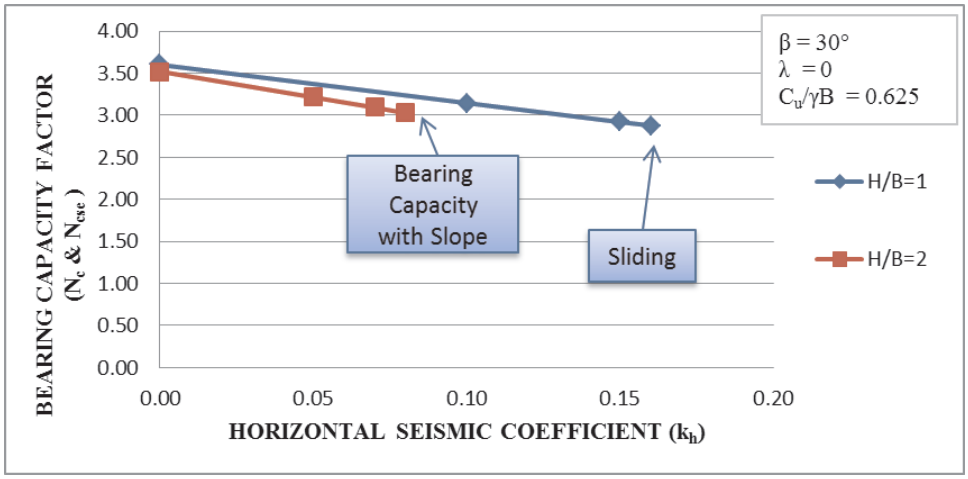

Figure A.24. Variation of Bearing Capacity Factor with Maximum Horizontal Seismic Coefficient for $C_u/\gamma B$= 0.625 and β= 30^o.

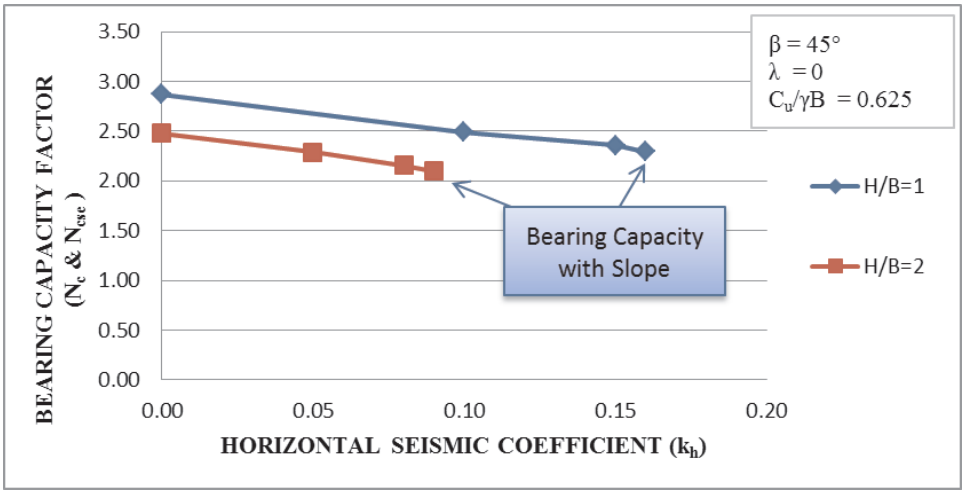

Figure A.25. Variation of Bearing Capacity Factor with Maximum Horizontal Seismic Coefficient for $C_u/\gamma B$= 0.625 and β= 45^o.

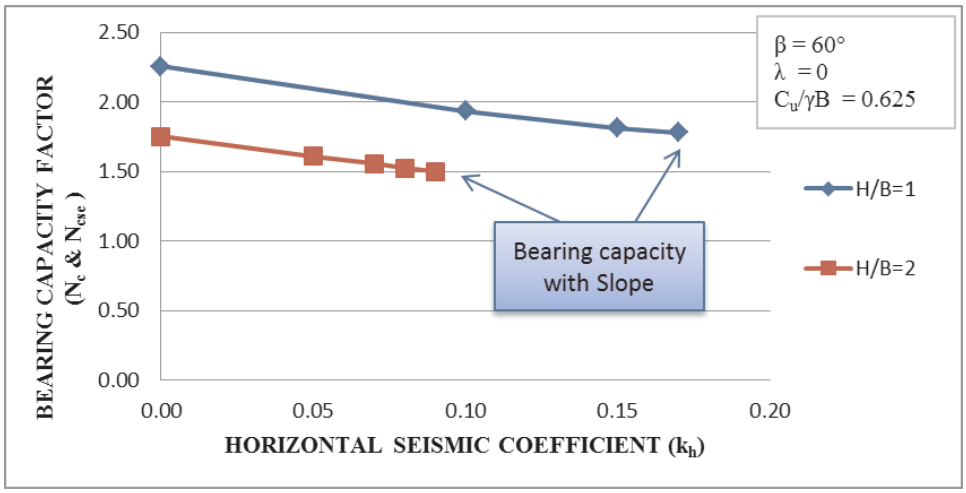

Figure A.26. Variation of Bearing Capacity Factor with Maximum Horizontal Seismic Coefficient for $C_u/\gamma B$= 0.625 and β= 60^o.

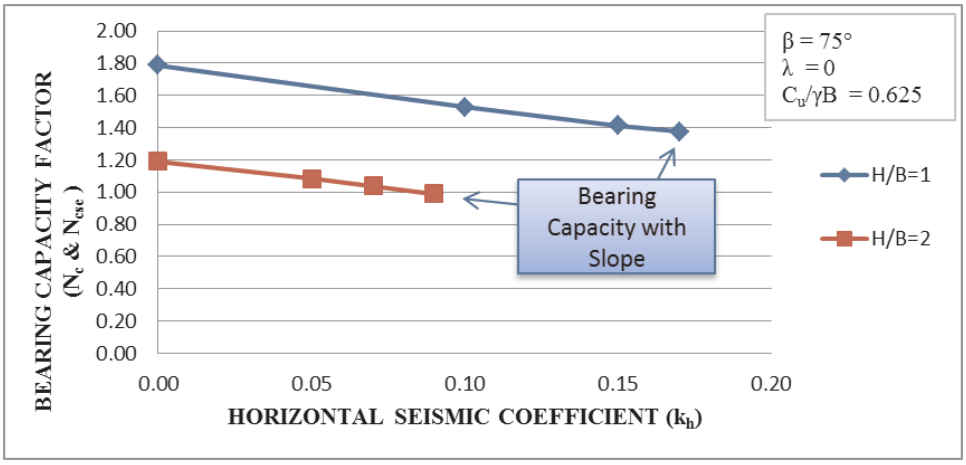

Figure A.27. Variation of Bearing Capacity Factor with Maximum Horizontal Seismic Coefficient for $C_u/\gamma B$= 0.625 and β= 75^o.

A.8. Relationship between k_{hMAX} and β^o for $C_u/\gamma B$= 0.625

In Figure A.28, owing to decreasing strength characteristic of soil, H/B=4 line couldn't be obtained.

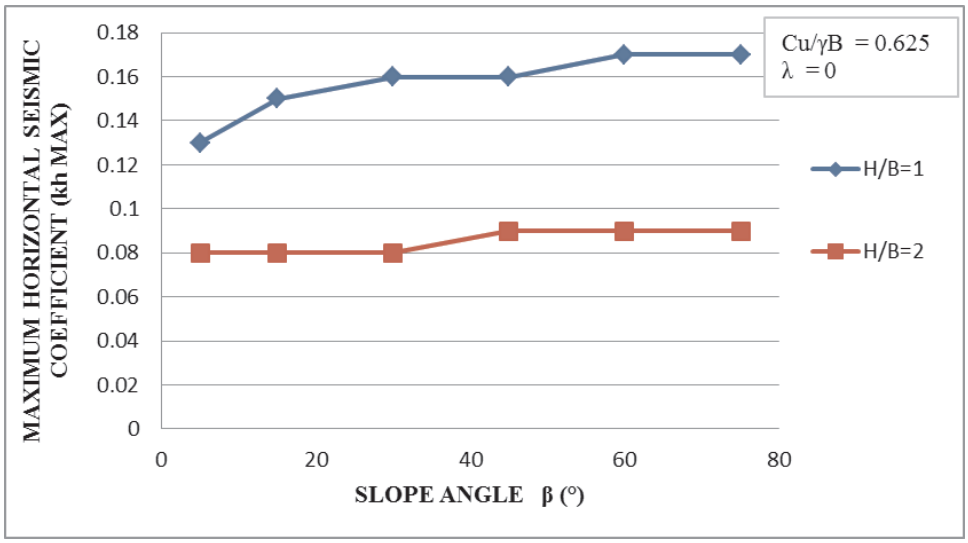

Figure A.28. Variation of Maximum Horizontal Seismic Coefficient With Slope Angle for $C_u/\gamma B$= 0.625.

A.9. Relationship between k_{hMAX} and β^o for H/B

In Figure A.29, Figure A.30 and Figure A.31, $C_u/\gamma B$= 5 lines have the highest maximum horizontal seismic coefficients due to being the greatest strength characteristic of soil in all material sets defined in PLAXIS. Hence, as $C_u/\gamma B$ ratio is increased, maximum horizontal seismic coefficients noticeably increase. However, as H/B ratio is increased, the maximum horizontal seismic coefficients drop.

As $C_u/\gamma B$ ratio is increased, the numeric difference among the maximum horizontal seismic coefficients for each line increases substantially. Likewise, as H/B ratio is increased, the numeric difference among the maximum horizontal seismic coefficients for each line increases as shown in Figure A.29, Figure A.30 and Figure A.31.

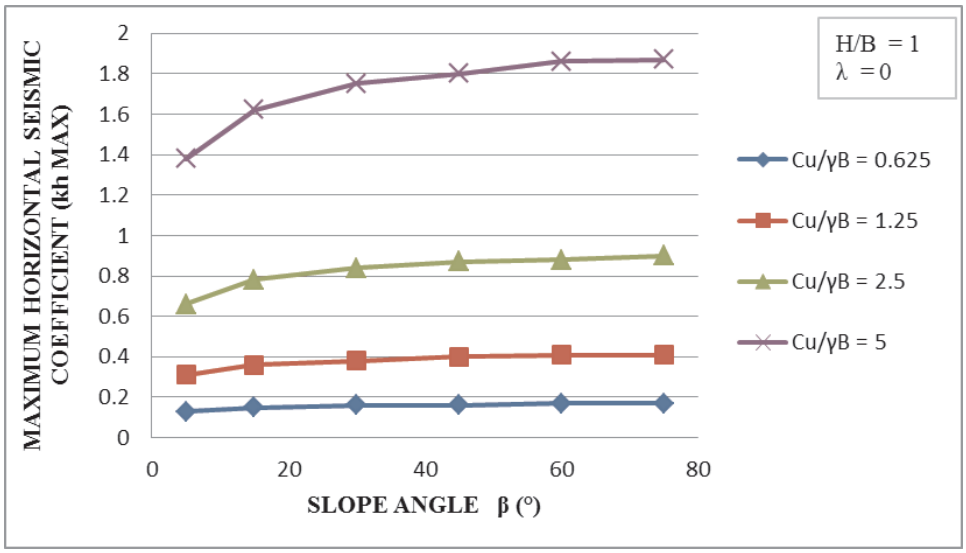

Figure A.29. Variation of Maximum Horizontal Seismic Coefficient with Slope Angle for H/B=1.

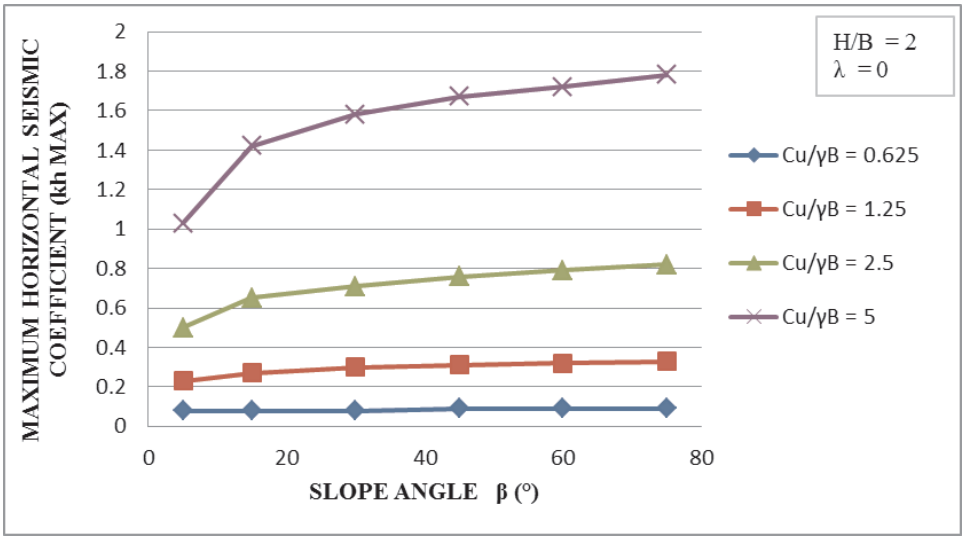

Figure A.30. Variation of Maximum Horizontal Seismic Coefficient with Slope Angle for H/B=2.

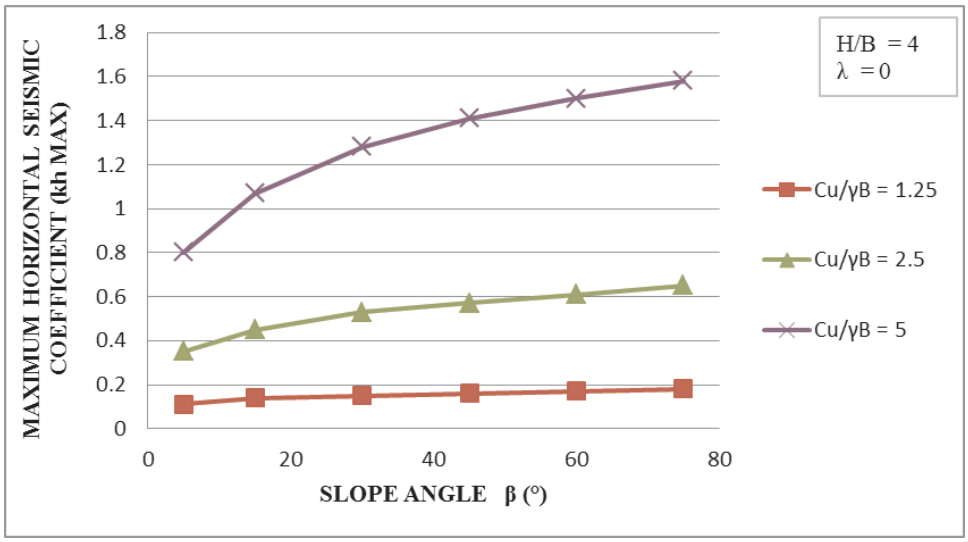

Figure A.31. Variation of Maximum Horizontal Seismic Coefficient with Slope Angle for H/B=4.

REFERENCES

Azzouz, A.S., and M.M., Baligh,1983,"Loaded Areas on Cohesive Slopes", *Journal of Geotechnical Engineering*, Vol. 109, No. 5, pp. 724-729.

Bishop, A.W., and N.R., Morgenstern, 1960, "Stability Coefficients for Earth Slopes", *Geotechnique*, Vol. 10, No. 4, pp. 129-150.

Castelli, F. and E. Motta, 2010, "Bearing Capacity of Strip Footings near Slopes", *Geotech Geol Engineering*, Vol. 28, pp. 187-198.

Chen, W.F., 1975, *Limit Analysis and Soil Plasticity*, Elsevier, Amsterdam.

Das, B.M., 2011, *Principles of Foundation Engineering*, Cengage Learning, SI 7th Edition.

Fang, H.Y., 1990, *Foundation Engineering Handbook*, Springer Science and Business Media, 2nd Edition.

Georgiadis, K., 2010, "Undrained Bearing Capacity of Strip Footings on Slopes", *Journal of Geotechnical and Geoenvironmental Engineering*, Vol. 136, No. 5, pp. 677-685

Hansen, J.B., 1961, "A General Formula for Bearing Capacity", *Akademiet for de Tekniske Videnskaber Geoteknisk Institut*, Copenhagen, Bulletin No. 11, pp. 38-46.

Hansen, J.B., 1970, "A Revised and Extended Formula for Bearing Capacity", *Akademiet for de Tekniske Videnskaber Geoteknisk Institut*, Copenhagen, Bulletin No. 28, pp. 5-11.

Houlsby, G.T. and A.M. Puzrin, 1999, "The Bearing Capacity of a Strip Footing on Clay under Combined Loading", *Procture Resistance Socienty London*, No. 2002,

455A, pp. 893-916.

Koppula, S.D., 1984, "Pseudo-Static Analysis of Clay Slopes Subjected to Earthquakes", *Geotechnique*, Vol. 34, No. 1, pp. 71-79, 1984.

Kumar, J. and V.B. K. Mohan Rao, 2003, "Seismic Bearing Capacity of Foundations on Slopes", *Geotechnique*, Vol. 53, No. 3, pp. 347-361.

Kusakabe, O., T. Kimura and H. Yamaguchi, 1981, "Bearing Capacity of Slopes under Strip Loads on the Top Surfaces", *Japanese Society of Soil Mechanics and Foundation Engineering*, Vol. 21, No. 4, pp. 29-40.

Meyerhof, G.G., 1957, "The Ultimate Bearing Capacity of Foundations on Slopes", *Proceedings of the Fourth International Conference on Soil Mechanics and Foundation Engineering*, pp. 384-386.

Michalowski, R.L., 1995, "Slope Stability Analysis: A Kinematical Approach", *Geotechnique*, Vol. 45, No. 2, pp. 283-293.

Michalowski, R.L., 2001, "Stability Charts for Uniform Slopes", *Journal of Geotechnical and Geoenvironmental Engineering*, Vol. 128, No. 4, pp. 351-355.

Pecker, A., 1996, "Seismic Bearing Capacity of Shallow Foundations", *Proceedings of Eleventh World Conference on Earthquake Engineering*, Elsevier Science Ltd, Paper No. 2076.

Pecker, A. and J. Salençon, 1991, "Seismic Bearing Capacity of Shallow Strip Foundations on Clay Soils", *Proceedings of the International Workshop on Seismology and Earthquake Engineering*, Cenapred, Mexico City, pp. 287-304.

Plaxis Version 8 Reference Manual, Plaxis bv, 2003.

Plaxis Version 8 Tutorial Manual, Plaxis bv, 2003.

Salençon, J. and A. Pecker, 1995, "Ultimate Bearing Capacity of Shallow Foundations under Inclined and Eccentric Loads Part I: Purely Cohesive Soil, *European Jony Mechanism, A/Solids*, Vol. 14, No. 3, pp. 349-375.

Salençon, J. and A. Pecker, 1995, "Ultimate Bearing Capacity of Shallow Foundations under Inclined and Eccentric Loads Part II: Purely Cohesive Soil without Tensile Strength, *European Jony Mechanism, A/Solids*, Vol. 14, No. 3, pp. 377-396.

Shiau, J., A. Lyamin and S. Sloan, 2006, "Application of Pseudo-Static Limit Analysis in Geotechnical Earthquake Design", *Numerical Methods in Geotechnical Engineering - Schweiger (ed.)*, Taylor and Francis Group, London, pp. 249-255.

Shiau, J.S., R.S., Merifield, A.V., Lyamin and S.W., Sloan, 2011, "Undrained Stability of Footings on Slopes", *International Journal of Geomechanics*, Vol. 11, No. 5, pp. 381-390.

Sivakugan, N. and M. Pacheco, 2011, "Design of Shallow Foundations", *Geotechnical Engineering Handbook*, B. M. Das, J. Ross Publishing.

Skempton, A.W.,1951, "The Bearing Capacity of Clays", *Proceedings of the Building Research Congress*, London, Vol. 1, pp. 180-189.

Taiebat, H.A. and J.P. Carter, 2002, "Bearing Capacity of Strip and Circular Foundations on Undrained Clay Subjected to Eccentric Loads", *Geotechnique*, Vol. 52, No. 1, pp. 61-64.

Taylor, D.W.,1937, "Stability of Earth Slopes", *J. Boston Soc. Civil Engineers*, Vol. 24, pp. 197-246.

Terzaghi, K., 1943, *Theoretical Soil Mechanics*, Wiley, New York.

Vesic, A.S., 1975, "Bearing Capacity of Shallow Foundations", *Foundation Engineering Handbook*, H.F. Winterkorn and H.Y. Fang, eds., Van Nostrand Reinhold, New York, pp. 121-147.